



Message from the Director General

SUMMARY OF A REPORT TO THE ESO STAFF

1. Audit

The team which was charged by the ESO Council to provide an audit report about ESO and in particular the VLT project, has now finished its work with a final discussion at the ESO Headquarters on April 28, 1994. The report has been published and was discussed by Council in its recent meeting.

I am glad to tell you that ESO came through this exercise "with flying colours" and that our earlier statements concerning the work done at ESO were largely confirmed by the Audit Team. In particular, it was agreed that the request for an increased VLT budget was reasonable and the need to add a number of staff positions was also supported.

The Audit Team proposed specific measures to the Council including increases in budget and staff and also improvements of various aspects of the work breakdown structure, the management system, as well as the plans for operations. A very important conclusion was that ESO will be able to manage the VLT project under these assumptions. It should be noted that this means that it has been possible to obtain support for a number of new positions since early last year. It is now our task to fill these positions with the best possible staff.

This will not be easy and will require a certain effort from all involved.

2. Chile

The situation of ESO in Chile has been the subject of many recent discussions and, as is known and has been made public through recent press releases, ESO appears to be under a concerted attack from some groups in that country. While ESO has meticulously adhered to its legal obligations in Chile, it is true that the wishes of the Chilean astronomers as well as the ESO Chilean staff were not always sufficiently taken into account. However, the Supplementary Agreement which is now in the final stages of negotiation, takes care of this. We are hopeful that it will become possible to conclude the signing and ratification procedure, so that this Agreement can enter into force and our Chilean colleagues can then profit from the new regulations. In fact, ESO has done everything it can reasonably do and the issues surrounding the ownership of Paranal is not ESO's problem, but a problem of the Chilean Government. We are confident that the Chilean Government will take the necessary actions in due time, but it is unfortunate that we may run into problems with the VLT

schedule, if a solution to this critical problem is not found soon. The recent visit by the ESO delegation to Chile during which meetings were held with the Foreign Minister and also the President of the Republic of Chile, reassured us that the Chilean Government fully adheres to the conditions laid down in the Chile-ESO Treaty, including ESO's immunities and privileges.

In view of the crucial importance of the Paranal issue for the VLT project and since we have at this moment committed approximately half of the total VLT budget, it is obvious that we must now do our utmost to "find a home" for the world's largest optical telescope.

3. OPC

The Observing Programmes Committee met for the first time under the new evaluation system at the end of May. The new process means that more scientists will be involved in the peer review and this will undoubtedly result in a better and more equitable assessment of the observing proposals. Things went extremely well and a very good job was done by Jacques Breysacher and his people despite the fact that a record number of applications was received for this round, close to 600.

4. STC

The Scientific Technical Committee also met recently and evaluated the scientific technical aspects of the ESO operations at La Silla. The STC again underlined that science must be the driver of all ESO activities and expressed the opinion that there are currently too many tasks for the astronomical/technical staff at La Silla. Reductions will be necessary, probably by the closure of some of the telescopes, or by transferring the operational responsibility to national groups.

The STC strongly supported the view that the VLTI must be re-introduced in the VLT as soon as possible since it is a unique feature of this telescope. The STC endorsed the new, smaller interferometry programme which was presented by ESO. It costs 30 % less and also further reduces the annual cost, since it will be stretched over twice the period earlier envisaged. In this connection, the interest of our Australian colleagues in VLT interferometry and the possibility of using in addition to the MPG/CNRS and ESO contributions the entry fee by Australia for this purpose, if and when it becomes a full member of ESO, is indeed very exciting.

5. Scientific Visiting Committee

This Committee has now delivered its report about the science carried out at La Silla and at the Headquarters. It is the intention to continue to rely upon its services as an Advisory Body for these questions. Certain problems were remarked on, in particular that more attention should be given to the involvement of ESO scientists in the development of new instrumental facilities, communications between the scientists inside and outside ESO and also the personnel policy of the Organization of which certain aspects, for instance salaries, are in the state of an undesirable lack of definition.

It is obvious that we must attempt to define better what we are really trying to do in the personnel area, but also that we must do everything possible to attract and keep the staff with the best qualifications. For this reason, special measures may become necessary during the period until the personnel policy has become better defined. The issue of a system based on merit is still open, but it is particularly important that the staff gets a feeling of fairness in the judgement of their performance. It will be my task to try to convince the Finance Committee and Council of what our "fair market value" really is. This will

become much clearer after the termination of the current comparative study of employment conditions (including salaries) at ESO and other national and private organizations.

6. Budget

I am happy to report that Finance Committee and Council approved the budget for 1994 as well as the forecast for 1995–1997. They also approved various management tools in connection with the cash flow, etc. which will facilitate the financial administration during the next years of heavy VLT expenditures.

7. Conclusions

In conclusion, I am glad to state that I do not see any real show-stoppers for ESO and its VLT project at this moment. We will surely be able to carry through successfully this great project but it is also true that we must improve ourselves in terms of management techniques and internal communication. There may still be some "cultural" problems within ESO, but I think that good will and enthusiasm for the common cause will make it possible to overcome these difficulties. *R. GIACCONI*

TELESCOPES AND INSTRUMENTATION

Work Starts on the VLT M2 Units

D. ENARD, ESO

The development and construction of the 4 VLT secondary mirror units is going to be carried out by Matra Marconi Systems together with REOSC, SFIM and MAN. The kick-off meeting was held on April 20 and 21 and the design work is already proceeding.

One of the basic features of the VLT is that there is only one secondary mirror to serve the different observing modes. The switch from Cassegrain to the Nasmyth and coudé foci is achieved by moving the tertiary mirror into different positions rather than – as is traditional – by exchanging the secondary mirror unit. There are important operational and cost-saving advantages in this approach. It gives a unique opportunity to change at any time of observing mode, reduces maintenance and significantly simplifies the operation software as well

as the adapters. This secondary mirror has a diameter of about 1.2 metre for the nominal aperture of F/15 at the Nasmyth focus. Because the VLT is largely optimized for the IR, the secondary mirror also defines the pupil which is slightly undersized with respect to the beam defined by the primary mirror outer diameter. This approach sets however a number of tough requirements on the M2 unit since all the requirements which traditionally are distributed on several mirror units of different sizes are concentrated into one single unit.

As part of the active optics scheme, the secondary mirror must be able to maintain the telescope geometry with respect to the primary mirror. To this effect, the secondary mirror can be positioned in three coordinates to correct for focusing and centring as it is already

the case for the NTT as well as for most modern telescopes.

In addition, the VLT secondary mirrors can be controlled in tilt around a point close to the vertex to correct for fast guiding errors. This mode is called field stabilization and was introduced at a very early stage of the project and was driven by the important wind loads to which the structure would have been subjected with the retractable enclosure originally foreseen. The later decision to revert to a conventional enclosure – essentially in order to better protect the primary mirror from wind loads – did not remove that need. As a matter of fact, numerical and wind tunnel simulations have shown that the enclosure did not contribute much to reduce the dynamic part of the wind loads and that, considering the strong winds at Cerro Paranal,

a fast guiding would be necessary if the very ambitious image quality goals were to be attained.

The VLT uses as a main criterion for image quality the Central Intensity Ratio which characterizes the peak intensity degradation induced by the telescope. The CIR is a direct indication of the telescope efficiency and is very sensitive to random image motion. As an example, a random image motion of 0.05 arcsecond will produce a CIR loss of about 10 % for a seeing of 0.4 arc-second.

Atmospheric image motion can also be corrected by the tip/tilt secondary mirror within the limit of the isoplanatic field and if an appropriate detection scheme is used.

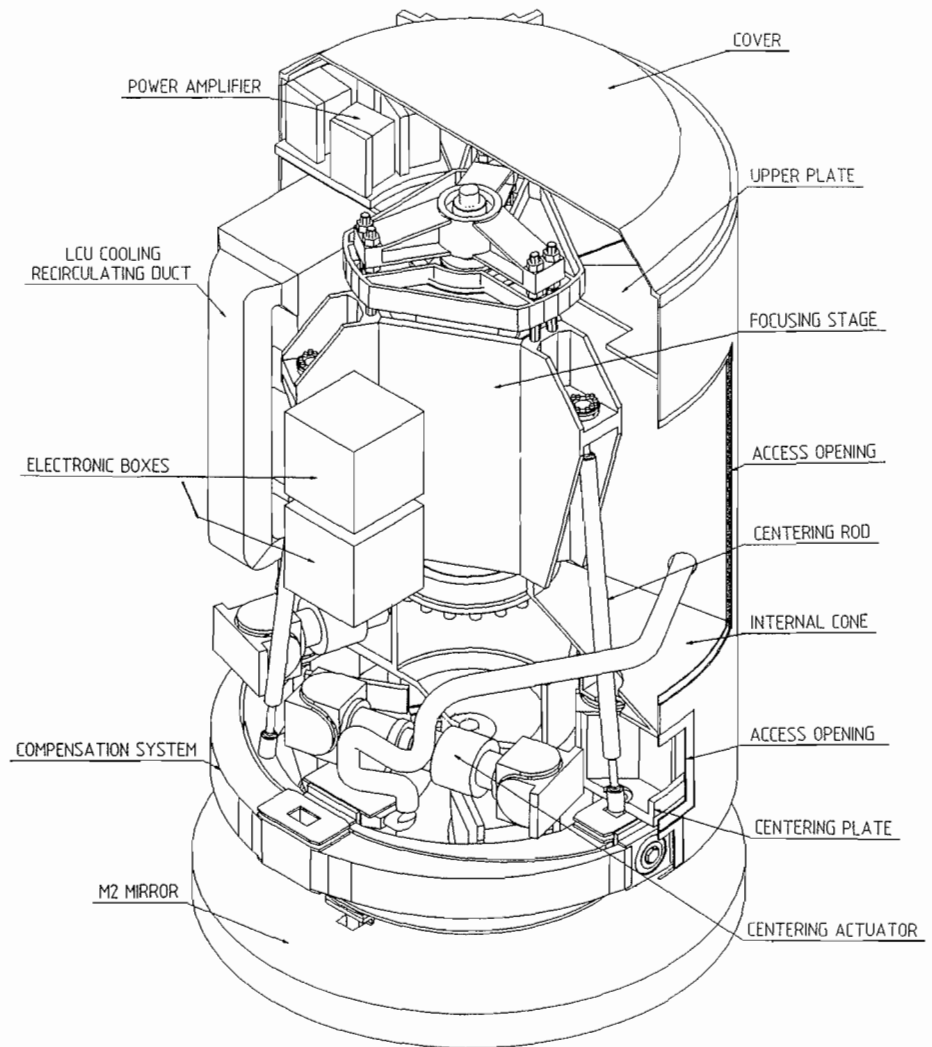
The accuracy requirement for field stabilization is 0.05 arcsecond which corresponds to about 0.01 arcsecond in sky coordinates. The correction bandwidth has been fixed to 10 Hertz which has been found adequate to correct for telescope guiding errors as well as for atmospheric image motion.

The third requirement for the secondary mirrors is square wave chopping for observing in the IR. The amazing development of IR detectors in the last 10 years has however much reduced the use of chopping which seems now limited to the longer wavelength range (10 and 20 μ). The requirements on frequency and tilt amplitude have been thoroughly analysed using the existing IR instruments. Though they have been considerably reduced with respect to what they were 10 or 15 years ago, they remain in terms of mirror bandwidth far above those necessary for the field stabilization mode and represent a technical challenge considering the relatively large size of the secondary mirror. The maximum chopping frequency is 5 Hertz for an amplitude of 2 arc-minutes.

Each secondary mirror unit is composed of a mirror assembly and of an electro-mechanical assembly.

The electro-mechanical assembly is composed of three independent stages: the focusing, centring and tilt/chopping stages. The mirror assembly is fixed to the tilt and chopping stage which itself is attached to the centring stage and to the focusing stage which provides the final attachment to the M2 unit structure.

The Focusing Stage consists of a servo-controlled electro-mechanical actuator generating a movement of the M2 mirror along the telescope optical axis. The same focusing system is used when changing between the Nasmyth and the Cassegrain foci which requires a change of mirror position of about 30 mm.



Architecture of the VLT M2 unit.

The Centring Stage is used to keep the lateral alignment of the M2 mirror with respect to the primary mirror. It is designed in such a way that the mirror vertex rotates around the mirror centre of curvature. This has the advantage of not modifying the telescope pointing so that only coma is corrected. The effective movement is achieved by three servo-controlled actuators acting on the mirror tilt and chopping stage which itself is attached to the focusing stage through a three legs pantograph.

The Tilt/Chopping Stage tilts the mirror around a point ideally located at the mirror vertex. This stage is equipped with a dynamically balancing system, intended to compensate the reaction forces which could cause oscillation of the electro-mechanical assembly.

The Control System consists of the Local Control Unit (LCU) and of all the electrical and electronic hardware used to control the operation of all the systems inside the M2 Unit. Except for the power supplies which are fixed on the telescope structure, the control system is physically integrated inside the M2 Unit.

All heat sources inside the M2 Unit are cooled in order to maintain the outer surface close to the ambient air temperature.

The M2 units are also equipped with a deployable Sky Baffle, which is used to obstruct an annular region of the sky immediately around the M2 Unit for particular observations.

The Mirror Assembly

The 1.2-metre diameter secondary mirrors are lightweighted convex hyperbolic mirrors made of Silicon Carbide. This material is together with Beryllium the most suitable for extreme lightweight structures. The Silicon Carbide has however the great advantage over Beryllium to be cheaper and probably more stable in the long term. The particular technology selected by Matra for the mirror substrate is the Reaction Bonded Silicon Carbide known as CERASTAR and produced by CARBORUNDUM. The weight of the finished mirror will be about 33 kg and its first eigenfrequency about 800 Hz. The mass

is about 10 % of that of a traditional glass mirror.

The optical surface will be generated by replication from a concave master. The development of a replication process applicable to astronomical large and highly accurate mirrors has been carried out for several years at the Observatory of Côte D'Azur with the financial support of INSU and ESO. Excellent replicas of a 1-metre concave mirror have been recently achieved, which

gives confidence that the M2 mirrors can be successfully replicated. In case of difficulties however, conventional polishing is foreseen as back-up. Replication is particularly suited for convex surfaces which, with conventional polishing, are much more difficult to produce and to test than concave surfaces. The mould to be used for replication is concave and can be tested quite easily. The mould can also be oversized which gives the possibility to attain an excel-

lent optical quality up to the very edge of the mirror which is hardly possible with traditional polishing. The main advantages of replica are therefore a lower cost, a shorter lead time and a better optical quality.

With the scheme proposed by Matra, the first unit is expected to be delivered well in time for the integration on the first Unit Telescope.

Hunting the Bad Vibes at Paranal!

B. KOEHLER, ESO

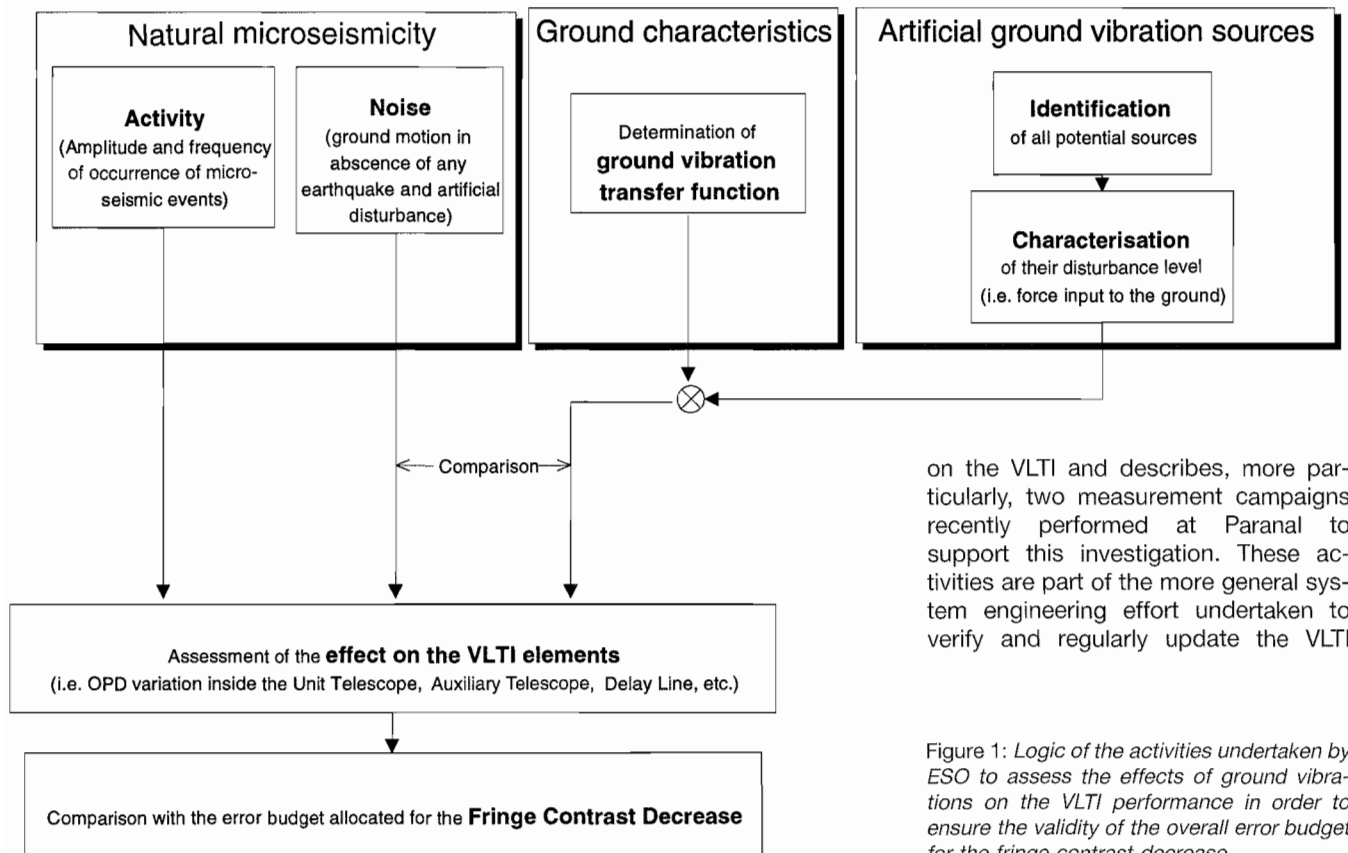
1. Introduction

It is well known that interferometric devices are extremely sensitive to vibrations. The VLT, in its interferometric mode (VLTi), is not an exception to this rule. Indeed, vibrations which generate relative displacement of the optical element of the interferometer at sub-micron level may blur the fringe pattern and result in a significant decrease of the fringe contrast, that is one of the prime observables of a stellar interferometer. Among many other sources of fringe contrast decrease, the vibra-

tions coming from the ground (referred to as microseismic noise) are especially critical and require particular attention during the design and development phase of the project. As a matter of fact, an important specificity of the VLTi with respect to laboratory interferometers is that the optical elements of the interferometer are firmly fixed to the ground and not isolated from the ground. This requires, therefore, a high dynamic stability of the ground itself. The reasons for which the optical elements cannot be isolated from the ground are: (i) the

site extension does not allow to place the complete interferometer on a single bench, (ii) individual isolation systems, because of their intrinsic low stiffness, would be incompatible with other requirements such as high tracking accuracy of the telescope under wind load and could, in some cases, deteriorate even more the fringe contrast because of their free relative motion at the support resonance.

This article provides an overview of the approach followed by ESO to investigate the effect of microseismic noise



on the VLTi and describes, more particularly, two measurement campaigns recently performed at Paranal to support this investigation. These activities are part of the more general system engineering effort undertaken to verify and regularly update the VLTi

Figure 1: Logic of the activities undertaken by ESO to assess the effects of ground vibrations on the VLTi performance in order to ensure the validity of the overall error budget for the fringe contrast decrease.

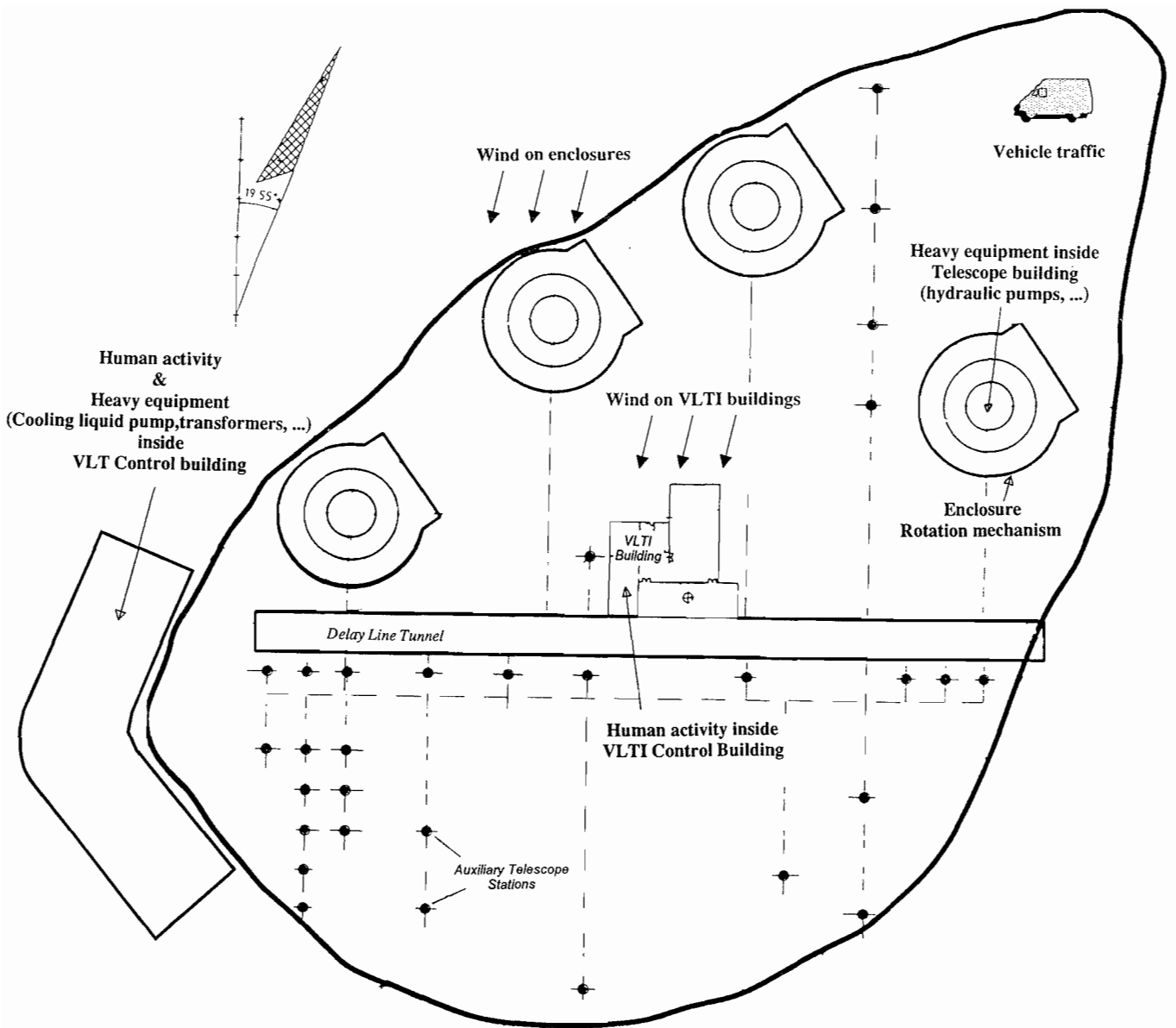


Figure 2: Overview of the different artificial sources affecting potentially the VLTI. All these sources are subject to a characterization of their disturbance level and to an assessment of their influence on the VLTI performance.

error budgets derived from the global VLTI performance requirements.

2. Overview

The logic of the investigation in the area of microseismic noise is schematically shown in Figure 1 and briefly described below.

Characterization of the natural microseismicity at Paranal: This consists in determining the natural ground motion at the site before any man-made disturbing sources are installed. Two types of seismicity are of interest: (i) the background noise which is the level of ground motion in the absence of any microseismic event, this level giving a reference for the “unpolluted” site, (ii) the microseismic activity characterized by the relation *intensity versus frequency of occurrence* of all micro-earth-

quakes. A specific campaign was dedicated to the measurement of these characteristics at Paranal (see section 4).

Determination of the Ground Vibration Transfer Function: Another important site characteristic related to the soil properties is the efficiency with which a disturbance at one location propagates through the ground to create a ground motion at a given distance where sensitive equipment is located. This characteristic is essential for the assessment of the effect of any artificial ground vibration source on a given VLTI element. It has been determined both theoretically and experimentally (see section 3).

Identification and characterization of all artificial ground vibration sources: An overview of the different artificial sources of microseismic noise potentially affecting the VLTI is shown in Figure 2. All these sources are subject to a

characterization of their disturbance level and to an assessment of their influence on the VLTI performance. The results are used to specify or to check the design adequacy for various subsystems of the VLT Observatory such as the antivibration supports of the hydraulic pumps and of the liquid cooling pumps, as well as to derive operational constraints such as prohibiting the traffic on the platform during interferometric observations.

Assessment of the effects of ground vibrations on the VLTI: As soon as the level of ground motion at the location of the VLTI elements is determined, the effect on the VLTI performance can be assessed by computing the Optical Path Difference (OPD) variation generated by this motion. For very simple and small elements such as the folding mirrors at the output of the light ducts,

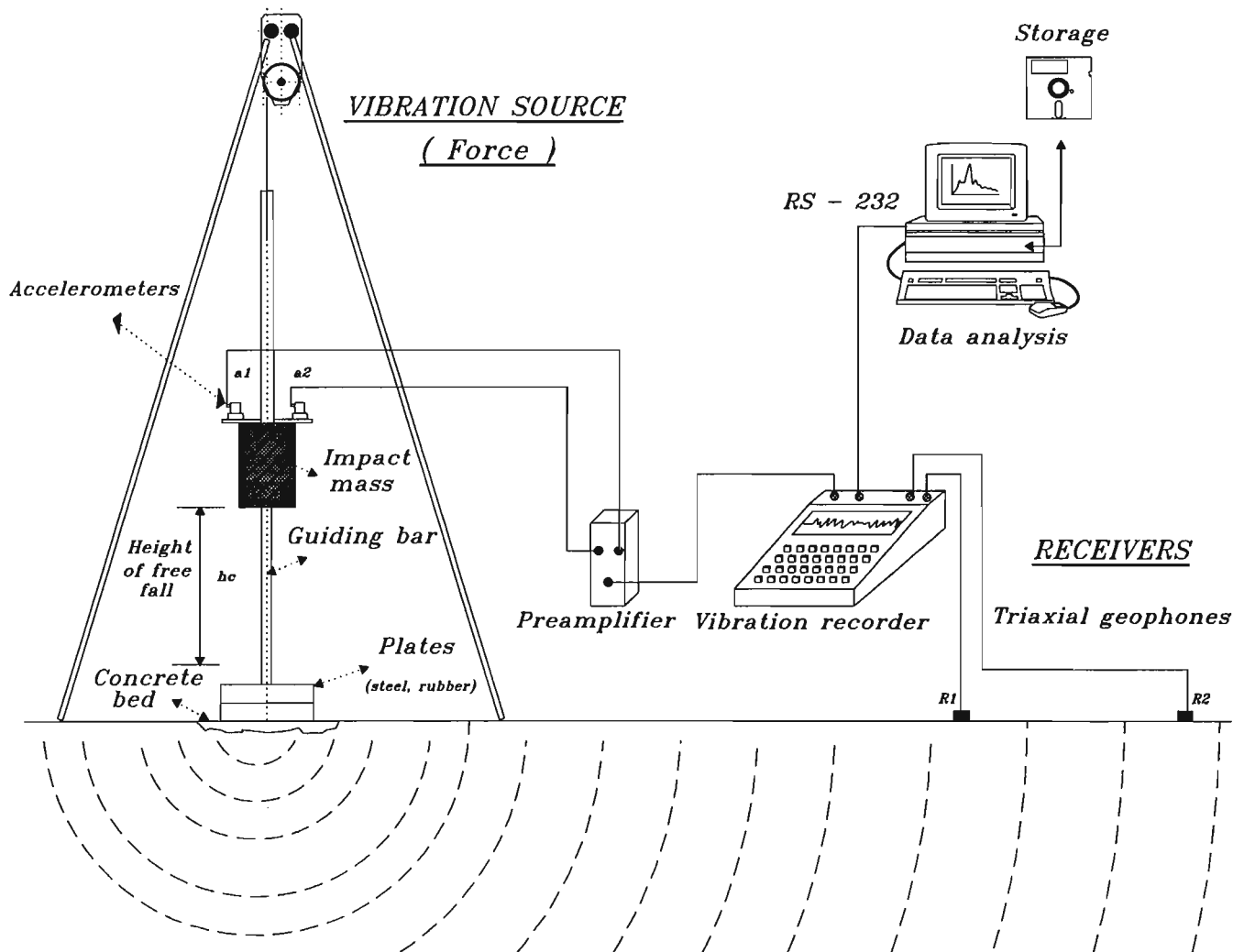


Figure 3: Measurement set-up for the in-situ determination of the Ground Vibration Transfer Function (GVTF).

the OPD variation can be directly derived assuming that the mirror follows exactly the ground motion. For complex elements such as the telescopes (or the delay lines), an accurate Finite Element Model is required. The ground motion is applied at the base of the telescope foundation and the OPD variation generated inside the telescope is computed from the displacements of the various mirrors. This computation is performed in the spectral domain.

The error budget for the OPD variation inside each telescope and each delay line is set to 14 nanometres RMS computed on any 10 millisecond time window corresponding to the detector integration time in the visible.

A level of $0.5 \mu\text{g}/\sqrt{\text{Hz}}$ (above 10 Hz) for the Power Spectral Density (PSD) of the ground acceleration during VLT operation has been set as a design criterion for the VLT. This level is used to easily compare the level of the various

microseismic sources and to assess the generic influence of the ground motion on the different elements of the interferometer. When the PSD of the disturbance significantly differs from this design spectrum, a particular computation is required.

3. Ground Vibration Transfer Functions

In order to assess the influence of a ground vibration source on any of the VLT elements (telescope, delay line, folding mirrors, beam combiner, instru-



Figure 4: View of the geophone (foreground) and of the hammer-handling machine (background) used to measure the GVTF.



Figure 5: Overview of the Observatory site showing the telescope excavations and, in the centre of the "Platform" the equipment used to measure the GVTF. The view is taken from the north.

ments, etc.), it is necessary to know how "well" the disturbance propagates through the ground between the source and the sensitive equipment. This ground characteristic, that we will call the Ground Vibration Transfer Function (GVTF), can be expressed in terms of the frequency-dependent amplitude (and phase) of the ratio: [Displacement of the ground at the location of the sen-

sitive equipment-called receiver-]/[Disturbance force input into the ground at the source location].

3.1. Preliminary computer estimates

A preliminary estimate of GVTF was performed in November 1991 through computer simulation to allow early assessment of the effect of some major

disturbance sources. The computer simulation, performed by the company Géodynamique et Structures (France), assumes a half-plan layered ground structure, horizontally isotropic, and makes use of the basic ground characteristics (mass density, compression and shear wave propagation velocities) previously measured on the site.

Results were obtained for different configurations of the source/receiver including different directions of the input force, different depths of the source and receiver, and different distances between the source and the receiver.

The results were used, in particular, to support the decision to install the main electrical transformers inside the Control Building located on the side of the Observatory Platform rather than inside the Interferometry Complex at the centre of the Platform.

3.2. In-situ measurements

In order to refine the above estimates it was decided to perform in-situ measurements of the GVTF at Paranal. This allows us to take into account the soil anisotropy and the particular geometry of the site not included in the above computer simulations. The one-week measurement campaign took place in September 1993 with the collaboration of the IDIEM company and Universidad de Chile (Chile).

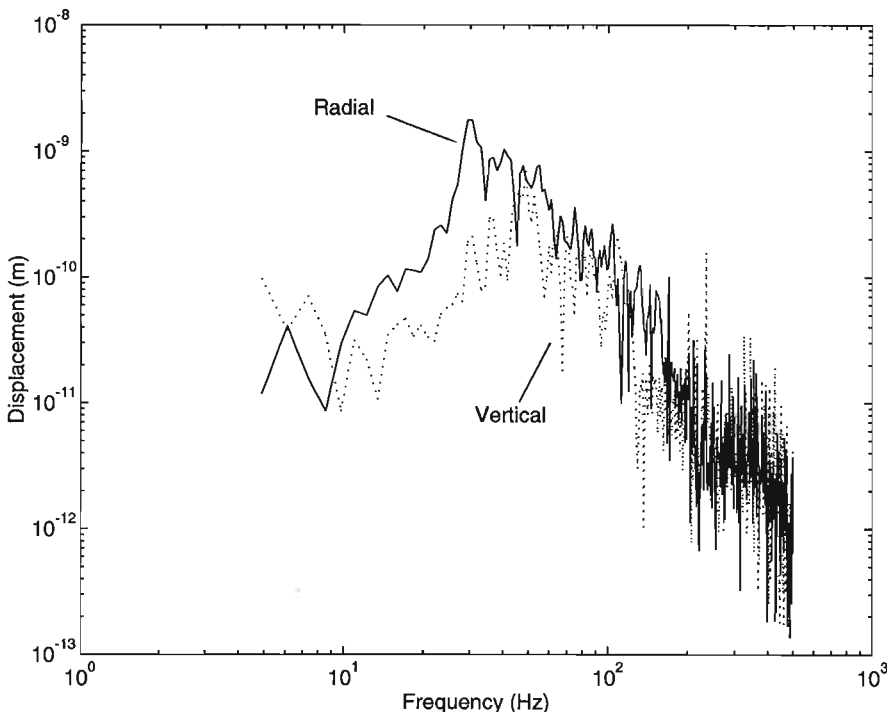


Figure 6: Examples of Ground Vibration Transfer Functions obtained from in-situ measurement. The curves represent the amplitude of the ground displacement in radial and vertical directions in response to a 1000 N vertical disturbance force, as a function of its frequency. The source is at the Control Building location and the receiver is 50 m away, on the central platform (west part of the interferometric tunnel).



Figure 7: Obtaining accurate microseismic measurements free from external disturbance such as wind buffeting requires the seismometer to be buried on firm rock at least 40 cm below the surface, and requires a polyvalent seismologist! Here, Luis Rivera is at work in the excavation of telescope No. 4.

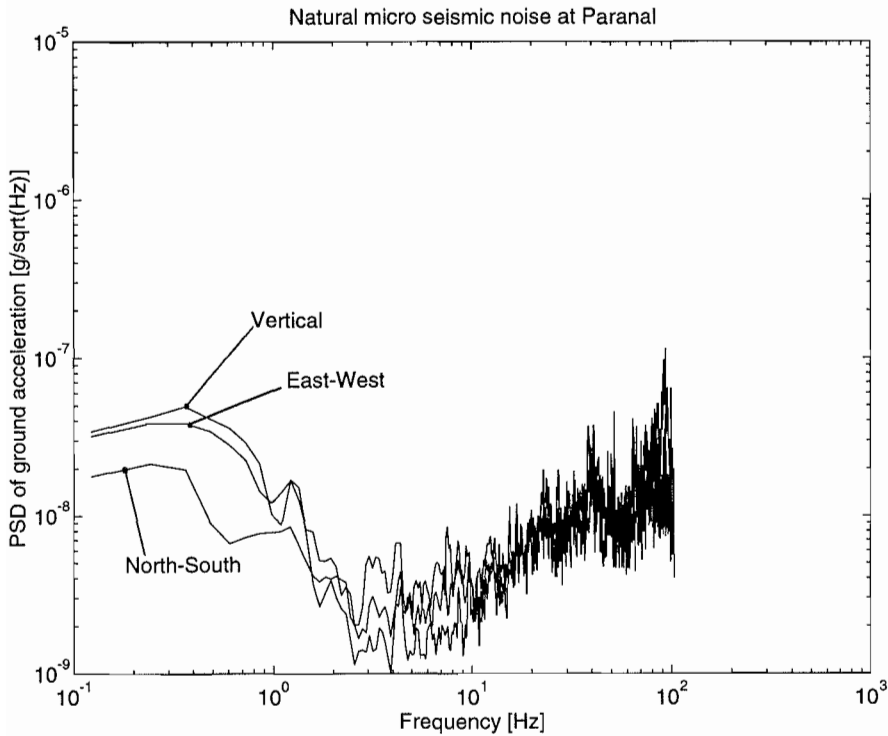


Figure 8: Natural micro seismic noise at Paranal in the absence of any seismic event and any artificial vibration source. The curves represent the PSD of the ground acceleration in the vertical, north-south, and east-west directions.

3.2.1. Measurement set-up

The measurement set-up, shown in Figure 3, uses a force source consisting of a free falling hammer monitored by accelerometers and a set of triaxial geophones monitoring the ground velocity. The signals from the accelerometers and the geophones are fed to an acquisition electronics and saved on a PC for later processing. Figure 4 shows one of the geophones together with the drilling machine used to handle the hammer in the background. Figure 5 provides an overview of the Observatory Platform with the measuring set-up installed at the centre.

3.2.2. Results

Measurements were performed in a total of 19 different configurations in the excavation of the first telescope, on the central platform, in the excavation of the Control Building, and in between these locations.

Figure 6 displays an example of the results obtained for a source located at the Control Building and a receiver located on the central platform at the western extremity of the delay-line tunnel. This configuration is of particular importance since most of the vibration-generating equipment will be located in the basement of the Control Building and could, if no precaution were taken, disturb the folding mirrors and delay lines located inside the tunnel. For some

show important spectral features in the transfer function due to rock inhomogeneity.

These results are being used to update the assessment of the effect of the various artificial micro seismic sources on the VLTI performance.

4. Natural Microseismicity

A second measurement campaign was undertaken at Paranal at the end of March 1994 to obtain a detailed characterization of the natural micro seismicity. This campaign was performed in collaboration with the Ecole et Observatoire de Physique du Globe de Strasbourg (EOPGS) (France).

The measurement campaign had the following goals: (i) measure the *natural ground motion noise* at Paranal in the absence of any seismic event and any artificial vibration source, (ii) characterize the *micro seismic activity* at Paranal (i.e. how often do micro seismic events – earthquakes – happen and which intensity do they have?).

In addition, we seized the opportunity to characterize some artificial vibration sources which can only be assessed by in-situ measurements, such as car driving on the access road and people walking on the Observatory Platform.

The measurement set-up included high-sensitivity seismometers (Kinemetrics SS-1 and MarkProduct L4) associated with acquisition electronics (Reftek). The seismometers were installed on firm rock and buried at least 40 cm

configurations, the experimental results could be checked against those of the computer simulations. A good agreement of the average levels of the GVTF was generally found (e.g. $\approx 5 \cdot 10^{-12}$ m/N in the 10–100 Hz region at 10 m distance), but the in-situ measurements

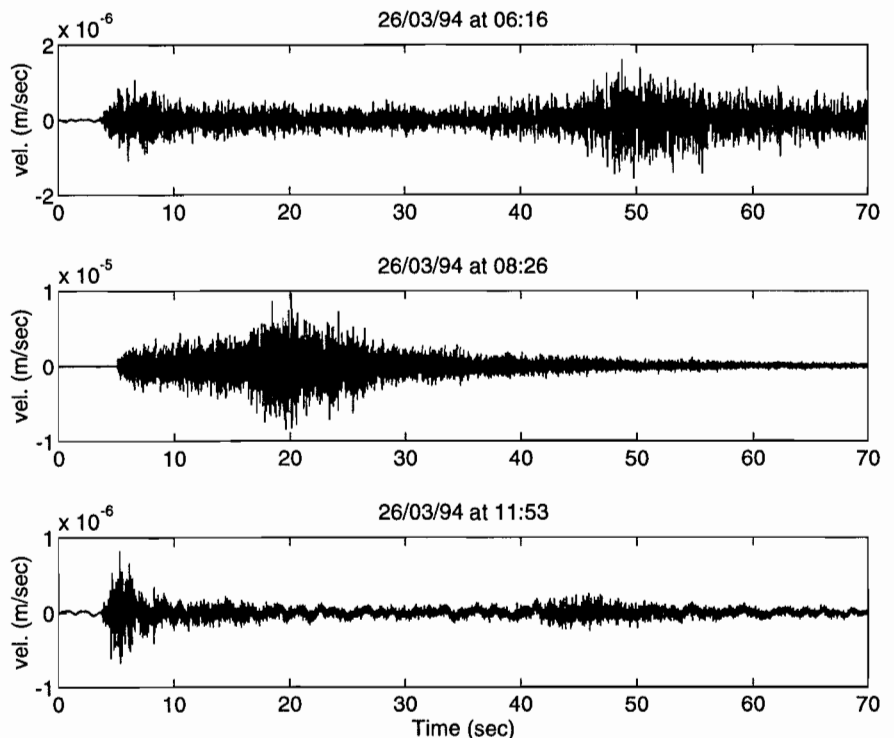


Figure 9: Examples of micro-earthquakes recorded at Paranal during the night of March 25/26, 1994. The curves represent the chronogram of the ground velocity in the vertical direction.

below the surface to avoid contamination by external disturbance such as wind buffeting (Fig. 7).

4.1. Natural background noise

Figure 8 shows the level of microseismic noise in the absence of any seismic event and any artificial vibration source for the vertical, north-south and east-west components of the ground motion. In the low-frequency part of the spectra, below 1 Hz, the effect of ocean waves is clearly visible, in particular on the vertical and east-west components, as expected from the Chilean coast geometry. This effect, which amounts to a few tenths of a micron, does not affect the VLTI because of its low frequency. In the medium (1–10 Hz) and high (10–100 Hz) frequency ranges, the level of ground motion ($<0.02\mu\text{g}/\sqrt{\text{Hz}}$) is extremely low, even when compared with that of very quiet sites available in the literature.

4.2. Microseismic activity

The microseismic activity was monitored during the ten-day campaign duration by placing the seismometers in trigger mode. The recording was triggered to any increase (by 30 % or more) of the signal RMS level. This allowed recording of very low-intensity earthquakes. These data will be complemented with the data obtained independently by the EOPGS with their permanent network installed 4 years ago in the Antofagasta area which monitors earthquakes of magnitude > 3.5 . The statistical distribution of macro- and microseismic events at Paranal will be derived from these data.

A large number of events were recorded during the campaign (about one every 20 minutes). Figure 9 provides examples of such events showing the chronogram of the ground velocity while Figure 10 displays the corresponding acceleration spectra. The high frequency level of the acceleration PSD ranges from small values ($\approx 0.1\mu\text{g}/\sqrt{\text{Hz}}$) to larger values ($\approx 3\mu\text{g}/\sqrt{\text{Hz}}$) potentially affecting the desired ultimate performance of the VLTI in the visible. A detailed statistical analysis of the events' amplitude versus their frequency of occurrence is therefore required to assess their real influence on the VLTI operation. This analysis is in progress at the date of writing. However, a first conclusion is the confirmation of our plan to install a set of seismometers on the VLT site in order to monitor the microseismic activity during VLTI operation and to store, in a database, the information necessary to implement on-line and/or post-processing strategies taking into

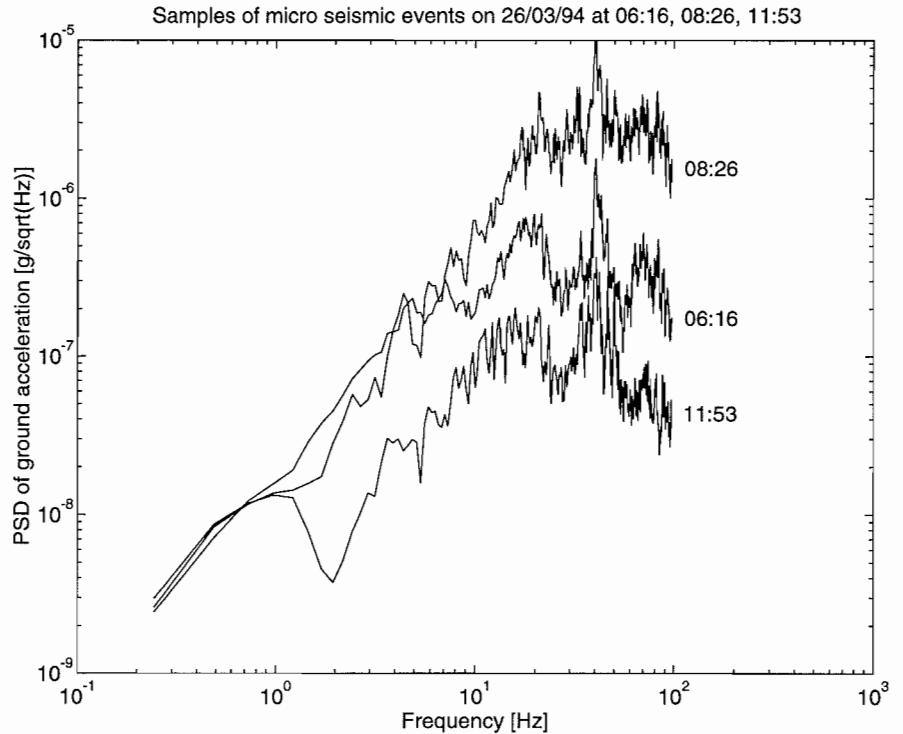


Figure 10: PSD of the ground acceleration corresponding to the three micro-earthquakes shown in Figure 9.

account the actual seismic activity experienced during the observations.

5. Conclusion

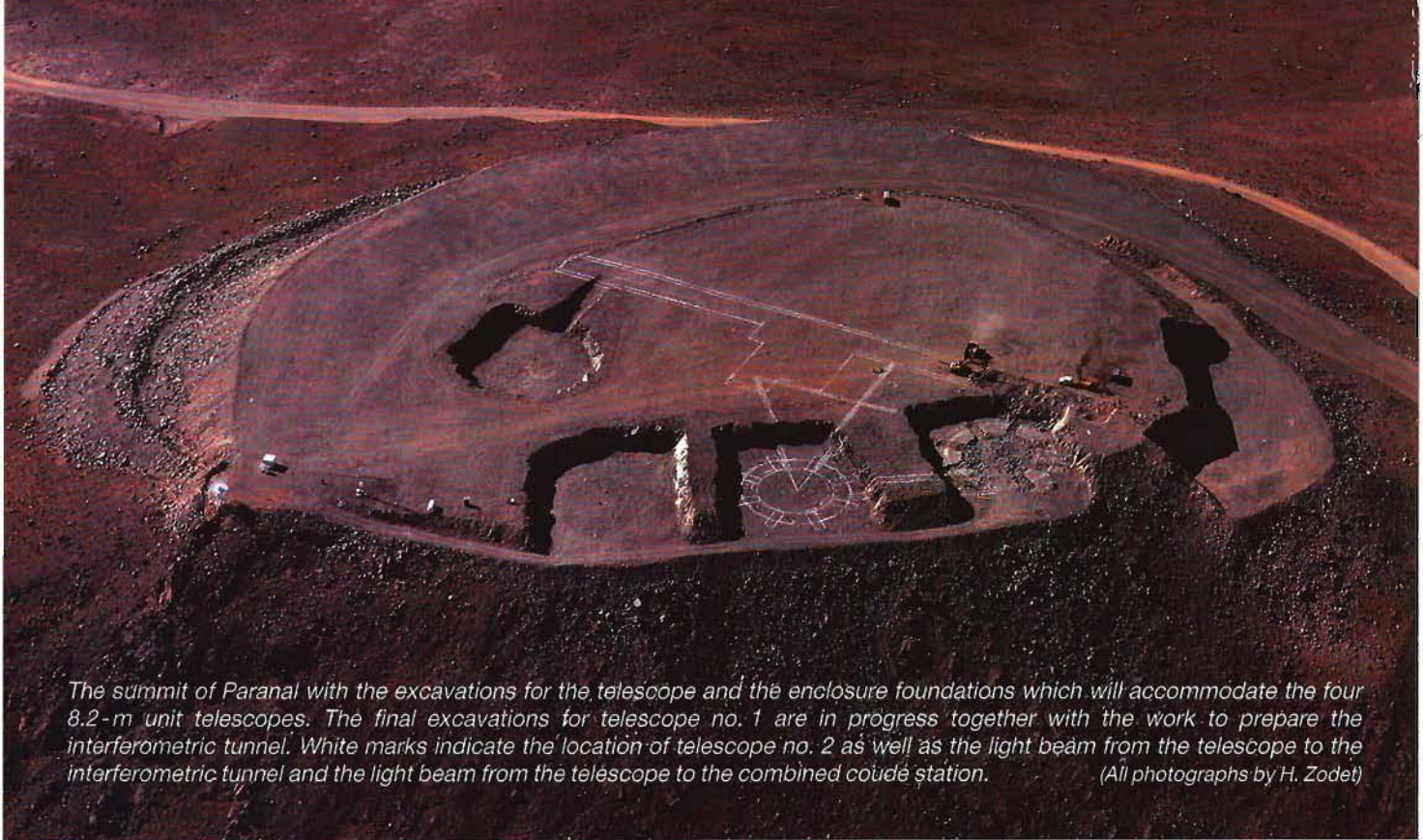
We have briefly described the activities undertaken by ESO to assess the effect of natural and man-made microseismic noise on the VLTI performance. First assessment of the ground vibration inside the VLTI facilities has been performed and is being updated as the detailed design of the VLT Observatory is progressing. The main conclusion is that the anticipated microseismic noise at the VLT site remains compatible with the error budgets derived from the required VLTI performance. A summary of the results obtained so far is given below.

- (i) The natural microseismic activity at Paranal is not insignificant when compared with the ultimate performance of the VLTI in the visible. It may mean that a fraction of the time, probably still very small, will be "polluted" by micro-earthquakes. Final results are still expected in this area.
- (ii) Vibration generating equipment inside the Control Building and inside the Telescope Building shall not transmit to the ground, at high frequency (> 10 Hz), a level of disturb-

ance force higher than 1000 N and 100 N respectively. This constraint is taken into account, for example, by selecting screw-type pumps for the oil bearing and liquid cooling systems as well as by a proper design of their isolating supports and foundations.

- (iii) People walking on the ground at 15 m distance, or less, start to contribute significantly to the level of microseismic noise. Control of the activity during interferometric observation as well as soft carpets in all service tunnels and in the VLTI Building are considered.
- (iv) The wind acting on the telescope enclosure, despite the high load induced, has negligible impact thanks to the low-frequency characteristic of the wind energy and thanks to the filtering effect provided by the soft earthquake safety device located below the metallic structure of the enclosure.
- (v) The enclosure bearing noise is not yet well known but does not appear very critical any more, thanks to the above-mentioned filtering effect.
- (vi) Vehicle traffic on the platform during interferometric observation shall be strictly prohibited and traffic to and from the Control Building shall be carefully controlled.

Recent Photographs of Paranal



The summit of Paranal with the excavations for the telescope and the enclosure foundations which will accommodate the four 8.2-m unit telescopes. The final excavations for telescope no. 1 are in progress together with the work to prepare the interferometric tunnel. White marks indicate the location of telescope no. 2 as well as the light beam from the telescope to the interferometric tunnel and the light beam from the telescope to the combined coude station. (All photographs by H. Zodet)



Aerial photograph of the Paranal region situated approximately 130 km south of the city of Antofagasta and about 12 km from the Pacific Ocean (clearly visible in the background). In the foreground on the right side of the main road one sees the Skanska Belfi camp and on the left side the ESO camp and the water tanks.



Close-up of the excavation for unit telescope no. 2.

The ESO base camp at the foot of the Paranal mountain. The base camp, which was installed two years ago, is becoming more and more the centre of activities of the VLT Division at the new ESO observatory. Particular attention has been given to the improvement of communications with the installations of antennas.



Site Surveys, from Pioneering Times to the VLT Era

M. SARAZIN, ESO

On December 4, 1990, ESO selected Cerro Paranal as the site for its future European Very Large Telescope, the VLT. The choice of this isolated summit in the Chilean Atacama desert, 700 km from the La Silla Observatory, followed one of the longest and most comprehensive site study campaigns ever undertaken in the history of astronomy.

The VLT concept was subjected to considerable modification from the moment the project received its funds in December 1987 and throughout the subsequent years. 1992 saw the finalized design, adapted to the orographic constraints of the site and aimed at preserving the intrinsic imaging quality. Albeit somewhat late in the day, it had become clear that the amplitude of the distortions of astronomical images introduced by the atmosphere was much smaller than those registered so far by classical telescopes. An innovative programme had been launched at the CFHT as early as 1981 involving the systematic monitoring of image quality at the telescope to understand better the reasons for local degradation of observing conditions. The enormous potential gain from such efforts was revealed at the La Silla Observatory on the night of 22/23 March 1989 when engineers began first tests on the newest ESO telescope, the NTT (New Technology Telescope). The images (*The Messenger* No. 56) surpassed all those ever obtained. So much so that the astronomical community had to admit that most existing large telescopes were simply not able to take advantage of the atmosphere during its best moments. Consequently, the operation of the NTT initiated vast improvement programmes for existing telescopes, both for the analysis of spherical aberrations of the primary/secondary mirrors and for the monitoring of thermal equilibrium and dome ventilation. The site study for the VLT also orientated itself towards research on the frequency and duration of prime conditions on the various listed sites.

The age of preconceived ideas attributing comparable image quality to all sites was past. Work by specialists in atmospheric optics was suddenly in great demand. For a decade they had been explaining how variable the atmosphere was and what the mechanisms were that made it so. With the help of these researchers who formed the first working group for the VLT site selection, special instruments were selected and installed on candidate sites. They also

helped to carry out an intensive measuring campaign on La Silla and later on at Paranal (*The Messenger* Nos. 44 and 68). The aim was not only to formulate the definitive characterization of an astronomical site but also to demonstrate the coherence of results from different measuring techniques using a single theory.

Over the centuries experimental astronomy has seen a gradual evolution both with regard to the observer's place in society and to scientific objectives. As far as the location of observatories was concerned, the majority were located, in the distant past, according to non-scientific criteria. The most important criterion was to be in the vicinity of religious, cultural or power centres. The Maya Observatory of Chichen Itza (Mexico) is one such example, as well as those found in most European capitals. It was only at the end of the last century when astronomers were encouraged by the improvements in photographic quality and the discovery of spectroscopy that they made resources available for site selection. The minimization of spectral absorption was one of the first priorities and this, of course, led to the selection of sites at a higher altitude. In France the Observatory of the Pic du Midi is a case in point; built in 1878 at an altitude of 2,877 m, it is still in use today. Then came the short-lived Janssen Observatory on the summit of Mont-Blanc (4,808 m) which was in operation from 1893 to 1909. 1926 saw the first attempt at characterizing the effects of atmospheric turbulence with the introduction by Danjon of a scale allowing the estimation of image quality from the visual observations of diffraction rings in small 25-cm diameter telescopes. Nevertheless, up until the middle of the century, sites which were economical and located near research centres were still preferable, regardless of the inevitable pollution induced by human activity. A prime example is the dramatic increase in sky luminosity above the 5-m Hale telescope on Mount Palomar (1,706 m) which was put into operation in 1948.

It was probably in the southern hemisphere that site studies were first carried out solely for science. In the 1960s several observatories were constructed there with the aim of receiving a new generation of telescopes 3 to 4 m diameter 10 years later. In 1962, the International Astronomical Union dedicated a symposium on the selection of observatory sites and assembled all experts (IAU Symp. No. 19). The study by

J. Stock which lasted from 1960 to 1963 in Chile resulted in the choice by AURA (Association of Universities for Research in Astronomy, USA) of Cerro Tololo (2,399 m), 600 km north of the capital Santiago, and Cerro La Silla (2,428 m), 100 km further north by ESO in May 1964, after an extensive search lasting seven years in South Africa (*The Messenger* No. 55). Then, some years later, the site Cerro Las Campanas (2,280 m) was chosen, 30 km north of La Silla, by CARSO (Carnegie Institution of Washington, USA). At about the same time Australia carried out its site selection for the Anglo-Australian Observatory which was built in May 1962 on Sidling Spring Mountain (1,164 m), 500 km from Sydney.

The main criteria during these campaigns were cloud coverage, air humidity and the image quality or "seeing". Instruments dedicated exclusively to the optical measurements of the effects of atmospheric turbulence were used in the 60s, proposed by J. Stock (1960), H.W. Babcock (1963), M.F. Walker (1965). The same instruments were used by the Max-Planck-Institut für Astronomie in the early 70s for a comparative study of the Gamsberg mountain in Namibia (then South-West Africa) and La Silla. However, while ESO's choice of La Silla in 1964 instead of South African sites was prompted mainly by scientific considerations, the 1982 decision of MPI to install the 2.2-m telescope at La Silla was taken more on political grounds (Namibia obtained independence in 1990). The two sites were found to be of quite comparable interest for astronomy.

From the attempts made in the 1960s up to the beginning of the VLT site study, considerable progress was made by theoreticians on the understanding of the influence of the atmosphere on astronomical image quality. What astronomers lacked in the past was a tool to relate quantitatively the physical laws of atmospheric turbulence to those of optical propagation. This gap was then filled by the unified theory of V.I. Tatarskii in the USSR in 1966. At the same time in the USA D.L. Fried was pursuing similar work. We have to thank Fried for the parameter named after him which is used internationally to characterize the perturbation of astronomical images by the atmosphere.

Work of that nature never went outside specialist circles due to its theoretical character and in fact reached the astronomical community with a few

years' delay. The latter, however, had already become aware of the increasing importance of spatiotemporals of the atmosphere by the discovery of interferometric speckle by A. Labeyrie in 1970 and by the limits imposed by the twinkling of stars in precision photometry. But engineers and instrument designers had to wait almost ten years to see work written in a more accessible style by e.g.: S.F. Clifford in 1978 or F. Roddier in 1981.

It was precisely during this period, the 1980's, that projects were introduced for the construction of large telescopes to become operational before the year 2000. They were to be equipped with sophisticated techniques to compensate, at least partially, for atmospheric effects on light waves. However, these techniques are only as effective and economical as the site quality is good. It was clear that the choice of a site was not just an unavoidable, rather administrative, formality but a decision with far-reaching consequences on the future performance of the observatory.

These were the favourable conditions in which a site study campaign for the VLT was launched. First there was a pre-selection of the candidate sites based on criteria such as logistics and large-scale meteorological analysis, followed in 1983 by inspection visits that led to the establishment of a team of observers on the summit of Cerro Paranal at the end of the same year (*The Messenger* Nr. 64). The chronology of a study of this kind was predetermined: first of all, the regions with the least

cloud cover, in other words offering the highest number of photometric and spectroscopic nights, had to be located before looking at atmospheric turbulence. The observers, who worked in fortnightly shifts, had the task of observing the quality of the sky both night and day. They also had conventional meteorological instruments and infrared radiometers that enabled them to measure the emissivity of the sky to deduce the precipitable water vapour content. Similar work was carried out simultaneously at the La Silla Observatory and after a few months the exceptional quality of the summits of the Atacama desert became evident, both for cloud cover and for water vapour content.

There are three mountain ranges at this latitude (23–25 degrees south): a coastal range of which Cerro Paranal is one of the highest summits, an intermediary or pre-Cordillera range 100 km more to the east and rising above 5,000 m, and then the Cordillera of the Andes with its volcanoes, some of which are higher than 6,000 m. Sporadic measurements taken on many of these summits confirmed the tendency to an increase in cloud cover near the Cordillera as well as a more marked seasonal influence. Worth mentioning is the infamous Bolivian winter that manifests itself in several weeks of wintry conditions in the middle of the southern summer.

The aridity of the Atacama desert is due to the low temperature of the Pacific Ocean, driven along the coastline by the cold Humboldt current that maintains

the inversion layer, and clouds, at an altitude of less than 1,000 m in the main. This phenomenon, in addition to the steep slope of the coastal range facing the ocean, guarantees Cerro Paranal's complete isolation which means no sea spray in the ambient air even though it is situated only 12 km from the sea. At the beginning of 1987 and in view of the first encouraging results, ESO decided, following agreement with the Chilean government, to make permanent changes to the landscape and constructed a rudimentary access road up to the summit. In April of the same year the first image quality measurements were available from a differential image motion monitor (DIMM). This instrument uses intensified CCD imaging. It was still being developed and became fully operational in October 1988. However, it was only one year later that the DIMM reached the required accuracy (better than 10 % down to 0.25 arcsec seeing). So it was on the basis of statistics on cloud cover and humidity collected over 7 years and 1 year of taking image quality measurements that ESO committed itself to the construction of a new observatory on Cerro Paranal. The same DIMMs are now in routine operation both at Paranal and La Silla and permit the estimation of the stability of ESO observatories with regard to the long-term climatic trends, as described in the next article.

(Part of this text was translated from the original French by S. Milligan.)

Seeing Update: La Silla Back on the Track

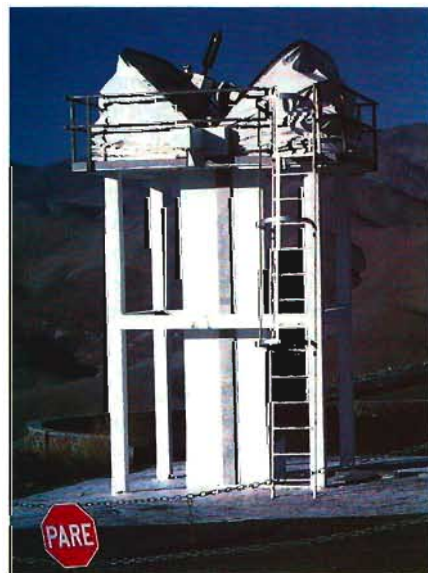
M. SARAZIN, ESO

The VLT at Paranal will be equipped with a new feature hitherto unknown at observatories: an Astronomical Site Monitor (ASM) whose function it is to deliver permanently and in real-time the status of the site parameters that affect astronomical observing and/or telescope performances. The ASM comprises several dedicated instruments locally controlled by a common unit and part of the observatory network. It will feed a database accessible by users, telescope subsystems and by the science archive management system.

Meteorological data and seeing have already been routinely monitored at Paranal, with one interruption period of

15 months during levelling work. A new 5-m-high tower based on a design for Galileo at La Palma by Capodimonte Astronomical Observatory (Italy) was erected last April for the differential image motion monitor (DIMM3). This tower has the advantage of being easily dis-

Figure 1: This fully retractable enclosure (here shown half open) was entirely designed and built solely for the La Silla DIMM by the Department of Maintenance and Construction. It was installed on the 5-m-high concrete tower in April 1993 and can be remotely controlled by the DIMM itself.



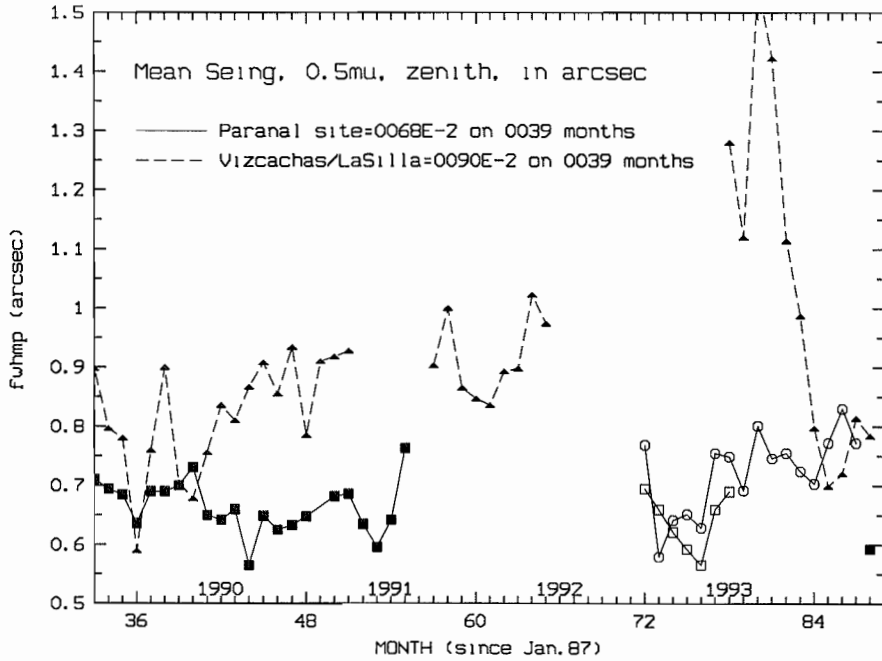


Figure 2: The statistics of monthly averages of seeing measured at ESO sites. The dotted line corresponds to measurements taken on 5-m-high towers (filled triangles) at Vizcachas (Sept. 1989 to March 1991) and La Silla afterwards. The full line corresponds to measurements made at Paranal on a 5-m-high tower (filled squares) before levelling (Sept. 1989 to Aug. 1991) and at the new VLT Telescope Area on a 1-m-high platform (Dec. 1992 to March 1994) where southern (open circles) and northern (open squares) edges have been monitored. Since April 1994 measurements resumed on a 5-m-high tower at the northern edge (filled square on the right end).

mantled if it disturbs VLT construction work during the years to come.

In the same way, although with less regularity, an identical monitor (DIMM2) was operated at La Silla after the Vizcachas candidate site was closed in March 1991. The instrument suffered serious damage from a thunderstorm in 1992 and was back in operation only in April 1993, with the addition of a remotely-controllable retractable enclosure (Fig. 1), and with an upgrade to the Unix operating system. In the meantime, the real-time dispatch of meteorological data to all La Silla telescopes was implemented (it is now also available with xmosaic). Since December 1993, DIMM2 has been fully automatized and the integration of seeing data in the starcat database has made it available to the community at large.

A comparative analysis of the trends in seeing quality at Paranal and La Silla was made regularly from September 1989 onwards on the basis of monthly averages (Fig. 2). It confirmed the steady degradation of observing conditions at La Silla in 1992 until the middle of 1993 which gave rise to increasing discontent on the part of users and was often misinterpreted as a general deterioration of telescope efficiency. But the most striking phenomenon has been the recent return of La Silla to the average level of 1989, in the three

months from August to November 1993. Several recent reports from astronomers visiting La Silla confirm that this positive trend is also noticeable in the final quality of astronomical work. As an illustration of this remarkable improve-

ment, Figure 3 shows the seeing record of the night before New Year's Eve where sub-half arcsec imaging was possible at La Silla for four consecutive hours.

Such a relatively rapid change teaches us something new about the dynamics of seeing and, although the climatic causes of low-frequency seeing variations are not yet understood, it should help us to improve our analysis of the results obtained during short-term surveys of potential observatory sites. A comparison with the evolution of Paranal, in spite of a slight increase of the average seeing at ground level in the past 8 months, also confirms the validity of the initial assumption that a site further north within the Atacama desert would be more stable than one located at its edge.

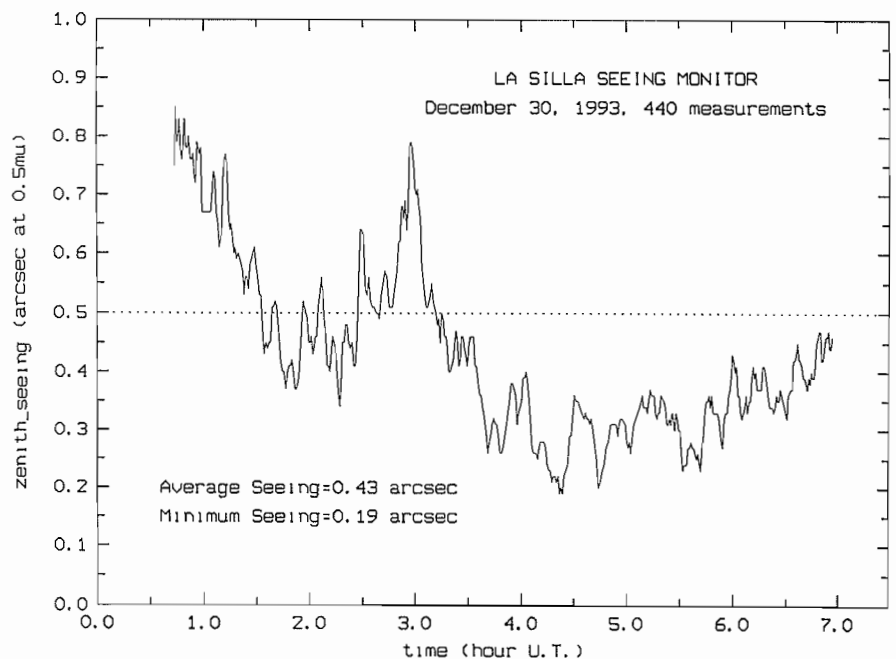


Figure 3: The DIMM2 seeing record at La Silla with a 120s temporal resolution during a particularly good night.

A F/5.2 Camera with a Thinned 2048² CCD at the EMMI Red Arm

S. D'ODORICO, ESO

Characteristics of the New Camera

The red arm of the EMMI spectrograph/imager at the Nasmyth focus of the NTT (D'Odorico, 1990, *The Messenger*, 61, 51) was designed and built to operate with a F/5.2 and a thinned 2048², 27- μm CCD. When the instrument was under construction, the development of large-size, thinned CCDs was delayed, forcing ESO to build a faster camera to feed a smaller-size CCD. The instrument started to operate in 1990 in this configuration. After the delivery of a thinned SiTe (former TEK) 2048², 24- μm CCD of relatively good quality, the F/5.2 camera was in February 1994 installed at EMMI. Figure 1 shows the camera and the CCD cryostat mounted on the side of the red arm of EMMI. In the imaging and spectroscopic mode, the new set-up provides a better sampling with a scale of 0.27 arcsec/pixel and an unvignetted field of view of 9.1 \times 8.6 arcminutes. The image quality is better than two pixels over the entire field, even with the current curved CCD (see below). Figure 2 shows the FWHMs for stellar images distributed over the CCDs from an image obtained during the test time.

The New CCD at the Red Arm of EMMI (ESO #36)

The new CCD with its dedicated ESO VME controller was fully characterized and optimized in its performance in the ESO Laboratory. The quantum efficiency curve is shown in Figure 3. With respect to the coated Loral chip which was installed until February 1994, the new CCD and the new camera bring an efficiency gain of 4.2 at 4500 \AA , 2.2 at 5500 \AA , 1.9 at 6500 \AA and 1.8 at 8000 \AA .

This gain has been confirmed by the determination of the efficiency curves of the instrument obtained from standard star observations. Other key parameters of the chip are summarized in Table 1. They have been confirmed by measurements at the telescope and will be regularly monitored.

It is important to notice two limitations of this CCD. The active surface is convex with a peak at its centre in the direction of the camera, an artifact of the manufacturing process which was not known in advance. The curvature can be well approximated by a paraboloid. The difference between the centre and the



Figure 1: The new camera and the CCD cryostat are shown on the red side of EMMI mounted on the Nasmyth adaptor of the NTT.

corners of the CCD is approximately 200 μm . If the instrument is focused on an intermediate plane, the image blur due to this effect will be one pixel or less, with the exception of the extreme corners of the image. A new field lens which matches this curvature has now

been ordered. The second limitation is the relatively long reading time of the large chip: a little less than six minutes are needed from the closure of the shutter to the display of a slow read-out frame. This is reduced to about 4 minutes for the fast readout mode.

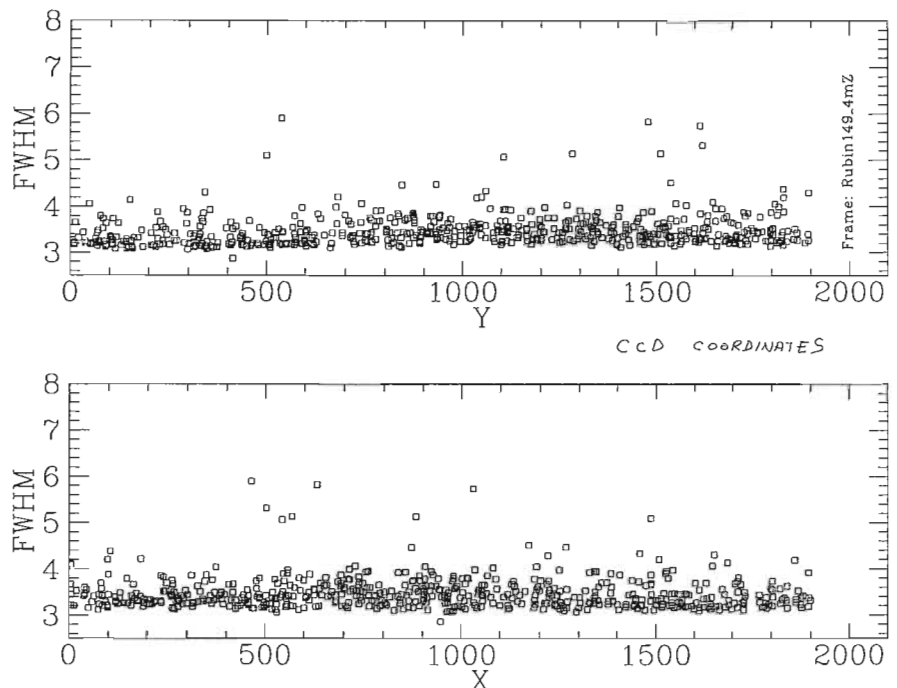


Figure 2: FWHMs in pixels of stellar images in the x and y directions measured by J. Storm at various positions of one 4-min CCD frame in the Z colour.

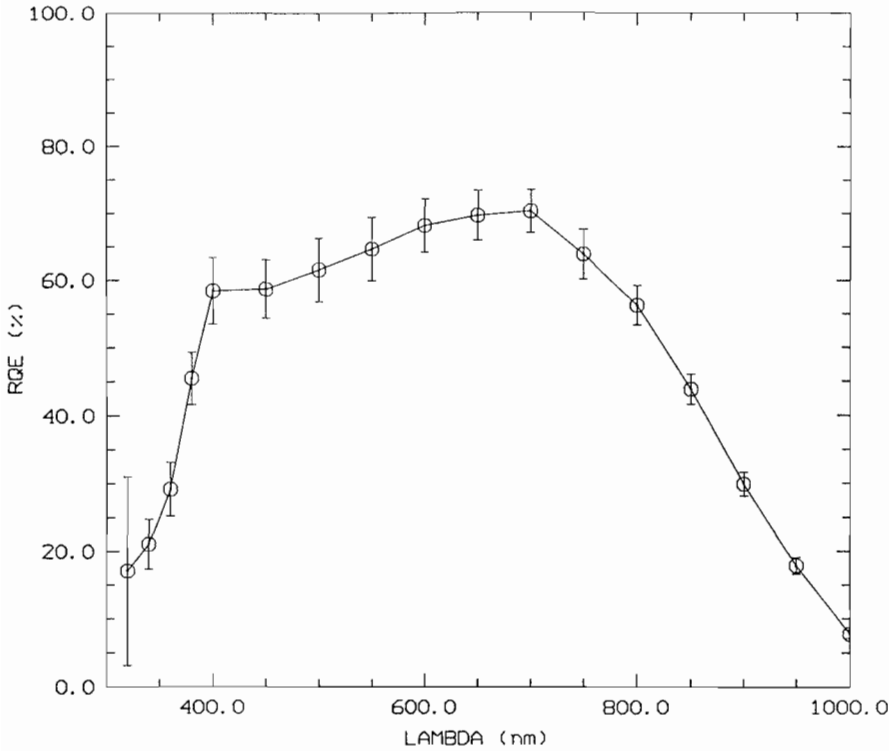


Figure 3: Quantum efficiency curve of the thinned 2048² CCD (ESO #36) as measured in the ESO detector laboratory.

This long reading time is due to the large number of pixels through a single output of the CCD but also to the limitation of the present ESO acquisition system based on the A900 computer. It is envisaged to replace it with a more efficient

system based on VLT standards at the end of 1995. At present an option available to the user is the read-out through two outputs of similar characteristics (but not identical, thus requiring separate calibrations). The gain in slow mode

Table 1: Main properties of the ESO CCD #36

Usable pixel number and size	2086×2046, 24 μm
QE	See Figure 3
Read-out noise (slow)	4.8 e/pixel
Read-out noise (fast)	8 e/pixel
Linearity	Better than 1% from 30 to 200,000 e/pixel
Cosmetics	~10 partially hot columns (Amplifier D)
Dark current	≤5 e/pixel/hr at 151 K
Cosmic ray event rate	4 events/min/cm ²

is then 80 seconds. A quick-look mode (2 outputs, fast read-out, binning 2×2) requires about 1 minute.

An Updated EMMI Operating Manual

As of April 1st, 1994, the NTT has entered a new operation scheme which also foresees a major upgrading of the control hardware and software with the goal to fully exploit the unique capabilities of this telescope (see Baade et al. in *The Messenger*, 75, 1). As part of this effort, version 2 of the EMMI and SUSI Operating Manual is being prepared by E. Giraud and it will be released in June 1994. More detailed information on performance and data format of the instrument with the new camera and CCD will be included there.

Acknowledgements

The successful installation of the new camera and CCD is the result of the effort of several persons. H. Dekker planned and coordinated the activities in Garching and La Silla. O. Iwert, S. Deiries and R. Reiss put into operation and tuned the CCD in the laboratory. Again O. Iwert, R. Reiss together with P. Moore and P. Sinclair installed the CCD and its controller at the telescope and optimized the performance there. T. Abbott has collected CCD test data at the telescope and verified the operating characteristics.

J.L. Lizon, H. Dekker and S. Moreau tested the optical camera in the laboratory. The first two later installed it at the telescope. They also conducted with Ph. Gitton a general check up of many EMMI functions. Astronomical test observations and/or their analysis were carried out by S. D'Odorico, J. Storm, and R. Mignani of the Dipartimento di Fisica of the University of Milano.

Test of an R4 Echelle Mosaic

H. DEKKER and S. D'ODORICO, ESO

A. FONTANA, Dipartimento di Fisica, II Università di Roma, Italy

Why an R4 Echelle Grating?

The term "R4" describes one of the most important characteristics of an echelle grating, namely the tangent of the blaze angle. An R4 grating has a nominal blaze of 76 degrees, whereas the classical R2 has 63.5 degrees. Multi-

plied by the beam diameter, the tangent of the blaze angle yields the optical depth of the grating which determines the resolution that can be attained. The R4 echelle mosaic described here has a size of 450×130 mm, it is a down-scaled prototype version of the UVES¹

echelle which will have a size of 840×214 mm. To manufacture it, a novel technique has been developed in

¹ UV-Visual Echelle Spectrograph. See *The Messenger* 70, p. 13 for a full description of this dual-beam, cross-dispersed VLT instrument.



Figure 1: Photograph of the R4 prototype. The dimensions are 450×130×70 mm; the dead space between the two segments is 14 mm wide.

which two copies of the same master ruling are replicated on a common substrate, with a 14-mm gap between the segments. With its length of 450 mm, it is presently one of the largest monolithic gratings world-wide (Fig. 1).

Use of a steep R4 echelle has important consequences for spectrograph design. For the same spectral resolution, the beam diameter, collimator focal length and camera dimensions are reduced by a factor of two compared to an R2, which leads to a less costly, more compact instrument that is less affected by gravitational or thermal effects. This is why an R4 echelle was selected for UVES. On the other hand, while R2's can be mounted with a fairly large angle between incident and diffracted beams to separate the beams, R4's are much less forgiving and effects like spectral line curvature, spectral line tilt, grating anamorphosis (beam widening and variation of the line spread function along the order) and efficiency loss due to groove shadowing become more important and require a special spectrograph layout with the smallest possible angle between incident and diffracted beams.

The main purpose of ordering the R4 mosaic prototype was to compare the optical properties with those of R2 gratings, to test the manufacturing process, to identify possible effects of the segmentation of the grating surface and to test its suitability for astronomy in actual observations and data reduction. Of the available ESO spectrographs on La Silla, only EMMI works with a fairly small angle between beams (5.5 degrees; UVES has 1.8 degrees) so the prototype dimensions were chosen in such a way that it would be possible to be mounted on the red arm of EMMI with the possibility to reach $R \approx 70,000$ in a cross-

dispersed format in the range 4100–7500 Å.

Design and Laboratory Characterization

There are several constraints for making large echelle gratings for astronomical instrumentation. According to information from grating manufacturers, present ruling engines cannot handle blanks larger than 300 mm×450 mm and still maintain the required groove positioning accuracy and surface flatness. Diamond wear limits the total length of the grooves that can be ruled. Funding the manufacture of a larger rul-

ing engine was anyway considered not feasible at ESO.

In order to overcome these problems, one basically has the options (i) to build a mosaic from smaller identical gratings, all individually mounted and separately aligned (Keck HIRES spectrograph), (ii) to introduce active control by sensors, actuators and computers of individual gratings in such a mosaic (studied for the high-resolution spectrograph for the JNLT) or (iii) to build a mosaic out of smaller gratings replicated onto a single, larger piece of glass.

The technique used here is to assemble and precisely align a mosaic of sub-master gratings and to replicate this mosaic in one single step onto a larger, single piece of glass. Main advantages of this approach are that it results in a maintenance-free, simple, robust and compact grating with constant performance. A first description of the concept was presented two years ago². The R4 prototype realized according to this technique was delivered to ESO in November 1992 and was tested in the ESO optical laboratory in the course of 1993.

Blaze angle, efficiency, diamond wear and ghosts were tested on the smaller replica of MR 103-3 which for these aspects is considered representative. The absolute efficiency was measured at the blaze centre with ESO's TNO universal spectrophotometer in off-plane mounting with 5 degrees between inci-

² H. Dekker and J. Hoose, 1992, ESO Workshop on High Resolution Spectroscopy, ed. M.-H. Ulrich.

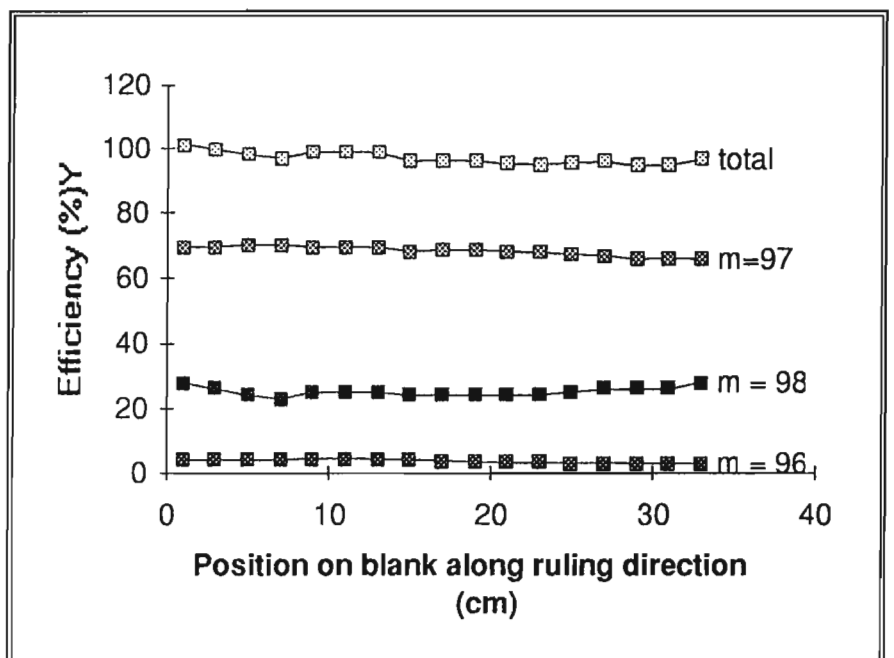


Figure 2: Diffraction efficiency as a function of laser beam position on the test grating in the main and neighbouring orders at the He-Ne wavelength 6328 Å.

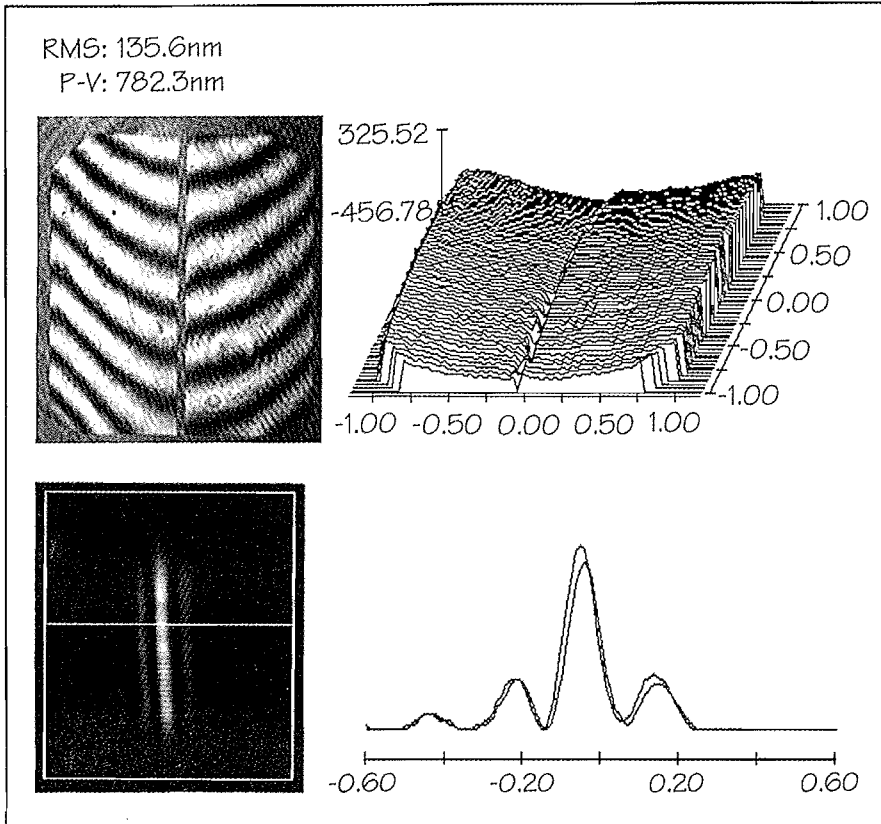


Figure 3: Top left: interferogram of the mosaic in order 97. – Top right: computer representation of the wavefront with tilt and focus removed. – Bottom left: spectrum of He-Ne laser taken with a 1.3-m laboratory collimator/camera. The astigmatism is evident. – Bottom right: horizontal trace through the spectrum. The mode spacing of the laser is 640 MHz or 8.5 mÅ.

dent and diffracted beams. The results and previous ESO measurements of R2 gratings are compared in Table 1 which shows that the efficiency of this R4 is almost as good as the 79 g/mm R2, which is one of the most efficient echelles.

The variation of diffraction efficiency at 632.8 nm in the main order ($m=97$) and in adjacent orders was measured as a function of beam position on the surface; see Figure 2. This type of measurement is sensitive to variations in the groove shape and groove angle along the ruled area as might be caused by diamond wear, but there is very little sign of this. The diffraction efficiency in order 97 varies only slightly from 69 % at the start of the ruling to 68 % and 66 % in the centre and at the end, respectively while comparison of the curves for orders 96 and 98 shows no sign of changing groove angle.

Tests of stray light and ghosts on a smaller replica of MR 103-3 with size 165 × 320 mm were carried out in the DAEC department of the Observatory of Meudon by J. Baudrand and P. Czarny using the Musicos fiber spectrograph³ which was at that time undergoing

laboratory tests. Since stray light is difficult to measure quantitatively as the level depends as much on the spectrograph as on the grating itself, the R4 grating was compared with its "sister" R2 grating MR 35-13*-411 (see

Table 1), the standard grating for this spectrograph. The fiber was illuminated with a red HeNe laser and the resulting spectrum recorded using a Thomson CCD cooled to -30°C and digitized to 12 bits. The R4 exhibits 4 ruling ghosts with a maximum intensity of 0.029 % (normalized to the intensity of the parent line) while for the R2 7 ghosts were detected in the CCD field of view; the brightest one was 0.037 %. Interorder stray light in this prism-cross dispersed spectrograph, measured with a flatfield lamp, was 10 % of the neighbouring continuum for the R2, 3 % on the R4.

Spectral and spatial resolution were measured on the R4 mosaic prototype itself in the ESO optical laboratory with a diffraction-limited interferometric optical set-up and a red He-Ne laser. Figure 3 illustrates the resolution performance. The main defect is the astigmatism which is already present in the master. In the mosaicking process, the local surface slope of the submasters at the intersection was aligned in order to generate a more or less contiguous wavefront, save for a phase jump, with a P-V astigmatic deformation of 1.3 waves.

The mode structure of the HeNe laser is easily resolved, indicating a spectral resolution that is well in excess of 760,000. Due to the astigmatism, the spatial resolution is not as good as could be desired; the height of the PSF in the slit direction is $\sim 100\ \mu\text{m}$, which corresponds to 0.55 arcsec (2 pixels with TEK CCD and F/5.3 camera) on the sky with EMMI.

The optical characteristics of the R4 mosaic prototype are summarized in Table 2 where its performance can be

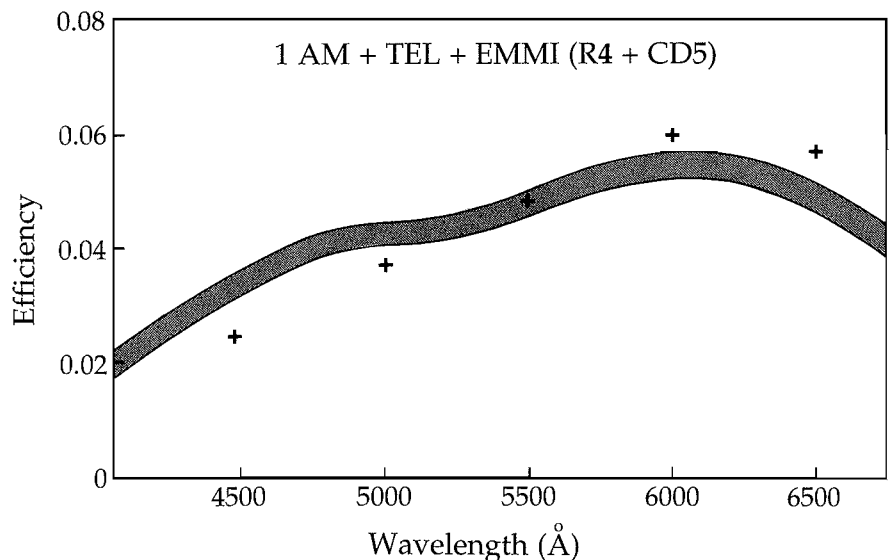


Figure 4: Global efficiency curve for atmosphere+telescope+EMMI with the R4 echelle grating and CD5. A thinned 2048² CCD from SITe was mounted as a detector. The width of the curve represents the difference between the observations of two different stars on two different nights. Crosses are average values for the same combination with the standard R2 grating (ESO #10 in the EMMI grating list).

³ J. Baudrand and T. Böhm, 1992, A&A 259, 711.

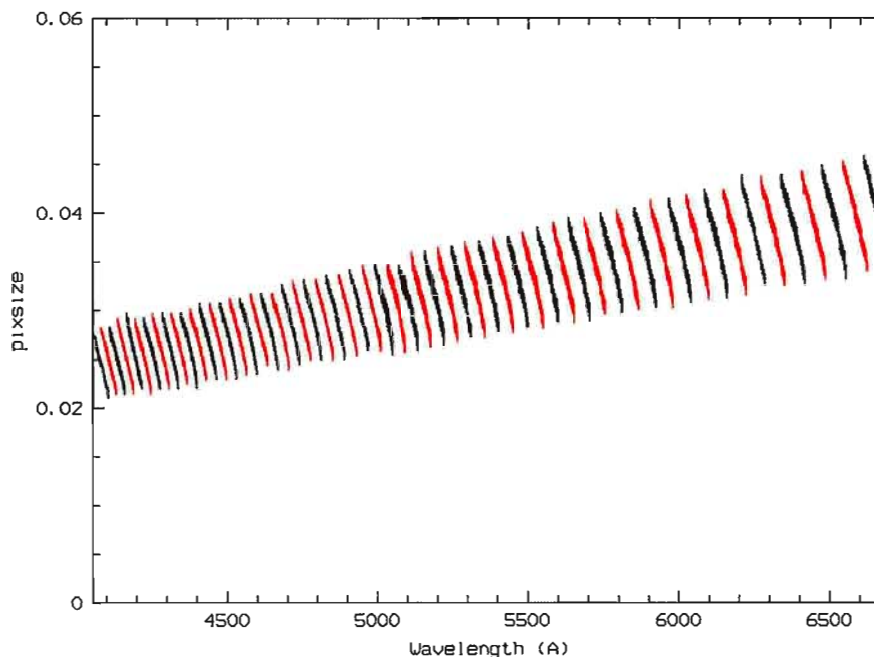


Figure 5: Variation of the pixel size in Å along the orders of an echelle spectrum with the R4 grating and CD5.

directly compared with the specifications of the UVES echelles that were agreed with Milton Roy and are now on order. The first delivery is expected by mid-1995.

Astronomical Tests on the EMMI Spectrograph

The EMMI spectrograph/imager at the NTT includes in its red arm an echelle mode which uses an R2 echelle grating and has a choice of four gratings as cross disperser⁴. For echelle observations, the

⁴ D'Odorico, 1990, *The Messenger* 61, 51.

standard grating unit is replaced by the unit which mounts the R2. A new mechanical housing was designed and built for the R4 prototype and installed on the spectrograph for two nights in February 1994. Table 3 summarizes the

main characteristics of this grating on EMMI. The configuration which was mostly used during the test was based on the use of grism #5 as CD.

The two nights of observations were mainly dedicated to operational tests. Due to a problem with the slit width calibration of the EMMI slit unit that was discovered following the analysis of the data after the observations, the spectra were obtained with a minimum slit width of 1.4 arcsec which resulted in a resolution of 45,000. The maximum resolving power which would correspond to a 2-pixel sampling of the slit on the detector, that is $\approx 70,000$, has to be confirmed by new observations.

Figure 4 shows the global efficiency of the atmosphere (at air mass=1) + telescope + instrument with the R4 grating and compares it with the values determined during the same run for the R2 grating (EMMI #10). The data are based on observations of two standard stars on two different nights. They show that R4 is generally as efficient as the R2 grating at most wavelengths and it surpasses it in the blue where the silver-coated R2 has lost some efficiency after 5 years.

The intensity of the interorder scattered light has also been measured from the standard star spectra. With or-

TABLE 1. Absolute efficiency in % at blaze as a function of wavelength of some echelles

	400nm	500nm	600nm	700nm
MR 103-3 (R4, 31.6 g/mm)	63	67	69	68
MR 35-13-*411 (R2, 31.6 g/mm)	57	60	61	61
MR 35-13-*401 (R2, 79 g/mm)	–	72	71	71

TABLE 2. Main parameters of the prototype mosaic and of the UVES echelles

	R4 mosaic prototype (results)	UVES echelles (specifications)
Dimensions	450×130×70 mm	840×214×125 mm
Number of segments	2	2
Ruling	existing ruling (Milton Roy 103-3) area: 165×320 mm blaze angle: ~75.5 degrees groove density: 31.6 g/mm	new rulings, nominal, nominal data: area: 214×420 mm blaze angle: 76 degrees groove density: 31.6 g/mm (red) 41.6 g/mm (blue)
Efficiency (surface average, including dead space between segments)	66 % at 550 nm	64 % at 550 nm
Spectral resolution	> 760,000	> 500,000
Spatial resolution	16 arcsec (0.55 arcsec on the sky with EMMI)	< 8 arcsec (0.2 arcsec on the sky with UVES)
Interorder stray light	<3 % of continuum (in Musicos spectrograph)	
Grating ghosts	<0.029 %	<0.015 %

der separations from 6.5 to 13.5 arcsec, the interorder intensity is below 3 % of the continuum intensity. No grating or optical ghosts were detected above the 1 % level. A systematic search at fainter levels has not been made yet.

Figure 5 shows the variation of wavelength bin size in Å as a function of order and within a single order. The strong variation of the wavelength bin within the order is an effect of the steep blaze angle of the echelle and has to be taken into consideration in the data reduction.

Finally, Figure 6 shows as an example of astronomical observations an untreated 1-hour spectrum of the nucleus of the Seyfert galaxy NGC 3783 ($m(v) \approx 14$).

In conclusion, the test of the R4 mosaic grating prototype on EMMI has confirmed the good performance which was indicated by the laboratory results and provides support to the choice of this type of solution for the VLT UVES spectrograph. Concerning a possible regular use of this grating in EMMI for scientific programmes, additional measurements will be needed to confirm the predicted limiting resolution and to test any flexure of the grating unit as the instrument rotates at the Nasmyth adapter. If these are successful, the R4 on EMMI would provide a unique possibility for obtaining spectra over a wide wavelength range at a resolution up to 70,000 for objects as faint as 16.5. If the users will express a strong scientific interest in such a facility, ESO will consider offering it as a standard option of EMMI as of 1995.

Acknowledgements

The R4 echelle was produced by Milton Roy (Rochester, USA) by the team led by John Hoose. The housing for mounting it on EMMI was designed at ESO by G. Hess. Thanks for the successful run at the telescope are due to the technical team which carried out the upgrading of the red arm of EMMI (see the report in this issue of the *Messenger*) and to P. Molaro (Trieste Observatory) for assistance during the astronomical observations.

TABLE 3. Performance data of the R4 echelle on EMMI

Resolution	45,000 with a 1.4 arcsec slit (measured) =70,000 with a 0.7 arcsec slit (to be verified, see text)	
Wavelength bin	30 mÅ at 5000 Å	
Spectral formats	Wavelength range	Order separation
Recommended grisms 3	4070–8370 Å	>3.7 arcsec
5	4070–6640 Å (gaps beyond 7450 Å)	>6.3 arcsec
Global efficiency (at air mass=1)	1 photon/Å/sec at 5500 Å for a star of $m(v)=16.6$	

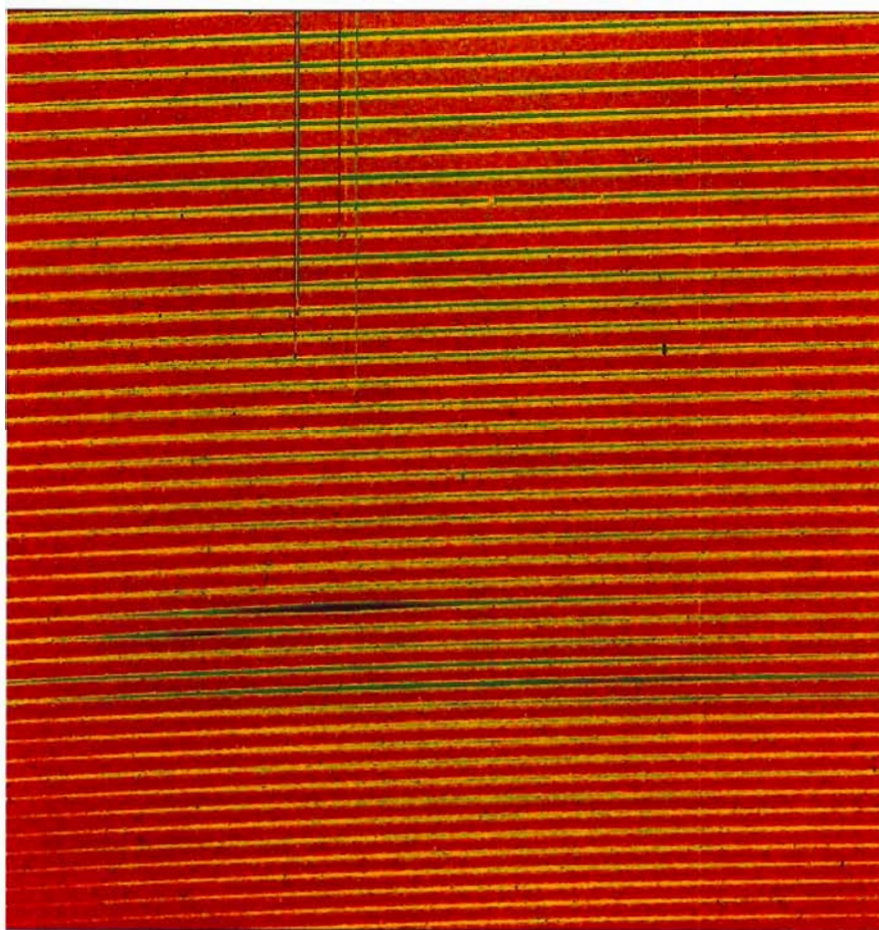


Figure 6: Central 1400×1400 pixels of an untreated 1-hour exposure of the nucleus of the Seyfert galaxy NGC 3783 with EMMI and the R4 grating prototype. The broad H β and the two [O III] emission lines are visible in the lower half and interstellar Na I absorption lines in the upper part of the frame. At a potential resolution up to 70,000, this spectrum of a $m(v) \approx 14$ object has a S/N ratio ≈ 40 in the continuum.

News from La Silla

J. MELNICK, ESO-La Silla

3.6-m Pointing

An effort has been done to understand the behaviour of the pointing model of the 3.6-m telescope for differ-

ent instruments. As a result, the methods for top-ring and top-end exchanges have been refined in order to avoid movement of the secondary mirror. Pointing is now stable. The software has been modified to permit fast models by adjusting only 8 parameters.

3.6-m Seeing

Progress has been achieved in understanding the bad seeing experienced at the telescope after the installation of the AIRCO cooling system. Measurements made by installing DIMM1 inside the

dome and comparing the seeing measurements with those of DIMM2 (permanently installed near the Schmidt telescope) indicate that, when operated correctly, the AIRCO system effectively eliminates dome seeing, at least for the conditions prevailing during the tests. This indicates that the seeing degradation experienced with most instruments, notably EFOSC, is due to heat sources at the telescope itself. A plan for monitoring and eliminating these heat sources is in preparation. In the mean time, the AIRCO system will not be used except in cases where considerable seeing improvement has been reported (i.e. Come-On+), since the tests clearly show that the cooling aggravates the effect of any uncontrolled heat sources in the dome like for example an outside door accidentally left open.

Manuals

New manuals are available for EFOSC2 and IRAC2. Also, updates for the EFOSC1, CES, and CASPEC manuals have been written. All are avail-

able from the Visiting Astronomers Section.

On-Line MIDAS

Workstations for on-line data reductions with MIDAS are now available at the 0.9-m, both 1.5-m telescopes, the 2.2-m telescope, the NTT, and at the 3.6-m telescope for TIMMI and Come-On+. It is expected that the CES and the 3.6-m EFOSC, MEFOS, and CASPEC will be connected to workstations very soon. Work is in progress to replace the old IHAP-based HP acquisition programmes by workstation-based systems.

B & C Gratings

A 2,400 gr/mm holographic grating was successfully tested at the ESO 1.5-m telescope. With a blaze at 400 nm this grating is more efficient and spectrally cleaner than the equivalent conventional unit (Grating #20 in second order; 2.9 nm/mm). The tests were done using a temporary support that introduces some astigmatism. The grating will be

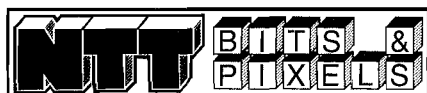
offered to visitors as soon as a permanent support has been manufactured.

Dutch Telescope Focus

The focus stability of the Dutch telescope has been substantially improved by the installation of a new secondary mirror support unit. The slow focus drift during the night which remained after the installation of the new unit, seems almost certainly related to overcooling of the unit by radiation during the night. Work is in progress to eliminate this effect.

ESO 50-cm Telescope

The automatization of the ESO 50-cm telescope, following a scheme similar to the one used at the Danish 50-cm, has been completed, although the debugging of the new system is still not complete. The pointing of the telescope is now excellent (typically 10" rms), and the autocentering device allows the telescope to be used fully automatically. Tests for remote operation will be conducted soon.



With this periodically compiled collection of short notes, the NTT Team intends to keep the community informed about changes in performances, configuration, and operation of the NTT and its subsystems.

NTT Coordinator

On a rotating basis, this new function is shared between the 4 NTT astronomers on La Silla (presently E. Giraud, R. Gredel, G. Mathys, and J. Storm). From early in the morning into the first hours of the night, the NTT Coordinator is supervising all activities at the NTT. He has full responsibility and authority for any decision which has to be taken on a short notice in response to the daily requirements. He can be reached via paging code No. 50 and in most cases is the primary on-site contact person for NTT observers.

Day Time Interventions

Any day-time work at the NTT requires prior approval by the NTT Coordinator. Every day, the period between 9 a.m. and 2 p.m. (may be extended by the NTT Coordinator) is reserved for maintenance, instrument setups, and repairs. Upon termination of the work (not only completion), the NTT Coor-

dinator has to be informed about the progress made and the effects on performance expected for the night so that night assistants and observers can prepare themselves accordingly.

NTT Calendar

The NTT Coordinator enters all maintenance and other work into a computer-based calendar. From any X-terminal connected to the workstations of the Astronomy Support Department and the NTT, this calendar can be viewed by typing `nttcal`. This simple but very useful tool has kindly been created by C. Levin.

Electronics Support Strengthened

The NTT Upgrade Plan (now available via anonymous ftp, cf. below) foresaw that initially only one electronician (D. Gojak) would work for the NTT but that the adequacy of this approach would be

carefully monitored. It has become evident that also in the respective other weekly shift electronics support is constantly required. We are, therefore, happy to announce that R. Parra has for a significant part of his time been assigned to the NTT. In fact, he is not at all new at the NTT, and many NTT (and other) observers will know him already.

Image Quality

Elongated images have been reported by many observers. It now seems probable that the main contributing factor is astigmatism. Its nature will be studied in more detail during the forthcoming test nights in May and June. Nevertheless, in one night in May images as good as 0.35 arcsec FWHM were obtained which is virtually identical to the results achieved at first light (cf. *The Messenger* No. 56, 1). A decisive factor contributing to this recovery has, of course, been the dramatic improvement in the average seeing on La Silla which has taken place since the middle of 1993 (see the article

by M. Sarazin on page 13 of this issue of the *Messenger*).

MIDAS Data Organizer

A customized version of the Data Organizer is now installed on-line at the NTT (cf. MIDAS Manual, Vol. B, Chapter 15). Each time an EMMI/SUSI FITS file arrives at the workstation, its header is appended to the so-called Observation Summary Table and selected keywords may be displayed in a scrolled window in an easily legible format. Each exposure is classified automatically according to its exposure type and the optical path used. This classification eases the monitoring of the on-going observing run and will in future be used also for on-line calibration and data reduction.

(M. PÉRON, Observation Support and Data Handling Group.)

Improved Pointing Expected

A bug has been found in the refraction correcting part of the telescope control software (we thank K. Wirenstrand for his help with the analysis). A quick analysis of pointing measurements obtained on side B (EMMI) in the night before this article was written suggests that a pointing accuracy of as good as 0.9 arcsec (rms) over the sky may be achievable. A new check of the tracking performance figures on the May test plan.

Early MOS Images in Service Mode

Effective July 1st, the NTT Team will on an experimental and best-effort basis

try to supply multi-object spectroscopists in advance with direct images of a few of their fields so that the operational efficiency of the MOS mode of EMMI is satisfactory from the first night. All observers who might take advantage of this new service during Period 53 have been informed by letter.

Furthermore, the Data Management Division has kindly offered support for the analysis of options for the export of the EMOS software package used at La Silla for the preparation of data files for the EMMI punching machine.

Rotator Tests

During the months of March and April, a large number of test data have been accumulated to identify the reason for occasional excessive friction which on both sides completely blocked the bearing of the rotator/adapters. A software modification has been introduced by B. Gustafsson to suppress the worst symptoms. A first model has been developed by F. Franza which will be scrutinized in the coming months. We thank all observers concerned by our extensive day time tests for their patience and cooperation.

Another problem associated with the rotators, namely the power amplifiers being suddenly switched off, has not yet been eradicated. But the frequency of occurrence could be reduced. Analysis continues.

Electronic Bulletin Board

A separate newsgroup `ntt` has been created on ESO's electronic bulletin board. It can be reached by telnetting to `mc3.eso.hq.org`, account `esobb` (no

password needed). It carries news which are too recent or too ephemeral for inclusion in the manuals.

Anonymous ftp Account

We aim at making PostScript versions of manuals, major test reports, etc. available via anonymous ftp. The node name is `ftp.hq.eso.org`. Select subdirectory `pub/NTT`. Announcements of the available documents are posted on the electronic bulletin board (cf. above). An updated version of the IRSPEC manual is being offered via anonymous ftp only (it will not be printed).

E-mail Info Service

Astronomers who find that the available manuals (a substantially revised EMMI/SUSI manual is in preparation) and the information channels mentioned above still do not answer all their questions about the NTT and its instruments are encouraged to send e-mail to `ntt@eso.org`.

Preview

In the next issue of the *Messenger* we hope to inform you about the results of field tests of the first components of the new, "VLT-like" control system, improvements of the current control software, results of extensive opto-mechanical tests planned for May and June (including the tracking of moving targets), experiences with the new computerized problem reporting and tracking system, the status of the parallel mode of the active optics system, and others.

Studies of Disks Around Main-Sequence Stars with the VLT

A.-M. LAGRANGE, *Laboratoire d'Astrophysique de Grenoble, France*

Since the IRAS mission in 1983 it is thinkable to observationally study outer Solar Systems in various stages of evolution, so as to give clues to the scenarios of formation and evolution of planetary systems. This paper reviews the observational work that has been done so far. It will also show how the forthcoming VLT is expected to contribute to a better understanding of these systems, especially thanks to its high angular resolution capabilities and performing IR instruments.

1. Introduction

The IRAS satellite measured unexpected infrared excesses at 25, 60 and 100 μm around some nearby ($d \leq 25$ pcs), Main-Sequence (MS) stars. The first such objects known were α Lyr (A0V), α PsA (A2V), β Pic (A5V), and ϵ Eri (K2V). In some cases the excesses are due to thermal emission from cold (≈ 100 K) dust orbiting the stars (Aumann et al., 1984). Typical sizes of these IR sources range between 10 and 400 AU. These systems might be planetary systems in various stages of evolution. As the central stars are on the Main Sequence, they may even have got time to form planets. Their proximity allows detailed studies: high-resolution imaging of the dust, high-resolution spectroscopy of the gas, if present. As they are numerous – more than 100 such objects are reported and there is evidence that indeed the occurrence of such properties for MS stars is common – statistical studies can also be done.

To better understand these systems, one has to determine their structure (disk?, spatial extension), the sizes (large bodies?), distributions, temperatures of the orbiting material, their chemical composition, and their origin: is the dust the remnant of the protoplanetary disk, or was it produced more recently through collisions of larger bodies? IRAS measurements already brought a wealth of information: the signature of circumstellar (CS) material, the evidence of extended 60- μm emission regions in the four cases mentioned above, the evidence of a relative lack of hot and then close dust, tentatively attri-

buted to former planetary accretion. Nevertheless, these IRAS data are not sufficient to constrain as tightly as possible all the unknown parameters. One in fact needs a large variety of observations: whenever possible, multicolour resolved images of the CS dust, and if not possible, multiwavelength aperture photometry or photometry. The spectral range from UV to radio is important, as cold and hot dust, large or small grains, with different optical properties may be *a priori* present around the candidate stars. The next section shows how a multiwavelength approach has allowed us to describe the CS dust around β Pictoris in detail, and how our knowledge on this disk can still be improved thanks to the forthcoming generation of telescopes. Section 3 will then give the status of knowledge on the other candidates, as well as the results of search for other disks and will give details on the progress expected with the VLT.

2. The Disk Around β Pictoris

2.1 Observations of the dust

2.1.1 Optical images

Shortly after the IRAS results, Smith and Terrile (1984) imaged at 0.89 μm the scattered light from the dust around β Pictoris, with a 2.2-m telescope at Las Campanas (Fig. 1a). The image revealed the dust concentrated in a thin disk, viewed nearly edge-on, from 100 to 400 AU. This was the first image of a disk around an extra-solar Main-Sequence star. To detect it, they had to use a coronagraph including a 7" (diameter) mask to remove most of the stellar light. Even with the coronagraph, the scattered light from the star is larger than the disk light. At 100 UA ($\approx 7''$), the disk magnitude per arcsec² is 16, to be compared to β Pictoris magnitude 3.8. Multiband images, from B to I, of the same region of the disk taken at ESO with the 2.2-m telescope led Paresce and Burrows (1987) to conclude that the typical size of the grains responsible for the observed scattered light is larger than 1 μm .

Gledhill et al. (1988) polarization maps

of the ≥ 80 AU region of the disk indicated a level of polarization of about 17 %; this, together with the other images, seems to favour the hypothesis that the properties of the grains are close to the ones of zodiacal dust for this region. Optical images of the inner part of the disk have recently been performed with two different techniques: one with antiblooming CCDs (Lecavelier et al., 1992; Fig. 1b), and the other one with tip-tilt correction (i.e. first-order adaptive optics correction) and a coronagraph (Golimowsky et al., 1992). In both sets of data, the disk is shown to be present down to 30 AU from the star, but a change in the slope of the surface brightness occurs at typical distances of 80 AU. The antiblooming images, made in various bands, B, V, R and I, moreover show a colour effect close to the star. At 3 arcsec (about 60 AU), a drop in the B band is observed, possibly due to changes in the chemical composition of the grains: grains with lower albedo such as silicates could produce such an effect.

2.1.2 IR and radio observations

IR aperture photometry on β Pictoris has been successfully performed to further constrain the SED and the models (Telesco and Knacke [1991], Knacke et al. [1993] and Aitken et al. [1993]). The observations showed that most of the 10 μm emitting region was closer to the star than 5" (90 AU). This was directly confirmed by resolved 10- μm images of the thermal emission of the β Pictoris disk with TIMMI at the ESO 3.6-m; this gave for the first time the disk brightness distribution in the thermal IR (see Lagage et al., *The Messenger* No. 75, p. 25, Fig. 1). Spectrophotometry revealed silicate emission at 10.8 μm , suggesting that small grains (≤ 1 μm) should be present close to the star. The silicate spectrum moreover appears to be similar in shape to the one of interplanetary dust which contains crystalline silicates, or to the one of comets. If so, comet-like bodies could then be at the origin of the inner part of the β Pictoris disk. This would also explain the presence in the disk of submicronic particles, which

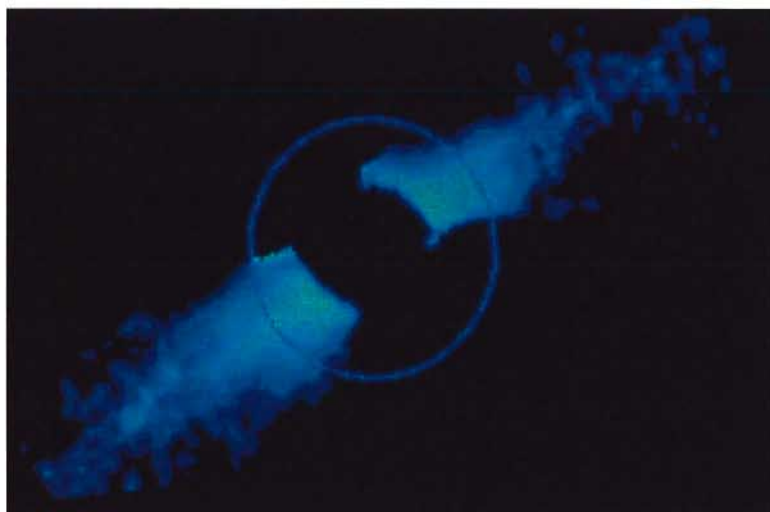
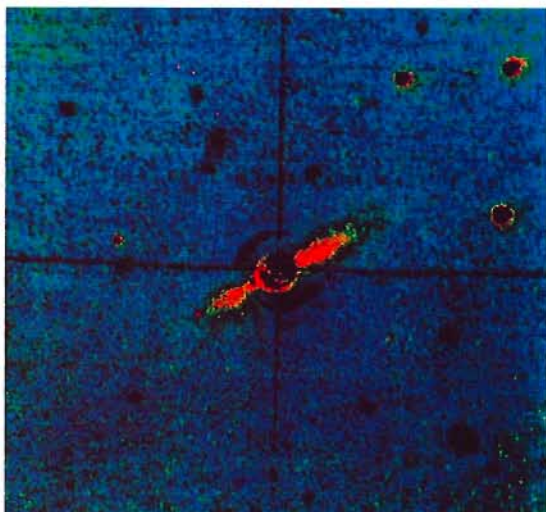


Figure 1: Optical images of the disk around β Pictoris: (a) the outer part from 7'' (100 AU) to about 25'' (400 AU) from the central star; (b) the inner part with the disk down to 30 AU; the circle corresponds to about 100 AU in radius.

cannot be primordial either, as they would have been removed on time-scales much smaller than the estimated age of the star under Poynting Robertson effect or radiation pressure effects.

Chini et al. (1991), with 1.3-mm observations showed that nevertheless larger grains (may be up to mm size) had also to be present around the star. From 800- μ m observations, Zuckerman and Becklin (1993) concluded that there are no large amounts of CS cold dust that could have escaped detection by IRAS.

2.2 A model for the dust

Several models have been proposed to explain the available data since 1985 (Diner and Appleby, 1986; Artymowicz, Paresce and Burrows, 1989...). A simple one has recently emerged to explain almost all available observational features. In this model (Backman, Gillet and Whitteborn, 1992) the disk is made of two regions: an outer one containing large ($\geq 1\mu$ m) grains, and with a distribution given by the classical images, and an inner part, in which the density distribution follows a less steep law and the size of the grains is small (down to submicronic size). The outer region extends at least to 1000 AU (optical data). The inward extension of the inner region is very model dependent, from 5 to 50 AU. The inner void thus evidenced could be the result of planet accretion. The boundary between both regions has to be between 60 and 100 AU, and could represent the limit of ice sublimation. Then the outer zone might be mostly made of icy material whereas the inner zone might contain more refractory material. Figure 2 summarizes the model.

2.3 Remaining questions

The use of several different and complementary data has obviously permitted to make remarkable insights in the knowledge of the disk since the IRAS discovery. Nevertheless, some important questions are still unanswered:

(1) are there planets already formed? where is the inner void of material pre-

dicted by most models located? (2) what is the chemical composition of the dust?

2.4 Future observations of the dust

2.4.1 Detection of planets

Direct detection of planets in the next decades is thinkable but needs dedi-

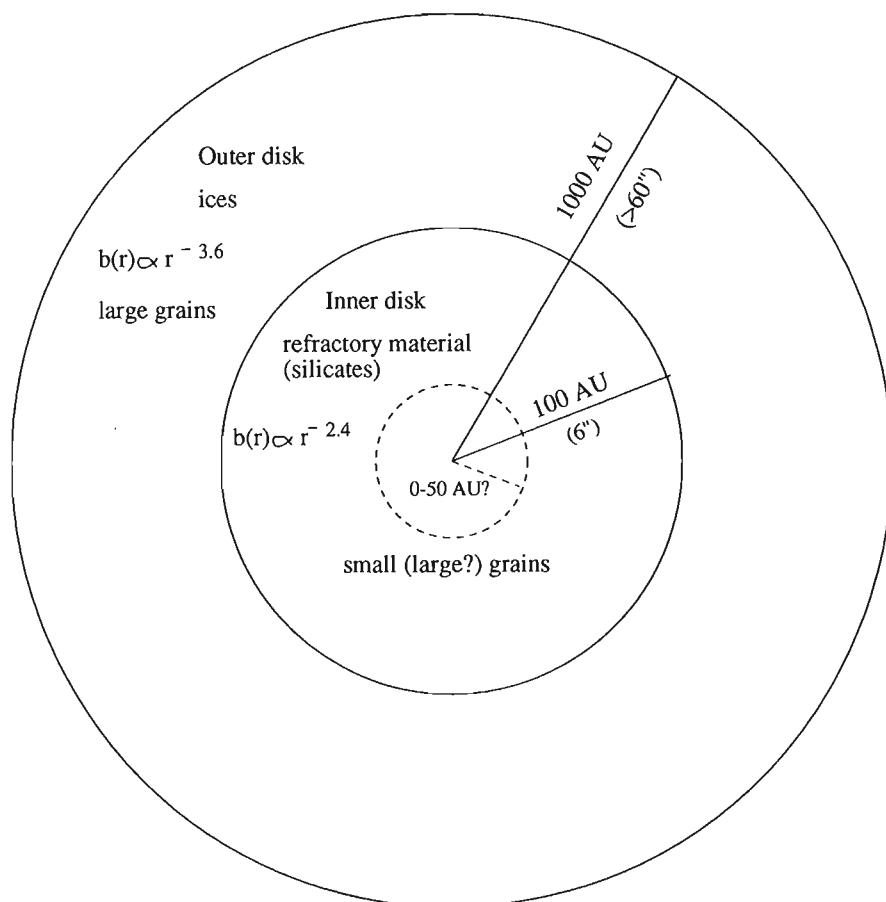


Figure 2: Model for the β Pictoris disk.

cated instrumentation (Watson et al., 1991). The basic problem is to detect $\Delta M \geq 25$ for Jupiter-like planets close to very bright objects ($\leq 1''$). This implies use of dedicated coronagraphs (apodizers), but also a very high image quality and then use of adaptive optics on the next generation of ground-based telescopes and dedicated instrumentation (Angel, 1994) or space observatories. Malbet, Shao and Yu (1994) have recently suggested an active system to correct for the imperfections of the primary and secondary mirrors of HST so as to possibly detect Jupiter-like planets around near-by stars.

Direct evidence of planets via Doppler shift has also been investigated in the previous years; it requires very accurate spectroscopy (precision of 10 m/s), and then also dedicated instrumentation.

Signatures of planets may relatively more easily be found in further investigating the structure of the disk (presence of gaps, location of inner void, asymmetries). Indeed, a planet is expected to produce gaps in the disk because of its gravitational perturbation on the close-by small grains (see for instance Sicardy et al., 1993). To detect such small-sized signatures (AUs), one first needs high angular resolution. Space observations (with HST), free of atmospheric distortion, or ground-based observations with adaptive optics are necessary. To observe very faint structures close to a very bright object, one needs a high dynamical range within a small spatial region. Coronagraphic techniques or use of antiblooming detectors are obviously needed.

2.4.2 Structures in the disk

Observations with the FOC and coronagraph on the refurbished HST are expected to provide diffraction-limited images from 1150 to 6500 Å, with a high efficiency towards 4000 Å. They are expected to test gaps size down to 0.2'' in size, i.e. 3 AU in the best case, and then hopefully test masses smaller than 0.1 M_{\odot} located at distances down to 20 AU from the star (Norman and Paresce, 1989). Near-IR diffraction-limited coronagraphic images with CONICA on the VLT will enable us to reach roughly similar performances, slightly better if we compare the resolution at 1 μm ($\approx 0.03''$) to the HST 0.4 μm one. Ground-based observations have the advantage of flexibility and offer the possibility to use dedicated masks. High-resolution images will also test the inner void down to less than 3 AU from the star.

FORS will unfortunately work at lower angular resolution (0.3'' in the best case) as it will give seeing-limited images. So

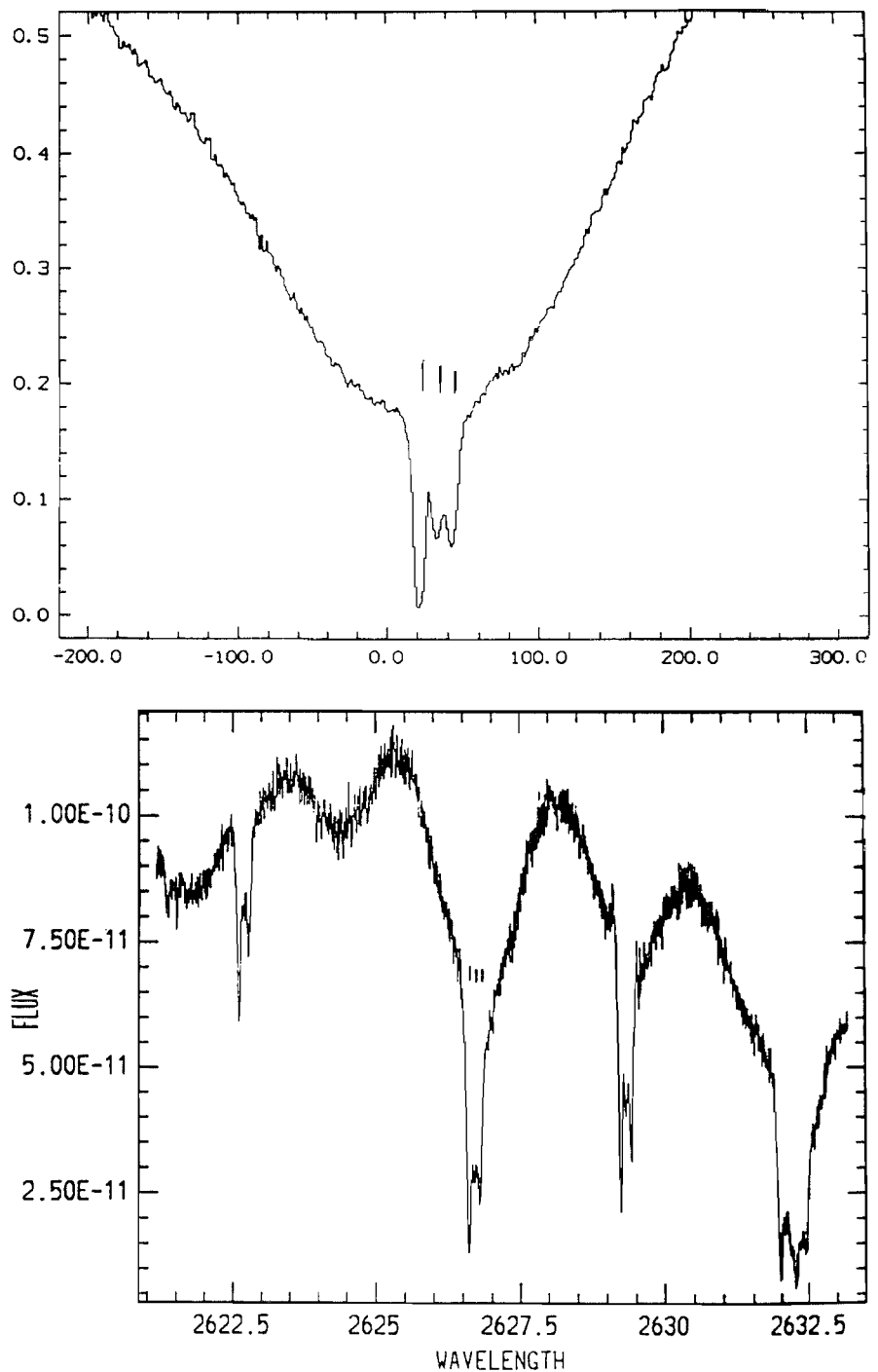


Figure 3: Variations in the CS lines of β Pictoris: simultaneous high-resolution observations of redshifted lines in Calcium II K (ESO) and Fe II (HST).

in principle, one could get the same type of information on 4-m-class telescopes if identical instruments were available. Adaptive optics correction in the visible, *even partial*, would drastically improve the image quality, and then the science to be done with. As an example, partially corrected (factor of 4 times the diffraction limit, which is quite a reasonable limit to be obtained when using the AO correction developed for the IR) images at 4000 Å would give a resolution of less than 0.05'' (i.e. 0.8 AU), comparable to the fully corrected HST images.

Of course, this assumes that the pixel size would correctly sample the resolution.

Next step, VLTI images with a resolution of 0.001'' would enable us to obtain details of less than 0.02 AU, otherwise undetectable, over a relatively large field of view (8'').

2.4.3 Radial distribution of the dust; optical properties of the grains

To further constrain those parameters, the best strategy is again to per-

form *multiwavelength* imaging, from the UV to the radio. The combination of disk responses from the UV to the IR at very high resolution with HST and CONICA images, and FORS, with, hopefully, at least partially corrected images in the optical range will undoubtedly bring a wealth of information.

10 and 20 μm structure of the disk with resolutions of 0.3 and 0.6" with MIIIs (see below) will also help to further constrain the models. Compared to the present TIMMI performances, a gain of more than a factor two might be expected. This is of course crucial. The lower resolution in this wavelength range compared to the visible or near-IR domains is partly balanced by the fact that conversely to the visible or near-IR domains, there is no need for a coronagraph. Direct imaging with ISOCAM up to 20 μm , with a nevertheless lower angular resolution, between 3 and 6", but a higher sensitivity, or with ISOPHOT aperture photometry up to 200 μm are also expected to further constrain the description of the disk.

The chemical composition of the disk will be further investigated with ISO, especially via spectroscopy: water ices as well as silicates can be searched for, with a very good sensitivity. From the ground with MIIIs, at higher resolution, silicate bands will be investigated with spectro-imaging or long-slit spectroscopy. Also, polarimetric and multiband observations with FORS should bring valuable information on the nature of the grains.

2.5 The gas

2.5.1 The stable gas

β Pictoris, viewed edge-on, is well suited for absorption line studies of its CS gas. The star exhibits indeed sharp absorptions at the bottom of the rotationally broadened photospheric lines of ionized elements present around the star (see Fig. 3). Those lines have been extensively studied in the optical range at high resolution ($R=10^5$) with the CES (Hobbs et al., 1985; Vidal-Madjar et al., 1986) and very recently at $R=10^6$ with the UHRF at AAT (Crawford et al., 1994), and in the UV with IUE (Kondo and Bruhweiler, 1985) and HST (Boggess et al., 1991; Vidal-Madjar et al., 1994; Lagrange et al., 1994), so as to investigate the composition of the CS gas, its density and location in the disk. A detailed review of the results is given in Lagrange (1994). The CS elements observed up to now in the stable gas are neutral: NaI, FeI, ClI, and mainly singly ionized, close to the star (FeII), MnII, CaII, ZnII...). The total Hydrogen density column is 10^{18} cm^{-2} and the typical

electronic density ranges between 10^3 and 10^6 cm^{-3} .

An interesting question concerning this gas is whether or not it is coupled to the CS dust, and whether or not they have a common origin. Vidal-Madjar et al. (1986) suggested that the gas close to the star could be the result of the evaporation of small grains at typical distances of 0.5 AU.

2.5.2 The variable gas; comets around β Pictoris?

Observations of β Pictoris at different epochs evidenced important infall of clumpy gas towards the star, with velocities sometimes as high as 300 km s^{-1} (see Fig. 3). This infall was tentatively attributed to evaporation of km s^{-1} sized, comet-like bodies grazing the star. Numerical simulations of such an event appeared to reproduce quite satisfactorily the variable lines (Beust et al., 1991, and references therein). Extensive monitoring of the variations both in the visible with CES, and in the UV with IUE, undertaken in 1985 and still going on now, has brought strong support to this scenario. It has also been shown (Mouillet et al., 1994) that the electronic densities and temperature of the infalling gas are very high, as predicted by models (Beust and Tagger, 1993).

This scenario can also account for the otherwise unexplained detections of infalling overionized species: A1 III and C IV (Lagrange et al., 1989; Deleuil et al., 1993; Vidal-Madjar et al., 1994) as well as the recent detection of molecular CO around β Pictoris.

A still open question is the triggering mechanism of these infalls observed at a high rate (a few hundreds of km-sized objects per year). Some possibilities have been suggested: perturbing bodies, collisions between km-sized bodies (Beust et al., 1991b; Gor'kavyz, 1994), which certainly deserve deeper investigations.

A chemical analysis of the variable gas can further test the cometary scenario. Visible and HST high-resolution and high S/N observations as well as ultra-high-resolution observations should bring decisive answers.

3. Other IR Excess Main Sequence Stars; Search for Disks

Most of the observational work done so far on α Lyr, α PsA and ϵ Eri, and to a lower extent on the other MS IR excess stars has been to observe them in the IR and radio domains, most of the time in photometry, but also in the optical range, to try to resolve CS disks. Also

spectroscopic searches for β Pictoris-like stars have been performed.

3.1 IR and radio observations

Far-IR and radio observations on α Lyr, α PsA and ϵ Eri showed that those objects exhibit excesses at all these wavelengths, sometimes extended (Harvey et al., 1984; Chini et al., 1991; and more recently Zuckerman and Becklin, 1993b). 800- μm maps showed that around these objects there is no important amount of cold dust which could have escaped detection by IRAS. Minimum masses of $6 \cdot 10^{-3}$, $2 \cdot 10^{-2}$ and less than $7 \cdot 10^{-4} M_{\odot}$ are deduced for the CS dust responsible for the 800- μm emission around Vega, Fomalhaut and ϵ Eri respectively.

Other IR excess MS stars have also been studied in some detail; a review of the current knowledge on these objects can be found in Lagrange (1994).

3.2 Spectroscopic search for CS gas

No atomic gas has so far been detected around any of the first four IR excess MS stars (Hobbs, 1985). Yamashita et al. (1993) also failed to detect CS ^{12}CO around α Lyr, α PsA and ϵ Eri. These non-detections should bring constraints to the production/destruction rates of CO around these objects. Spectroscopic similarities have been searched for in the CaII and NaI lines of a number of IRAS excess or already known shell A-B stars. Among more than 80 stars thus observed (Lagrange-Henri et al., 1990), very few exhibit spectroscopic similarities in these lines with β Pictoris. Some of them do show variations possibly similar to the β Pictoris ones. In conclusion, even though no strong correlation has been found up to now between the presence of CS dust and CS gas, some IR excess stars deserve further high-resolution spectroscopic studies. For these bright objects, the resolution of the instrument is a more important factor than the telescope collecting surface.

3.3 Optical search for disks

Many efforts have been made to find new IR excess candidates in the IRAS database and to detect disks around these candidates. Smith, Fountain and Terile (1991) extensively surveyed 100 stars with their coronagraph and did not find any disk. There might be several reasons for these negative results:

- the disk phase is very transient.
- the disks are too faint to be detected with the techniques used so far. Actually, among the IR MS excess stars,

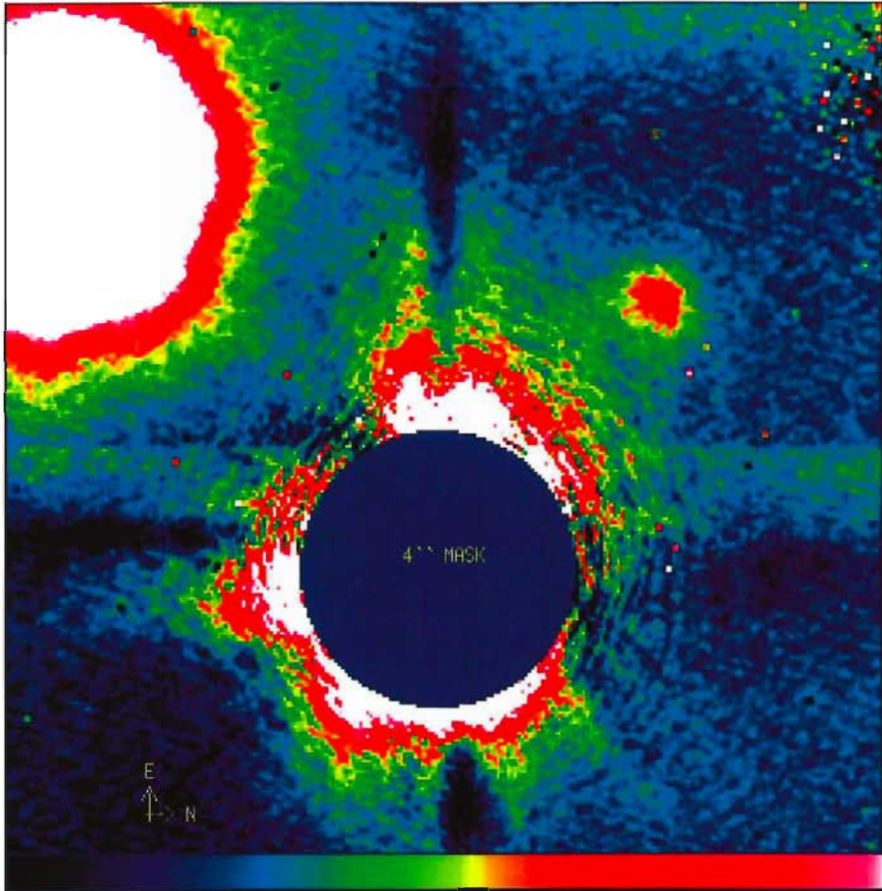


Figure 4: COME-ON+ observations with a coronagraph of the close environment of the IRAS excess MS star HR 4796 (H band, 300 sec exposure). The observations were made with a 2'' (diameter) mask. On the present image, the dark disk is a 4'' software mask used to hide the immediate vicinity of the physical mask, which in this case contains no useful information. A faint object ($m \approx 16$) is detected at less than 5'' from the 5th magnitude HR 4796.

β Pictoris exhibits the highest disk luminosity.

- the disks are unfavourably oriented. An inclination of the disk with respect to the line of sight obviously increases its magnitude, but also makes it much more difficult to detect it with the available techniques.
- the grains are no good scatterers in the visible.
- the candidate star environment is complex and other, colder field objects contribute to the part of IRAS large beam fluxes.
- the dust is closer to the star than in the β Pic disk and cannot be detected with 5–20'' masks. This is certainly true for some objects such as 51Oph (Waters, Cote and Geballe, 1988), HR4796 and HD98800 (Zuckerman and Becklin, 1993; Jura, 1993), for which models show that the CS dust lies within 1'' from the star. However, in most cases, the largest part of the dust cannot be too close as it would produce a 12- μ m excess detectable with IRAS.

To significantly progress in the study of the close environment of those stars,

and detection of disks, one needs to observe closer to the stars and/or have a much better sensitivity further away.

The next section focuses on the expected progress with the VLT in the domain of CS disk detection around other stars. Of course, once detected, an approach similar to the one adopted for the study of the β Pictoris disk should be followed.

3.4 Observations of disks with the VLT

3.4.1 CONICA

To observe very faint signatures very close to bright objects, one needs high image quality as well as coronagraphs or antiblooming detectors. Again either space observatories (HST) or ground-based diffraction-limited telescopes are needed.

Recent coronagraphic observations with the COME ON + system at the ESO 3.6-m telescope have already demonstrated that small masks can be used indeed: sizes down to 0.8'' in diameter have been tested, and we expect to use

even smaller sizes, hopefully down to the first Airy ring. Actually, the most tricky point is to stabilize the object behind the mask. Also, these coronagraphic COME-ON + observations demonstrated that high dynamic ranges could be reached as well (see Fig. 4; Beuzit et al., 1994).

With CONICA on the VLT one can reasonably expect to observe down to less than 0.1'' from the star. For typical distances of 10–50 pcs, it means distances closer than 5–25 AU. The field of view, 15'' of CONICA is indeed well suited for the study of the inner parts of the disks. The possible inner void of material can be tested. The gain in the scientific output with the high resolution facility provided is obvious. In summary, CONICA + coronagraph is very well suited for observations of the close environment of the candidates, and disk detection, from 0.1'' to 7''.

3.4.2 FORS

With the present FORS specifications, only outer parts of the disk will be observed ($\geq 0.6''$), but the gain in sensitivity, thanks to the higher collecting surface and the use of better detectors is a very promising issue. Figure 5 gives for the candidates proposed by Backman and Paresce (1993) in their master list of IR excess stars the expected disk luminosities in the visible (scattered light), assuming the dust distribution is similar to the β Pictoris one, and fractional luminosities of the disks are 100 times lower than the β Pictoris one. The differences in distances and stellar luminosities have been taken into account. One sees that the $\geq 7''$ regions, accessible to classical coronagraphs on 2–4-m telescopes are very faint. FORS + coronagraph should in principle detect the disks. Polarimetric facilities will provide useful information to further characterize the disks. Again, even partly corrected visible images would result in a significant gain, as they would enable us to observe more inner parts of the disks with very high sensitivities. Also, interferometric VLT observations would enable us to test the innermost parts of the disks.

3.4.3 MIRS

Another important issue is expected from 10–20- μ m observations on diffraction-limited 8-m-class telescopes. Actually, the 20- μ m window is more promising for early-type MS stars than the 10- μ m one since, with the exception of two cases, there has been no detection of 10- μ m excess, while 20- μ m excess has been detected in all cases (Auman and Probst, 1991). The expected resolu-

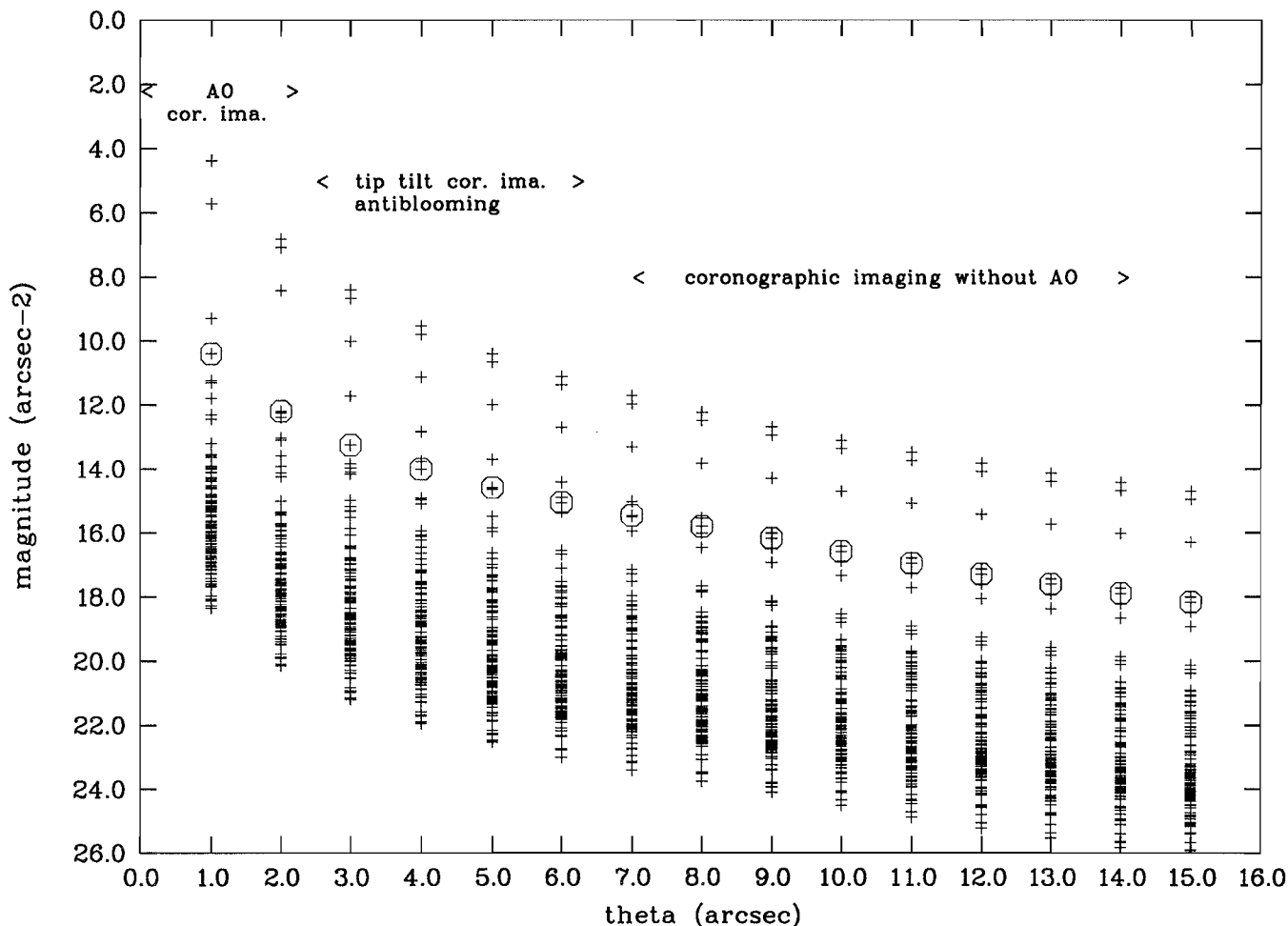


Figure 5: Expected disk magnitude per arcsec as a function of angle for the candidate stars proposed by Norman and Paresce (1993). The disks are supposed to be similar to the β Pictoris one (same intrinsic brightness and same radial distribution). An arbitrary, but reasonable factor of 100 in the relative disk luminosity compared to the β Pictoris one has been taken. Circles are the values for the β Pictoris disk.

tion of $0.6''$ is well suited to resolve the $20\text{-}\mu\text{m}$ emitting region for these nearby objects. In most cases, one should detect extended structures. Long-slit spectroscopy in the $17\text{-}\mu\text{m}$ silicate band range can also be performed.

4. Conclusions

The study of outer planetary systems will help to understand the way those systems form and evolve. Very important observational work will certainly be devoted to this subject in the next years and decades. The disk around β Pictoris has been successfully studied with various approaches: imaging, photometry (dust) and spectroscopy (gas). For β -Pictoris as well as for the other candidates, significant progress is expected from observations in the UV (HST), visible, near and mid-IR (ground-based diffraction-limited 10-m-class telescopes; ISO) and radio. Diffraction-limited images in the near IR should enable us to detect other disks close to the star; $20\text{-}\mu\text{m}$ imaging is expected to study the inner part as well, with less angular resolution, but in the thermal

domain; optical imaging should enable us to detect more remote parts of the disks. Table 1 summarizes for the first generation of VLT instruments what kind of observations and science can be done on the β Pictoris disk and on the other stars.

The author thanks A. Vidal-Madjar, A. Lecavelier and D. Mouillet for fruitful discussions and P. Corpron for his help in some parts of the work.

References

- Angel, J.R.P., 1994, *Nature* **368**, 203.
 Auman H.H., et al., 1984, *ApJ* **278**, L23.
 Auman H.H., and Probst, R.G., 1991, *ApJ*, **368**, 264.
 Artymowicz P., Burrows C. and Paresce F., 1989, *ApJ* **337**, 494.
 Backman and Paresce, 1993, *Protostars and Planets III*, Levy, E.H., Lunine, J.I. and Matthews, M.S. Ed., University of Arizona Press.

TABLE 1.

Instrument	Resolution	Science	Why the VLT?
CONICA	$0.02\text{--}0.15''$	β Pictoris: structure of the inner disk (gap, inner void, inhomogeneities) other stars: detection of disks, disk structure inner void	high angular resolution id
MIIS	$0.3\text{--}0.6''$	β Pictoris: structure of the disk at 10 and $20\text{ }\mu\text{m}$ angular resolution spectro-imaging of the silicate bands other stars: structure of the disks at $20\text{ }\mu\text{m}$ spectro-imaging of the silicate bands	angular resolution id
FORS	seeing	other stars: detection of disks, polarization	very good sensitivity

- Backman D.E., Gillet F.C. and Witteborn F.C., 1992, *ApJ*, **385**, 670.
- Beust H., Vidal-Madjar, A., Ferlet, R., Lagrange-Henri, A.M., 1991, *A&A* **241**, 488.
- Beust H., Vidal-Madjar, A., Ferlet, R., 1991, *A&A* **247**, 505.
- Beust, H., and Tagger, M., 1993, *Icarus* **106**, 42.
- Beuzit et al., 1994, *A&A*, to be submitted.
- Boggess, A., Bruhweiler, F.C., Grady, C.A., Ebbets, D.C., Kondo, Y., Trafton, L.M., Brandt, J.C. and Heap, S.R., 1991, *ApJ* **377**, L49.
- Chini R., Krugel E., Shsutov B., Tutukov A. and Kreysa E., 1991, *A&A* **252**, 220.
- Crawford, I.A., Spyromilio, J., Barlow, M.J., Diego, F., and Lagrange, A.M., 1994, *Mon. Not. R. Astron. Soc.*, **266**, L65–L68.
- Deleuil, M., Gry, C., Lagrange, A.M., Vidal-Madjar, A., Ferlet, R., Moos, T.A., Liven-good, T.A., Ziskin, D., Feldman, P.D. and McGrath, M., 1993, *A&A*, **267**, 187–193.
- Diner, D., and Appleby, J., 1986, *Nature* **332**, 436.
- Gledhill, T.M., Scarrott, S.M. and Wolsten-croft, R.D., 1991, *Mon. Not. R. Astron. Soc.* **252**, 50.
- Golimowsky, D.A., Durrance, S.T., and Clam-pin, M., 1993, *AJ* **105**, 1108.
- Harvey, P., Wilking, B.A. and Joy, M., 1984, *Nature* **307**, 441.
- Hobbs, L.M., Vidal-Madjar, A., Ferlet, R., Albert, C.E., Gry, C. 1985, *ApJ* **293**, L29.
- Jura M., Zuckerman, B., Becklin, E.E. and Smith, R.C., 1993, *ApJ* **418**, L37.
- Knacke, R.F., Fajardo-Acosta, S.B., Telesco, C.M., Hackwell, J.A., Lynch, D.K. and Russell, R.W., 1993, *ApJ* **418**, 440.
- Kondo, Y., Bruhweiler, F.C., 1985, *ApJ* **291**, L1.
- Lagage, P.O., 1994, *Nature*, in press.
- Lagrange, A.M., Ferlet, R., Vidal-Madjar, A., 1987, *A&A* **173**, 289.
- Lagrange, A.M., Ferlet, R., Vidal-Madjar, A., Beust H., Gry, C., Lallement, R., 1990, *A&A Sup.* **85**, 1089.
- Lagrange A.M., et al., 1994, *A&A*, submitted.
- Lagrange A.M., 1994, in "Planetary systems: formation, evolution and detection"; 2nd TOPS conference.
- Lecavelier, A., et al., 1992, *A&A* **274**, 877.
- Malbet, F., Shao, M and Yu, J., 1994, in "SPIE Symposium Astronomical Telescopes and Instrumentation for the 21st Century".
- Mouillet, D., et al., 1994, *A&A* submitted.
- Norman, C. and Paresce, F., 1989, in "Formation and evolution of planetary systems".
- Paresce, F. and Burrows C., 1987, *ApJ* **319**, L23.
- Sicardy, B., 1994, in *Asteroids, Comets and Meteors*, 1993 (A. Milani and Di Martino Eds.), Kluwer Academic Publ., in press.
- Smith B.A., and Terrile, 1984, *Science* **226**, 1421.
- Smith B.A., Fountain J.W. and Terrile R.J., 1992, *A&A* **261**, 499.
- Telesco C.M. and Knacke R.F., 1991, *ApJ* **372**, L29.
- Vidal-Madjar, A., Hobbs, L.M., Ferlet, R., Gry, C., Albert, C.E., 1986, *A&A* **167**, 325.
- Vidal-Madjar et al., 1994, *A&A*, in press.
- Waters, L.B.F.M., Cote, J. and Geballe, T.R. 1988, *A&A* **203**, 348.
- Watson et al., 1991, *Applied Optics* **30**, N 22, 3253.
- Yamashita, T., et al., 1993, *ApJ* **402**, L65.
- Zuckerman, B., and Becklin, E.E., 1993, *ApJ* **406**, L25.
- Zuckerman, B., and Becklin, E.E., 1993, *ApJ* **414**, 793.

The History of Star Formation in the Large Magellanic Cloud

A. VALLENARI¹, G. BERTELLI², C. CHIOSI² and S. ORTOLANI²

¹Astronomical Observatory of Padua, Italy; ²Department of Astronomy, Padua, Italy

1. Introduction

The history of star formation in the Magellanic Clouds greatly differs from that in our own Galaxy and, despite the many efforts it is still poorly known.

Studying the luminosity functions (LFs) of field stars of the Large Magellanic Cloud (LMC), Butcher (1977) first suggested that the bulk of stars formed about 3–4 Gyrs ago. Subsequently, Stryker (1984), Frogel & Blanco (1983), and Hardy et al. (1984) confirmed this conclusion.

However, all those results were based either on data at the limits of reliability of photographic photometry or made use of age calibrators that were affected by significant uncertainties.

Recently, Bertelli et al. (1992) proposed a new method based on suitable ratios of star counts in the Colour-Magnitude Diagram (CMD) and used it to analyse CMDs of three areas approximately located at 4° north from the LMC centre. These areas, named from the nearest cluster, are NGC 1866, NGC 1783, and NGC 2155. They concluded that star formation underwent an intense burst-like episode of activity (other kinds of star formation did not lead to satisfactory results) and that this prominent activity commenced at nearly the same epoch (3–4 Gyrs ago) in each region. Bertelli et al. (1992) thus confirmed the conclusions reached in the older studies, i.e. that the LMC has been quiescent for about 70 % of its history.

This kind of star formation is compatible with the age distribution of star clusters in LMC, whose vast majority is not older than 3–4 Gyrs (Chiosi et al. 1988, Da Costa 1991, Girardi et al. 1994).

However, despite the above hints about the history of star formation in LMC, there are still several questions to be addressed: Has this burst affected the whole LMC? What is the physical process responsible for the star formation enhancement 3–4 Gyrs ago? How was the star formation rate at ages older than 3–4 Gyrs?

To this aim, a programme has been undertaken to observe with the ESO telescopes at La Silla several selected

areas all across the LMC (and SMC) and get deep, good quality B, V CCD photometric data. As part of this programme, frames for six regions have already been acquired. The six areas are located approximately at the centre of the V-charts of the Hodge & Wright (1967) catalogue after which they are named. The areas in question are LMC-30, LMC-45, LMC-56, LMC-61, LMC-60, and LMC-69. They are shown in Figure 1 superposed to a map of the LMC reproduced from Smith et al. (1987) indicating several regions of star formation, like 30 Doradus and Constellations II and III.

This paper presents the preliminary results for the region LMC-56 and a progress report of the overall programme.

2. The Data

The observations of the six fields have been taken during two observing runs in December 1991 and November 1993 using the 2.2-m ESO telescope equipped with EFOSC2 and the Thompson ESO CCD #19.

In the fields observed in the first run (LMC-56, LMC-69 and LMC-60) about 4,000 stars are measured down to $V \sim 23$ mag because of the mean seeing of 1.5", whereas owing to the better seeing conditions (about 1.0") in the fields observed in the second run (LMC-30, LMC-45 and LMC-61), about 9,000 stars per frame are detected down to $V \sim 24$ mag.

Figure 2 shows the BV-CMD of one area, namely LMC-45.

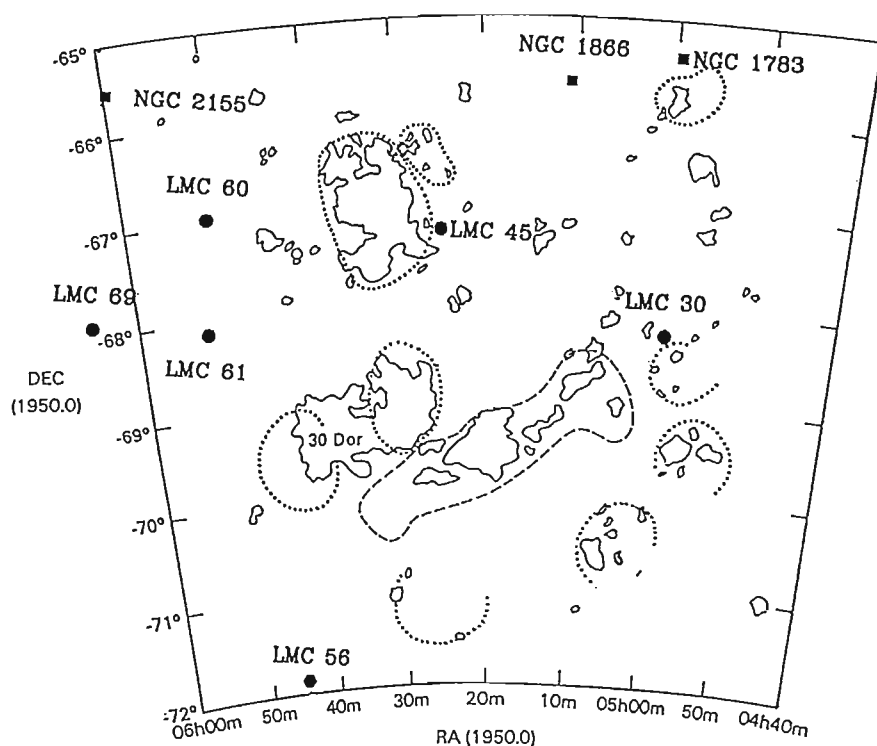


Figure 1: The map of LMC reproduced from Smith et al. (1987). In this map are shown both regions of ongoing (30 Doradus) or very recent star formation (Constellation III), together with the selected areas. The filled squares indicate the three regions studied by Bertelli et al. (1992), the filled diamond shows LMC-56 presented in this paper, finally the filled circles mark the remaining areas of the programme.

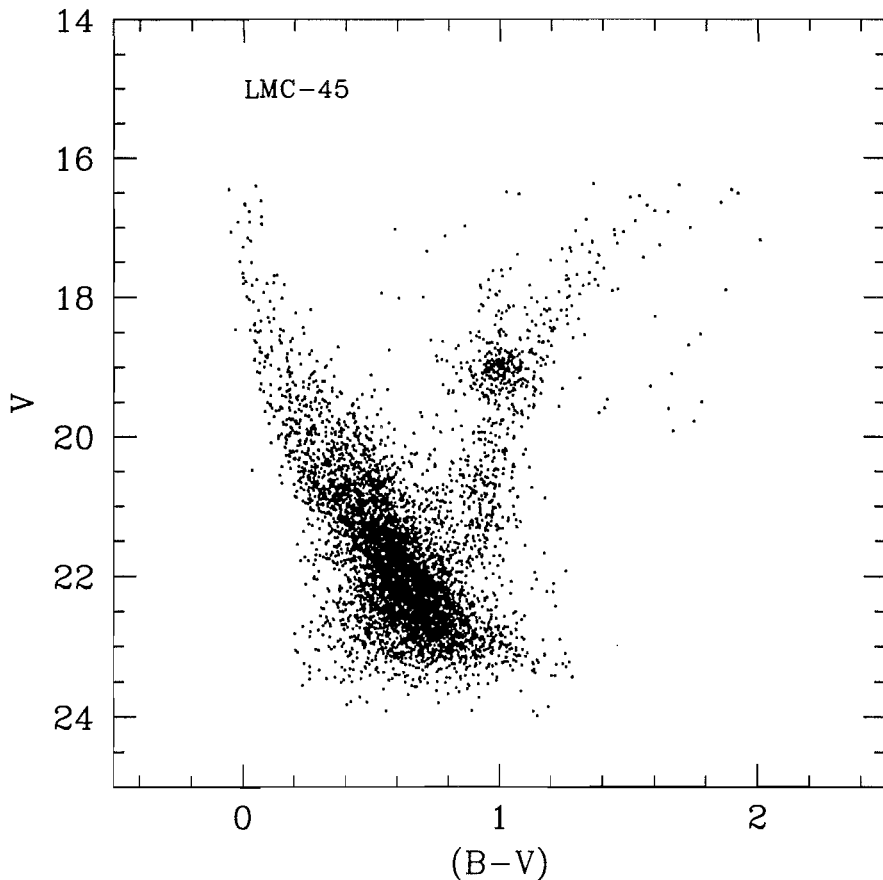


Figure 2: CMD of the region LMC-45.

3. Theoretical Rationale

The Bertelli et al. (1992) method is based on the use of suitable ratios of star counts effected in the giant and main sequence regions of the CMDs and their comparison with the CMDs and their comparison with theoretical simulations at varying laws of star formation. This is parameterized by the age of the initial episode and the intensity.

The analysis is made by means of the library of theoretical isochrones of Bertelli et al. (1994), which is based on the stellar models of Bressan et al. (1993) and Fagotto et al. (1994 a, b) calculated with core and envelope overshoot, the new radiative opacities of Iglesias et al. (1992), and a large range of metallicities (from $Z=0.0004$ to $Z=0.05$). In addition to this, theoretical luminosities and effective temperatures are translated into magnitudes and colours by means of the transformations described by Bertelli et al. (1994).

Assumed a suitable value for the metallicity Z and hence a particular set of isochrones, we derive the age τ_F from the luminosity of the youngest main-sequence stars existing in the CMDs.

Because the ratios of star counts are defined with the aid of characteristic magnitudes which are related to corresponding luminosities of the underlying evolutionary phases, a choice for the

distance modulus and colour excess is needed to compare the theoretical results with the observational data. We adopt the distance modulus to the LMC $(m-M)_0=18.5$ mag of Panagia et al. (1991) and the colour excess $E_{(B-V)}=0.07$ from the maps of Schwing & Israel (1991).

4. The Results for LMC-56

The comparison of the counts in LMC-56 with their theoretical counterparts allows us to derive the following results:

No solutions exist for the law of star formation for metallicities lower than $Z=0.005$ and in most cases higher than $Z=0.008$.

No solutions are found for slopes of the IMF lower than $\kappa=2.35$, whereas there are solutions for $\kappa=2.85$ and $\kappa=3.35$. However, the detailed LF of the main-sequence stars for the case $\kappa=3.35$ does not agree with the observation. Therefore, only the case with $\kappa=2.85$ leads to fully satisfactory results.

The age for the start of the bulk activity of star formation is significantly older than the value of 3–4 Gyrs found by Bertelli et al. (1992) for the areas NGC 1866, NGC 1783 and NGC 2155. For LMC-56 we found an age of 7–8 Gyrs.

Finally, it is worth recalling that these results do not change significantly with the distance modulus and reddening. Similar remark holds if we had adopted classical models instead of those with convective overshoot.

5. Final Remarks

Combining the results of the present study with those of Bertelli et al. (1992) and the very preliminary ones obtained for other regions of our list, there is some indication that the age of the most recent, perhaps dominant, episode of star formation has changed across the LMC. We should remind the reader that because of the adopted modelization of the SFR and the internal resolution of the method in usage, recurrent episodes of star formation cannot be singled out. What the method allows us to get is the mean age of the last, prominent episode of star formation. More detailed study is necessary before confirming whether the LMC suffered from recurrent episodes of star formation. It is tempting to attribute the LMC star bursts at 3–4 and 7–8 Gyrs to some sort of tidally induced shock caused in the past by a passage near the Galaxy, as suggested by Murai and Fujimoto (1980) and Gardiner et al. (1994).

References

- Butcher, H. 1977 *Astrophys. J.* **216**, 372.
- Bertelli, G., Bressan, A., Fagotto, F., Nasi, E. 1994, *Astron. Astrophys. Suppl. Ser.*, in press.
- Bertelli, G., Mateo, M., Chiosi, C., Bressan, A. 1992, *Astrophys. J.* **388**, 400.
- Bessel, M.S., Freeman, K.C., Wood, P.R. 1986, *Astrophys. J.* **310**, 710.
- Bressan, A., Bertelli, G., Fagotto, F., Chiosi, C. 1993, *Astron. Astrophys. Suppl. Ser.* **100**, 647.
- Chiosi, C., Bertelli, G., Bressan, A., 1988, *A196*, 84.
- Da Costa, G.S. 1991, in *The Magellanic Clouds*, IAU Symp. 148, eds. R. Haynes & D. Milne, Dordrecht: Reidel, P. 183.
- Fagotto, F., Bressan, A., Bertelli, G., Chiosi, C., 1994a, *Astron. Astrophys. Suppl. Ser.*, in press.
- Frogel, J.A., Blanco, V.M., 1984, *Astrophys. J. Lett.* **274**, L57.
- Gardiner L.T., Sawa T., Fujimoto M., 1994, *MNRAS* **266**, 567.
- Girardi L., Chiosi, C., Bertelli, G., Bressan, A., 1994, *A&A* submitted.
- Hardy, E., Buonanno, R., Corsi, C.E., Janes, K.A., Schommer, R.A., 1984, *Astrophys. J.* **278**, 592.
- Hodge, P.W., Wright, F.W., 1967, *The Large Magellanic Cloud*, Smithsonian Publication 4699, Smithsonian Press, Washington.
- Iglesias, C.A., Rogers, F.J., Wilson, B.C., 1992, *Astrophys. J.* **397**, 717.
- Murai, T., Fujimoto, M., 1980, *Publ. Astron. Soc. Japan* **32**, 581.
- Panagia, N., Gilmozzi, R., Macchetto, F.,

Geminga, 10 Years of Optical Observations

R. MIGNANI^{1,3}, P.A. CARAVEO¹ and G.F. BIGNAMI^{1,2}

¹*Istituto di Fisica Cosmica del CNR, Milano, Italy;*

²*Dipartimento di Ingegneria Industriale, Università di Cassino, Italy;* ³*Università degli Studi di Milano, Italy*

1. Introduction

The high energy source Geminga was discovered in γ rays about 20 years ago by the NASA satellite SAS-2 (Fichtel et al., 1975); between 1975 and 1982 the source was observed several times by the ESA COS-B satellite and, in parallel, a possible X-ray counterpart (1E0630+178) was found by the EINSTEIN Observatory (Bignami et al., 1983).

The detection of Geminga at X-ray wavelengths reduced the radius of error box by a factor ~ 300 . It then became possible to search for its optical counterpart. First deep inspections of the HRI error circle ($r = 4''$) were done with the 3.5-m CFHT (Bignami et al., 1987) and led to the observations of three possible candidates, namely stars G, G' and G'', the last one being the fainter of the three ($m_v = 25.5$). Later observations with the ESO 3.6-m (Bignami et al., 1988) and with the 5-m Hale (Halpern and Tytler, 1988) demonstrated that the first two were quite normal field stars while the unusual colours of G'' made it the most probable candidate for the optical counterpart of Geminga.

The high energy brightness of the source coupled with its faintness in the optical ($L_X/L_{opt} > 1000$) was one of the arguments which led Bignami et al. (1983) to suggest that Geminga was an isolated neutron star, in spite of the lack of detectable radio emission.

In the 1990s, GRO and ROSAT observations greatly contributed to understanding the nature of the source. First came the detection of a 237 msec. pulsation in soft X-rays (0.1–2 Kev) by ROSAT (Halpern and Holt, 1992) soon followed by a similar discovery in γ rays by EGRET (Bertsch et al., 1992). This was immediately found also in old COS-B (Bignami and Caraveo, 1992) and SAS-2 (Mattox et al., 1992) archived data. This discovery of a common periodicity confirmed the identification between the γ and X-ray source and provided important information about the nature of the object. The observed

pulsation at high energies can be explained only as due to the fast rotation of a highly magnetized isolated neutron star ($B \sim 1.5 \cdot 10^{12}$ G), up to now the only one detected through its γ/X emission but quiescent at radio wavelengths.

The evolution of the period of the X/ γ pulsar, computed over a time span of about 10 years (1982–1992), provided a good measure of its period derivative ($\dot{P} \sim 1.09 \cdot 10^{-14} \text{sec sec}^{-1}$) and hence of its age (about $3-10^5$ years). According to the standard relation adopted for radio pulsars ($\dot{E} = I\Omega\dot{\Omega}$) the overall energy output for Geminga is $\sim 3 \cdot 10^{34}$ ergs sec^{-1} . Assuming that all the rotational energy of the pulsar is converted in γ rays, an upper limit for its distance can be estimated (~ 340 pc). The actual distance to Geminga is then a function of the assumed γ ray efficiency ϵ_γ . For an efficiency similar to that of the Vela pulsar ($\epsilon_\gamma \sim 0.01$) a value of 30–40 pc is found.

2. The Optical Counterpart

If Geminga is, indeed, an isolated neutron star, it should move with a high tangential velocity typical of radio pulsars (~ 100 km/sec.). This, coupled with the upper limit on the distance, could lead to a measurable proper motion of the proposed optical counterpart G''

(Bignami and Caraveo, 1992). The expected proper motion can be written as:

$$\mu = 0.2v_{100} d_{100}^{-1} \text{ arcsec yr}^{-1}$$

(where v_{100} is the pulsar velocity in units of 100 km sec^{-1} and d_{100} its distance in units of 100 pc). Thus, a proper motion $\mu = 0.2''/\text{year}$ should be observed for a neutron star at 100 pc travelling at 100 km/sec.

Working with images taken in 1984, 1987 and 1992, Bignami, Caraveo and Mereghetti (1992, 1993) indeed found an overall displacement to NE corresponding to a proper motion of G'' $\mu = 0.17''/\text{year}$. This value is fully consistent with the hypothesis that G'' is a close ($d < 340$ pc) neutron star.

Thus, Geminga joins the restricted group of the optically identified neutron stars including PSR0531+21, PSR0833-15 and PSR0540-69, detected as pulsating sources, and PSR1509-58 and PSR0656+14 for which a likely identification was recently reported (Caraveo et al., 1994 a, b).

New V filter images of G'' have been taken in January 1994 by G.F. Bignami and P. A. Caraveo with the ESO New Technology Telescope equipped with the SUSI (Superb Seeing Imager (SUSI)). In order to reduce contamination from cosmic ray hits, the whole observation was subdivided in four exposures of

TABLE 1

Date	Telescope	Filter	Pixel size	Seeing	Exp. time
1984 Jan. 7 ¹	CFHT	R	0.412''	0.9''	180 min
1986 Feb. 3 ²	5m-Hale	g	0.336''	1''.8	120 min
1987 Jan. 28 ³	ESO 3.6-m	V	0.675''	1.6''	120 min
1992 Nov. 4 ⁴	NTT/SUSI	V	0.13''	0.6''	150 min
1994 Jan. 11 ⁵	NTT/SUSI	V	0.13''	1''	80 min

¹Bignami et al. (1987); ²Halpern and Tytler (1988); ³Bignami, Caraveo and Paul (1988); ⁴Bignami, Caraveo and Mereghetti (1992, 1993); ⁵This paper.

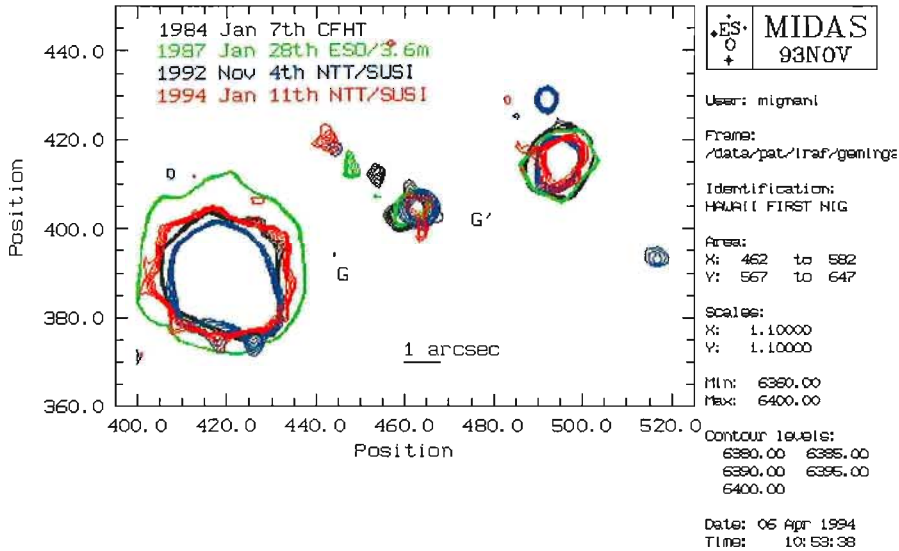


Figure 1: Superposition of contour plots corresponding to four observations of the field of Geminga taken at various epochs and with different telescopes. The displacement of G'' over a period of 10 years appears evident (north and east are approximately to the top and to the left of the frame, respectively). All the frames were set at the same pixel scale and orientation using standard programmes in MIDAS. Given the position of at least 10 reference stars (computed with CENTER/GAUSS), linear fits to coordinate transformations were computed with ALIGN/IMAGE. As a reference we used the SUSI 92 frame because of its finer pixel scale and the better image quality (see Table 2). The coordinates of the 1984, 1987 and 1994 frames were finally corrected using REBIN/ROTATE. The final precision was very good with all the images overlapping within a few hundredths of a pixel.

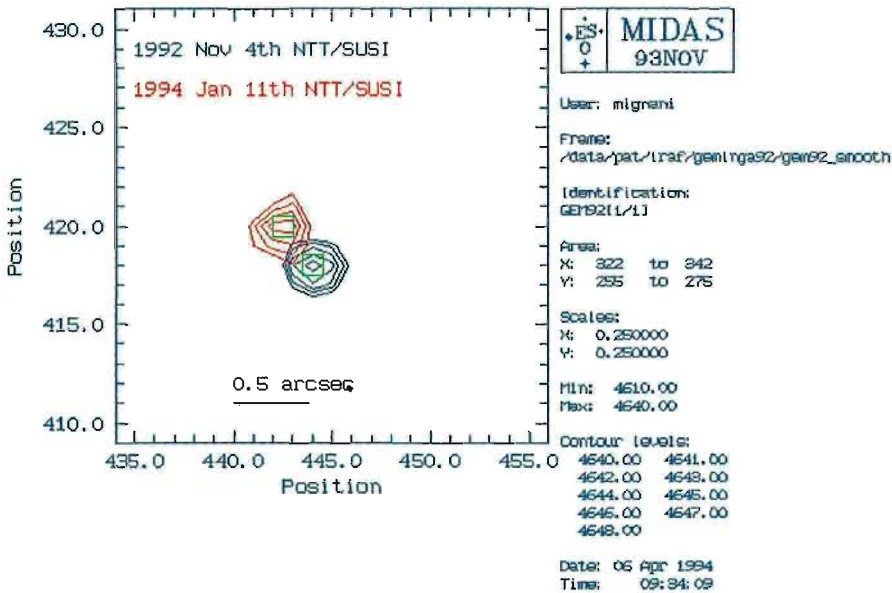


Figure 2: A zoom of Figure 1 showing the proper motion of G'' as observed with two SUSI/NTT images taken 14 months apart. The difference in image quality is due to different seeing conditions, 0.6–0.8'' in November 1992 and about 0.9'' in January 1994 with a greater air mass.

20 minutes each which have been later summed. For an immediate comparison between several images of the same field, taken with different telescopes and detectors (Table 1), all frames were tilted and rebinned to match exactly the same pixel scale and orientation (see caption to Fig. 1).

In order to check the displacement of G'' and to get a new measure of the proper motion, contour plots were pre-

pared for each set of available observations. The overplot of the four images (Fig. 1), covering a period of 10 years, shows the object's proper motion to NE. This result confirms and continues the previous work of Bignami, Caraveo and Mereghetti (1992, 1993). In addition, we can now compare for the first time two sets of SUSI observations which, thanks to their finer pixel scale (0.13 arcsec/pix.), make it possible to observe clearly the proper motion of G'' even on time scales as short as one year. This is better shown in Figure 2 where the two NTT/SUSI observations of November 1992 and January 1994 are compared. The displacement of G'' over 14 months is evident, even taking into account the uncertainty in the centring of the object, which is less than 1 pixel.

For each original frame, the sky coordinates of G'' were then computed taking as a reference the pixel positions of several field stars (from 7 to 12) taken from the HST Guide Star Catalogue; the UK STARLINK programme ASTROM (available under anonymous ftp from the ST-ECF domain) was then used to compute the astrometric solution.

The coordinates of G'' computed at each epoch are listed in Table 2.

The quoted errors reflect both the uncertainty in measuring the pixel position of G'', which is about 1 pixel for each original frame, and the RMS of the astrometry fits, typically, a few hundredths of arcsecond. A linear fit to the coordinates in Table 2 was then computed to give an average annual displacement of 0.149''/year in RA and 0.109''/year in DEC (with an error of $\pm 0''.044$) which is in very good agreement with previous results reported by Bignami, Caraveo and Mereghetti (1992, 1993). The coordinates of Halpern and Tytler were not used in the linear fit because they were not computed with the same set of standard stars, the original image not being available to us.

3. The Future

Having secured the optical identification of Geminga, the next step should be the precise measurement of the source distance, possibly through a parallax

TABLE 2

Date	R.A. (1950)	DEC. (1950)	Error
1984 Jan. 7	6 ^h 30 ^m 59 ^s .06	17°48'32.7"	±0.46"
1986 Feb. 3	6 ^h 30 ^m 59 ^s .06	17°48'32.9"	±0.5"
1987 Jan. 28	6 ^h 30 ^m 59 ^s .10	17°48'33"	±0.68"
1992 Nov. 4	6 ^h 30 ^m 59 ^s .15	17°48'33.6"	±0.141"
1994 Jan. 11	6 ^h 30 ^m 59 ^s .17	17°48'33.82"	±0.144"

measurement of G'' . At a distance of 100 pc the expected annual parallax would be 0.02", a value within the capability of the WFPC2 on the Hubble Space Telescope.

This is the aim of a set of observations approved for Cycle 4. The need to pursue this programme with HST is obvious. Only the PC on board HST has the resolution (0.043"/pixel, i.e. about one third that of SUSI) required to compute the position of G'' with the necessary precision. Even if the PC field of view (35×35 arcsecs.) is smaller than that of SUSI (~ 2×2 arcmin.) it should have a number of reference stars to do accurate astrometry on the target. Exposures at the vernal and autumn equinoxes in 1994 and 1995 are foreseen.

The interest of an absolute distance

measurement of Geminga would be outstanding. The optical, X and γ -ray observed fluxes could be converted accurately in luminosities, to be compared with the object's rotational energy loss, also precisely measured. This would then become the first case of a pulsar for which the energy output in each electromagnetic channel could be measured precisely as a test vs. pulsar theory.

Acknowledgements

We wish to thank F. Murtagh and R. Hook (ST-ECF) for providing the astrometry software.

References

Bertsch, D.L. et al., 1992 *Nature* **357**, 306.

Bignami, G.F., Caraveo, P.A. and Lamb, R.C., 1983 *Ap.J.* **272**, L9.

Bignami, G.F. et al., 1987 *Ap.J.* **319**, 358.

Bignami, G.F., Caraveo, P.A., 1992 *Nature* **357**, 287.

Bignami, G.F., Caraveo P.A. and Mereghetti, S., 1993 *Nature* **361**, 704.

Bignami, G.F., Caraveo P.A. and Mereghetti, S., 1992 *The Messenger* No. 70, p. 30.

Bignami, G.F., Caraveo, P.A. and Paul, J.A., 1988 *A.A.* **202**, L1.

Caraveo, P.A., Bignami, G.F. and Mereghetti, S., 1994a *Ap.J.Lett.* **422**, L87.

Caraveo, P.A., Bignami, G.F. and Mereghetti, S., 1994b *Ap.J.Lett.* **423**, L125.

Fichtel, C.E. et al., 1975 *Ap.J.* **198**, 163.

Halpern, J.P. and Tytler, D. 1988 *Ap.J.* **330**, 201.

Halpern, J.P. and Holt, S.S., 1992 *Nature* **357**, 222.

Mattox, D.G. et al., 1992 *Astr.J.* **103**, 638.

Jet/Cloud Interactions in Southern Radio Galaxies?

M. SHAW, C. TADHUNTER, N. CLARK, R. DICKSON, Sheffield, England

R. MORGANTI, Istituto di Radioastronomia, Bologna, Italy, and ATNF, Australia

R. FOSBURY, R. HOOK (ST-ECF), Garching, Germany

The role of jet/cloud interactions in high redshift radio galaxies is controversial, although there can be little doubt that radio jets have a profound influence on the interstellar medium which surrounds them. Cospatial radio and optical emission-line regions, extreme emission-line gas kinematics and extended blue continuum structures may all be manifestations of this phenomenon.

The importance of jet-induced phenomena has been stressed largely from the theoretical perspective, observa-

tional support for jet-induced star formation being, at best, suggestive (e.g. van Breugel & Dey 1993). This article corrects this imbalance. We present the preliminary results of our study of the southern radio galaxy PKS2250-41, an object displaying particularly clear evidence for such an interaction.

1. Observations of PKS2250-41

We are conducting a study at ESO of low and intermediate redshift radio galaxies, such objects being sufficiently

distant to show characteristics typical of high redshift galaxies, but sufficiently nearby to allow detailed study (Tadhunter et al. 1993, Morganti et al. 1993). As part of this survey, PKS2250-41 ($z=0.31$) was observed with the ESO 3.6-m in July 1993 using EFOSC in broad/narrow-band imaging, spectroscopic and polarimetric modes.

The narrow-band [OIII] image is shown in Figure 1. The striking morphology of this object, in particular the emission-line arcs, are clearly indicative of a strong jet/cloud interaction; the west-

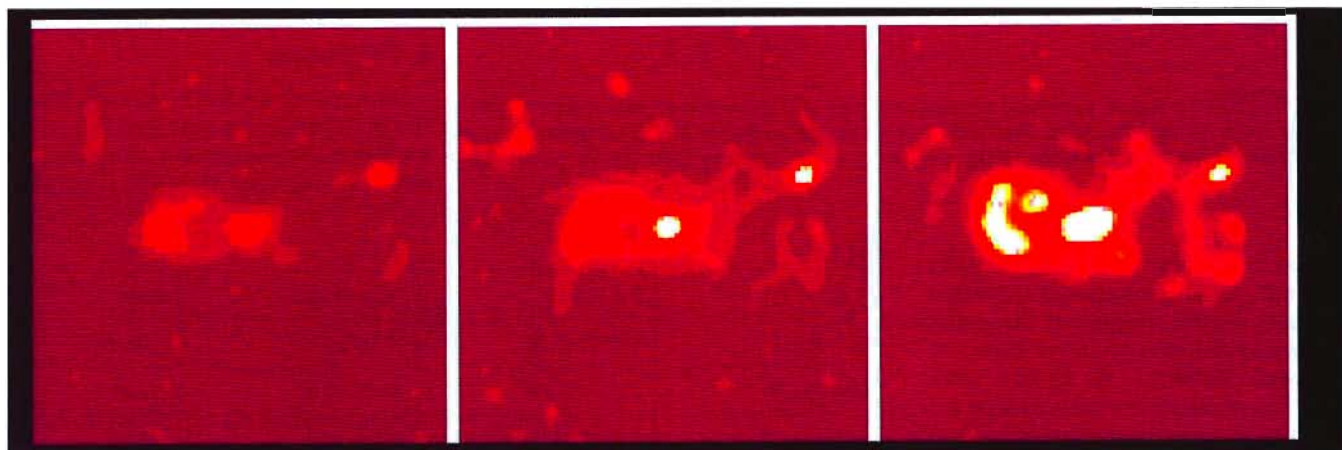


Figure 1: A montage of 5-min B (left), 5-min V (centre) and 30-min [OIII] ($\lambda 5007 \text{ \AA}$ - right) images of a 58 arcsec square area centred on the nucleus of PKS2250-41. The images have been derived after undertaking Richardson-Lucy restoration using PSF's derived from stars on the original EFOSC frames, although all of the structure evident in these frames are also clearly seen in the original images. North is up, east to the right.

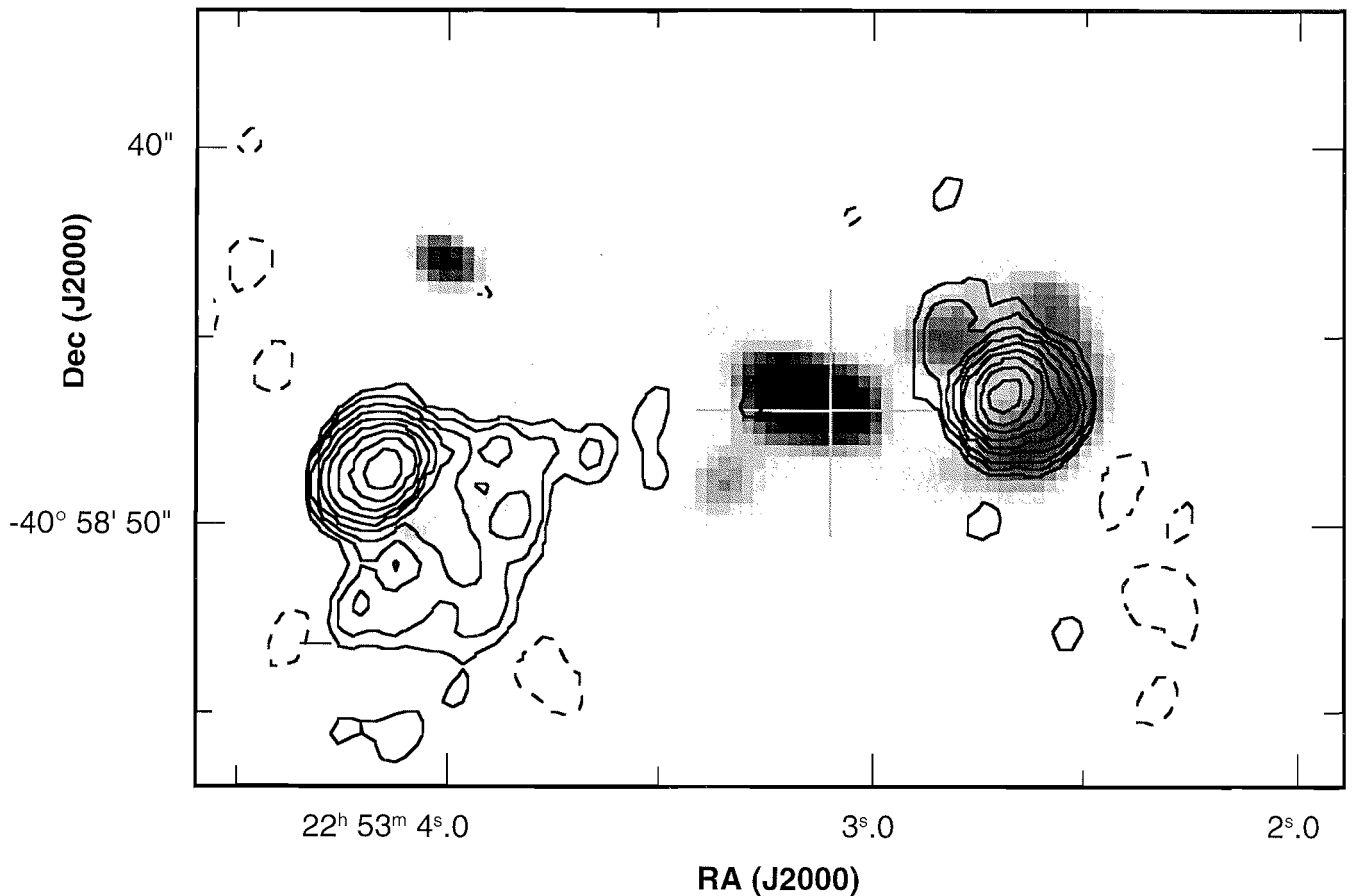


Figure 2: Greyscale of the original (unrestored) [OIII] image with superposed 8 GHz radio contours derived from ATNF observations in February 1994. The large cross marks the location of the optical nucleus, and the radio beam size is 1.2×0.9 arcsecs along a P.A. of -30° .

ernmost arc has the appearance of a bow shock, whilst east of the nucleus two (fainter) concentric arcs are evident. There also exist holes through each eastern arc, these being aligned with the nucleus/jet axis and possibly implying subsequent excavation of a cavity in the emission-line gas by the radio jet. A similar instance has recently been inferred by Jackson et al. (1993) from HST observations of Cygnus A. The dimensions of the structures evident in this figure are also impressive: the western and (innermost) eastern arcs are 35 kpc and 60 kpc from the nucleus ($H_0 = 50 \text{ km s}^{-1} \text{ Mpc}^{-1}$ and $q_0 = 0.0$).

The spatial correspondence between the emission-line arcs and radio lobes is excellent (Fig. 2), and suggests a causal link between the structures. Interestingly, the western and eastern arcs are also sites of continuum emission, both components being seen in broad-band B and V images (Fig. 1).

Further support for the jet/cloud hypothesis comes from our spectroscopic and polarimetric observations. The 60-min blue spectra show the nucleus to possess line ratios typical of a photoionized narrow line region in an AGN, whilst the western arc is more consistent with photoionization or shock excitation. Moreover, our 3-hour B-band

polarimetry results place a 3σ upper limit of $\lesssim 3.5\%$ on the degree of polarization in the western arc within 2.5–6.2 arcsec diameter apertures. By contrast, the nucleus is polarized at $5.0 (\pm 0.7)\%$ over equivalent apertures, at a position angle misaligned from the innermost optical isophotes by $77 \pm 6^\circ$.

2. Implications

Our polarization measurements suggest that the rest wavelength UV continuum of the nucleus in PKS 2250-41 is dominated by scattering from an AGN. Conversely, the western arc appears to possess continuum flux generated locally, possibly from the light of hot stars and/or by recombination continuum flux from warm ionized gas.

To our knowledge, this is the most striking evidence to date for jet-induced phenomena in powerful radio galaxies. The question arises as to why the emission-line arcs are so clear in this object. Also, why do they show such excellent spatial coincidence with the radio lobes, even though shock models imply that the primary emission lines arise in regions considerably downstream from the shock? We believe the most likely reason is that the radio jets have encountered a particularly dense region of the ISM in the host galaxy, or in a merg-

ing companion, in a manner similar to that inferred by van Breugel et al. (1985) in the case of 3C277.3.

If PKS 2250-41 is indeed typical of its high redshift radio galaxy counterparts, the importance of jet/cloud interactions implied by our observations is significant. For example, although scattered light is undoubtedly a contributory factor in the alignment effect (e.g. Tadhunter et al. 1992, Cimatti et al. 1993), objects like PKS 2250-41 suggest that scattering is not the whole story. A more detailed account of this work is being submitted to *Astronomy and Astrophysics Letters*.

References

- Cimatti, A., di Serego Alighieri, S., Fosbury, R., Salvati, M., & Taylor, D., 1993. *MNRAS*, **264**, 421.
- Jackson, N., Sparks, W., Miley, G., & Macchetto, F., 1993. *A & A*, in press.
- Morganti, R., Killeen, N., & Tadhunter, C., 1993. *MNRAS*, **263**, 1023.
- Tadhunter, C., Scarrott, S., Draper, P., & Rolph, C., 1992. *MNRAS*, **256**, 53p.
- Tadhunter, C., Morganti, R., di Serego Alighieri, S., Fosbury, R., & Danziger, I., 1993. *MNRAS*, **263**, 999.
- van Breugel, W., & Dey, A., *ApJ*, **414**, 563.
- van Breugel, W., Miley, G., Heckman, T., Butcher, H., & Bridle, A., 1985. *ApJ*, **290**, 496.

The Lithium Isotope Ratio in Metal-Poor Stars

P.E. NISSEN¹, D.L. LAMBERT² and V.V. SMITH²

¹*Institute of Physics and Astronomy, University of Aarhus, Denmark*

²*Department of Astronomy, University of Texas at Austin, U.S.A.*

1. Introduction

In the present article the scientific reasons for studying the lithium isotope ratio in stars are briefly reviewed, and the reduction and analysis of recent observations of the Li I 6707.8 Å resonance line in spectra of metal-poor stars are discussed in some detail. The aim and prospects of obtaining similar observations for fainter and more interesting stars with the ESO VLT are also touched upon.

2. Scientific Background

It is evident from the hundreds of astronomical papers of lithium published in the last 10 years that knowledge about the Li abundance in stars is of fundamental importance in studying the history of the Universe as well as the structure and evolution of stars. This is due to the many interesting processes by which lithium can be made at different times and places in the Universe. Most important is that Big Bang nucleosynthesis leads to a primordial abundance of Li, which depends on the physical conditions in the Big Bang phase, e.g. the baryon density and the degree of inhomogeneity. Measuring the primordial Li abundance therefore constrains Big Bang models. The discovery by Spite & Spite (1982) that the hotter Pop. II subdwarfs have a nearly constant Li abundance ($\log \epsilon(\text{Li}) \approx 2.1$, where $\epsilon(\text{Li}) = N_{\text{Li}}/N_{\text{H}} \cdot 10^{12}$) suggests that this is the value of the primordial Li abundance in agreement with predictions from the Standard Big Bang model. Other processes may, however, have affected the Li abundance in the atmospheres of Pop. II stars. Li is produced by cosmic ray spallation of C, N, O nuclei and $\alpha + \alpha$ fusion in the interstellar space. Possible stellar sources of Li include envelope burning in AGB stars and $p + \alpha$ reactions in flares. In addition Li is destroyed by protons at the bottom of the convection zone if the temperature there is higher than about 2×10^6 K. Hence, both Galactic and stellar evolution of lithium is a complicated affair, but by understanding the various processes better we will learn more about stellar and Galactic evolution and may be able to determine an accurate value of the primordial Li abundance.

In order to disentangle the relative importance of the various processes

that produce or destroy lithium it is important to know not only the total Li abundance but also the lithium isotope ratio ${}^6\text{Li}/{}^7\text{Li}$. The reason for this is that in some cases, e.g. Big Bang nucleosynthesis and envelope burning in AGB stars, ${}^7\text{Li}$ only is produced, whereas other processes, e.g. $\alpha + \alpha$ burning and flare events, produce both ${}^6\text{Li}$ and ${}^7\text{Li}$. In addition, ${}^6\text{Li}$ is destroyed more quickly than ${}^7\text{Li}$ at the bottom of the convection zone in F and G stars.

The lithium isotope ratio in the solar system is known to be ${}^6\text{Li}/{}^7\text{Li} = 0.08$ from analysis of meteorites. Recently, about the same ratio has been measured in the interstellar gas (Lemoine et al., 1993; Meyer et al. 1993). From earlier attempts to measure the isotope ratio in both Pop. I and II, F and G main sequence stars (Andersen et al. 1984, Maurice et al. 1984 and Pilachowski et al. 1989) an upper limit ${}^6\text{Li}/{}^7\text{Li} < 0.10$ has been set. Recently, ${}^6\text{Li}$ has, however, probably been detected in one Pop. II star (HD 84937, $T_{\text{eff}} \approx 6200$ K and $[\text{Fe}/\text{H}] \approx -2.4$) at a level of ${}^6\text{Li}/{}^7\text{Li} = 0.05 \pm 0.02$ by Smith, Lambert & Nissen (1993). This abundance of ${}^6\text{Li}$ in HD 84937 is about the value one would expect from the measured Be and B

abundances in metal-poor stars (Gilmore et al. 1991, Edvardsson et al. 1994) and the known cross sections for producing the isotopes of Li, Be and B by $\alpha + \alpha$ fusion and C, N, O spallation, assuming a small degree of Li depletion as predicted by standard (non-rotating) stellar models. Models predicting a strong (factor of 10) ${}^7\text{Li}$ depletion in subdwarfs seem to be excluded because according to these models there should be practically no ${}^6\text{Li}$ left in HD 84937. Hence, the detection of ${}^6\text{Li}$ supports the idea that the Li abundance in the hotter subdwarfs really represents the primordial abundance except for a small (10 %) contribution from Galactic cosmic ray processes.

In view of the important consequences of the detection of ${}^6\text{Li}$ in HD 84937 independent determinations of the lithium isotope ratio in HD 84937 and other turnoff halo stars are very desirable. Furthermore, it would be interesting to study the ${}^6\text{Li}/{}^7\text{Li}$ ratio as a function of $[\text{Fe}/\text{H}]$ in order to see how the various processes mentioned above contribute to the evolution of Li in the Galaxy. In the following some new observations at ESO with this aim are described, and problems connected with

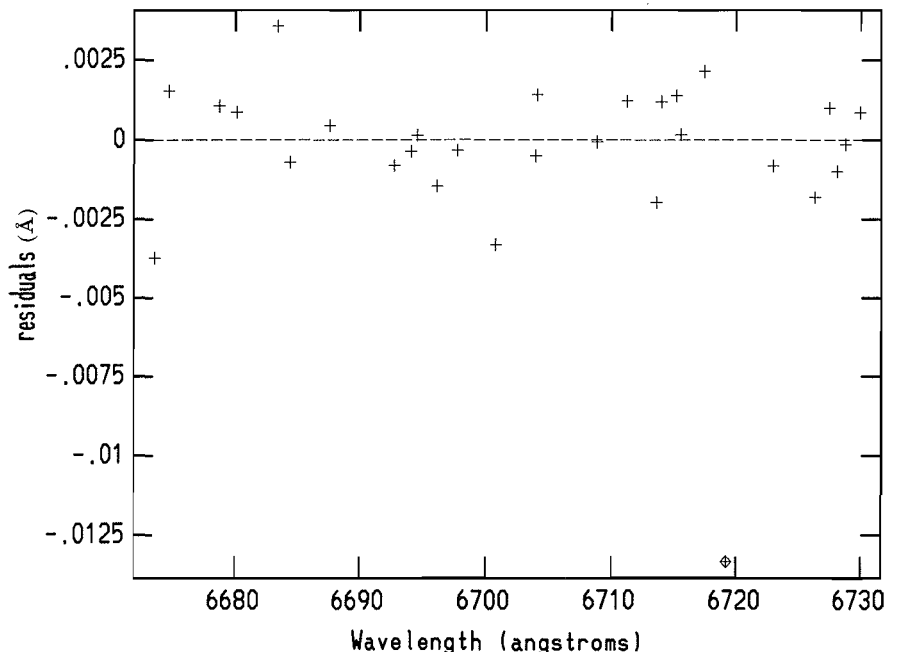


Figure 1: The residuals of the wavelength of 29 thorium lines from a 2nd-order dispersion solution. One strongly deviating line at 6719.2 Å is indicated by a special symbol. As discussed in the text this is caused by an argon line blending the thorium line. The rms deviation of the other lines is 1.5 mÅ.

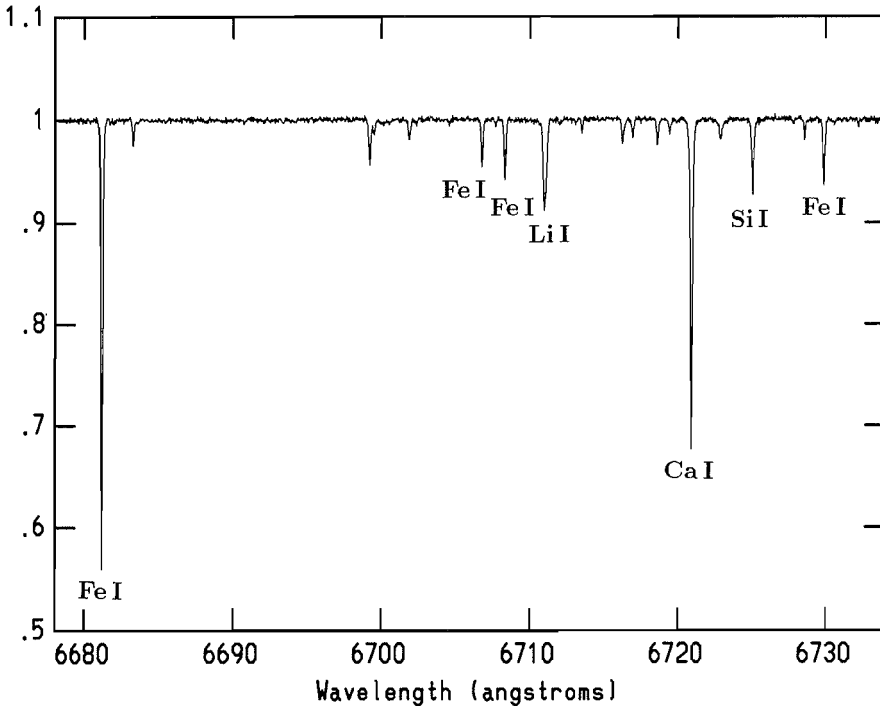


Figure 2: The spectrum of HD 76932 ($V=5.8$) as observed with the ESO Coudé Echelle Spectrometer connected to the 3.6-m telescope by a fibre link. The lines used in connection with the determination of the lithium isotope ratio are identified. The spectrum has not been corrected for the Doppler shift due to the radial velocity of the star.

an accurate determination of the lithium isotope ratio are discussed.

3. Observations and Reductions

The spectral region around the Li I 6707.8 Å resonance line was observed with the ESO Coudé Echelle Spectrometer (CES) during 8 nights in October 1992 and 4 nights in June 1993. In October the 1.4-m CAT telescope was used, whereas the 3.6-m and the fibre link to the CES were used for the June observations. In both cases the long camera of the CES was applied providing a resolution of $R=115,000$. The corresponding entrance slit width of the CES for the CAT observations was 1.2 arcsec. In connection with the 3.6-m observations an image slicer was used so that the entrance aperture at the 3.6-m could be as large as 3.4×3.4 arcsec. The detector was a 2048×2048 FA chip with 15 micron pixels and a read-out noise of about $10e^-$.

The observing run with the CAT telescope was primarily used to observe a number of metal-poor ($[Fe/H] \approx -0.8$) thick disk stars with magnitudes between 4 and 7, whereas the 3.6-m run was used for fainter halo stars with metallicities between -1.5 and -2.1 . The stars were selected to be in the turnoff region of Pop. II main sequence stars. Each star was observed on typically 4 different nights with slightly different settings of the central wavelength of the

CES to minimize the influence of possible defects of the CCD detector as well as irregularities in the flat-fielding procedure.

The spectra obtained were reduced with IRAF using tasks for subtraction of background, flat field correction, extraction of spectra, and wavelength calibration. Due to the use of an image slicer in connection with the 3.6-m observations each CCD frame consists of 8 individual spectra with different exposure levels. These were reduced separately and coadded after wavelength calibration. Finally, the spectra were rectified and normalized by fitting 5 pieces of cubic spline functions to the continuum.

Several aspects of the reductions are critical for the accuracy of the final spectra, in particular the wavelength calibration, the flat field correction and the determination of possible variations of the instrumental profile along the CCD caused by e.g. focus variations due to non-flatness of the CCD.

The wavelength calibration was performed by the aid of 29 thorium lines from a Th-Ar comparison lamp. A second order polynomial was adopted for the dispersion solution, i.e. wavelength vs. pixel coordinate. Residuals in the fit are shown in Figure 1. As seen the scatter is satisfactorily small, except for one strongly deviating line at 6719.2 Å. After contact with H. Hensberge, Brussels, who has made a detailed list of wavelengths of thorium lines including

notes on blends, it was cleared up that this deviating line is a close blend with an argon line. Excluding the 6719.2 Å line the rms deviation from the fit is 0.0015 Å or about 5% of the pixel width. We conclude that errors in the wavelength calibration are less than 0.002 Å or 2 mÅ. It should be noted that in the case of the 3.6-m observations the light from the Th-Ar lamp is sent via the fibre and through the image slicer. Hence, the light-pass through the optics of the CES is the same as for the star light. The same is true for the light from the flat fielding lamp. In the case of the CAT observations we don't have this favourable situation, so it is important that these observations are checked by observing some stars with both systems.

Figure 2 shows the combined spectrum of HD 76932 ($T_{\text{eff}} = 5970$ K, $[Fe/H] = -0.8$) obtained on June 6 and 8, 1993 with the fibre link to the 3.6-m telescope. The S/N of the spectrum is about 600. Figure 3 shows a detail of the region around the Li I line. For comparison the spectrum of HR 7121, an early B-type star with no spectral lines in this region, is also shown. It was reduced in the same way as HD 76932. As seen the spectrum of HR 7121 is indeed flat within its S/N of about 800.

Figure 3 also shows the profile of an unblended thorium line. It is symmetric and is well fitted by a Gaussian profile with a FWHM = 58 mÅ corresponding to a resolution of $R=115,000$. It was checked that there is no significant variation of this profile along the CCD; the FWHM varies between 58 and 60 mÅ only. Hence, we can assume that there are no focus variations along the spectrum, which is important when applying the profile method to determine the lithium isotope ratio.

In Figure 3 it is not possible to see the very broad, low-intensity wings that are always present in the profile of a spectrometer. The effect of these wings is equivalent to stray light in the dispersion direction, which one cannot account for by subtracting the light scattered perpendicular to the dispersion direction. From measurements of the profile of the laser line at 6328 Å it is, however, known that the equivalent amount of stray light for the CES in the red part of the spectrum is 1–2% only. Hence, it has only a marginal effect on the profiles of weak lines, but may in any case be included in the reductions.

4. Analysis

The Li I resonance line is a doublet with hyperfine structure. Accurate interferometric wavelength measurements have been carried out by Meissner et al.

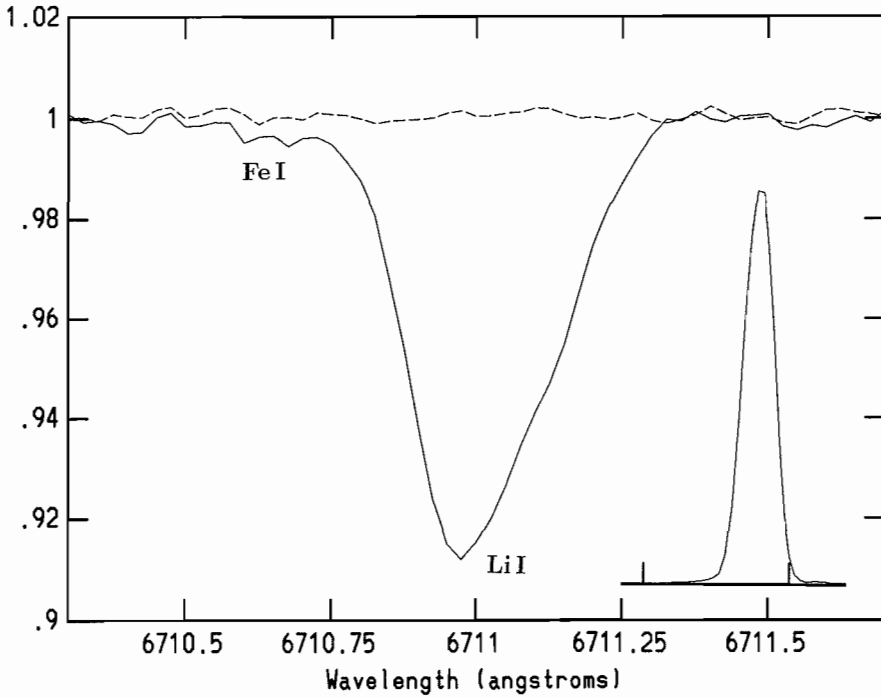


Figure 3: Detail of Figure 2. In addition to the Li I line a weak blending Fe I line is seen. For comparison the spectrum of an early B-type star, HR 7121 ($V = 2.1$) having no spectral lines in this region is shown with a dashed line. Furthermore, a thorium line is inserted in order to illustrate the instrumental profile of the CES.

(1948). The doublet splitting is 0.152 \AA and the isotope shift is 0.158 \AA with ${}^6\text{Li}$ having the longest wavelength (see Table 1 of Andersen et al. 1984). Hence, the stronger doublet component of ${}^6\text{Li}$ is superimposed on the weaker ${}^7\text{Li}$ component. Due to the various line broadening effects in a stellar atmosphere a rather complicated profile results. Figure 5 shows a model-atmosphere calculation of the Li line in HD 76932 for three values of ${}^6\text{Li}/\text{Li}$. As seen an increase of the ${}^6\text{Li}$ abundance has two effects: (i) a shift of the centre-of-gravity wavelength of the Li line amounting to 15 m\AA when ${}^6\text{Li}/\text{Li}$ is increased from 0.0 to 0.1, and (ii) an increase of the FWHM of the line, which amounts to 18 m\AA for the same increase of ${}^6\text{Li}/\text{Li}$. It means, that we have essentially two methods to determine the ${}^6\text{Li}/{}^7\text{Li}$ ratio: The centre-of-gravity method and the profile method. In the following we discuss these methods separately.

4.1 ${}^6\text{Li}/{}^7\text{Li}$ from centre-of-gravity (cog) wavelengths

When measuring the cog-wavelength of the Li line we must reduce the observed wavelength for the Doppler shift due to the radial velocity of the star and the gravitational redshift. In the case of HD 76932 the Doppler shift was determined from the lines identified in Figure 2. In metal-poor stars these lines are practically unblended. Very accurate wavelengths of the Fe I lines have recently been published by Nave et al. (1994). Furthermore, M. Rosberg and S. Johansson, Lund, have kindly measured a similar accurate wavelength of the Ca I line. The error of these wavelengths (Table 1) is less than 2 m\AA . The wavelength of the Si I line was adopted from Kurucz & Peytreman (1975) and is less accurate.

How well do the Doppler shifts determined from the various lines agree?

Table 2. The difference $\Delta\lambda$ between the measured cog-wavelength of the Li I line and the cog-wavelength corresponding to ${}^6\text{Li}/{}^7\text{Li} = 0.0$. The last column gives the equivalent width of the Li line.

Night	$\Delta\lambda$	W(Li)
Oct. 24, 1992	6.8 m\AA	24.9 m\AA
Oct. 25, 1992	6.2	24.4
Oct. 26, 1992	8.8	23.5
June 6, 1993	3.7	24.5
June 8, 1993	4.7	26.0
Average	6.0 m\AA	24.7 m\AA

Table 1 shows for each night the difference between the Doppler shift (in km s^{-1}) determined from an individual line and the mean Doppler shift for the six lines. As seen, there are some systematic differences which repeat from night to night. The weak, high-excitation lines appear to be slightly blueshifted (about 0.2 km s^{-1} or 4 m\AA) relative to the stronger, lower excitation potential lines (Fe I at 6678.0 \AA and Ca I at 6717.7 \AA). It may be due to small errors in the laboratory wavelengths, but it could also be caused by convective motions. In fact, similar systematic differences are seen in the solar spectrum (Dravins et al. 1981), and have been explained by a hydrodynamical model in which hot, rising bright granules are balanced by a downflow in darker (cooler) inter-granular regions. The result is a convective blueshift of the lines, which is more pronounced for the weak high-excitation lines because they are formed deep in the atmosphere where the convective motions are more vigorous.

Assuming that the convective blueshift of the Li I resonance line is the same as the mean shift of the Fe I 6678.0 \AA and Ca I 6717.7 \AA lines, the observed cog-wavelengths have been corrected for Doppler shift. The resulting difference, $\Delta\lambda$, relative to the cog-wavelength corresponding to ${}^6\text{Li}/{}^7\text{Li} = 0.0$ (6707.812 \AA) is listed in Table 2. As seen, the results from the various nights agree quite well. The average value of $\Delta\lambda$ is 6.0 m\AA , which would correspond to ${}^6\text{Li}/{}^7\text{Li} = 0.04$ if the shift was due to

Table 1: Values of $\Delta V = V_{\text{indv.}} - V_{\text{mean}}$ for HD 76932 as observed on 5 different nights. $V_{\text{indv.}}$ is the Doppler shift in km s^{-1} determined from a single line and V_{mean} is the mean Doppler shift for all six lines. The first 3 nights are from the Oct. 1992 observing run with the CAT, and nights 4 and 5 are from the June 1993 run with the fibre link to the 3.6 m. In col. 2 the excitation potential of the lower level of the line is given. Col. 3 lists the laboratory wavelength taken from sources given in the text and col. 4 the measured equivalent width of the line.

Line	χ	λ_{lab}	W	ΔV_1	ΔV_2	ΔV_3	ΔV_4	ΔV_5	ΔV_{mean}
Fe I	2.69 eV	6677.987 \AA	73 m\AA	0.14	0.15	0.10	0.25	0.13	0.15
Fe I	2.76	6703.567	6	0.27	0.05	-0.04	-0.07	0.04	0.04
Fe I	4.61	6705.102	9	-0.24	-0.10	0.07	-0.15	-0.04	-0.09
Ca I	2.71	6717.677	61	0.21	0.25	0.25	0.25	0.23	0.24
Si I	5.86	6721.848	13	-0.34	-0.34	-0.48	-0.28	-0.39	-0.37
Fe I	4.61	6726.667	10	0.05	-0.01	0.12	0.02	0.04	0.04

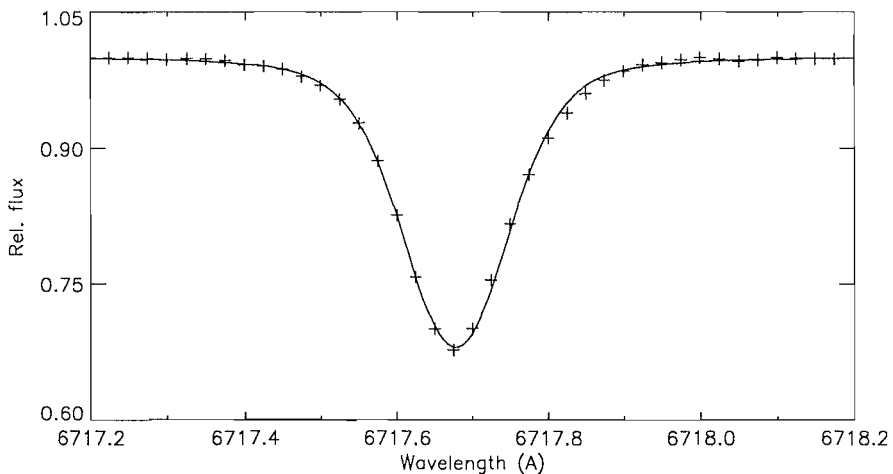


Figure 4: The observed profile of the CaI line of HD 76932 (+) compared with a synthetic model atmosphere profile convolved with a radial-tangential broadening function with the FWHM = 4.7 km s⁻¹. A slight asymmetry in the right wing of the observed profile is evident. It corresponds to a C-shaped line bisector.

the presence of ⁶Li. Differential convective blueshifts between the LiI line and the comparison lines may, however, be responsible for the positive value of $\Delta\lambda$. It is therefore doubtful that ⁶Li has been detected in HD 76932.

The total Li abundance of HD 76932 derived from the equivalent width ($W = 24.7$ mÅ) of the LiI line is $\epsilon(\text{Li}) = 2.06$, close to the value at the “Spite” plateau for halo stars. Two other stars observed (HD 22879 and HD 63077), have a much weaker Li line ($W = 7$ mÅ) despite the fact that they have about the same T_{eff} and $[\text{Fe}/\text{H}]$ as HD 76932. Their atmospheres are depleted in Li by a factor of 4–5, and we would therefore expect that they are totally depleted in ⁶Li. Still, the apparent ⁶Li/⁷Li ratio derived from the cog-wavelength is about 0.04. This points to a zero-point error in the method, probably due to differential convective blueshifts between the Li line and the FeI and CaI lines used for determining the Doppler shift of the star. We conclude that ⁶Li has not been detected in HD 76932. The upper limit for ⁶Li/⁷Li is about 0.03.

4.2. ⁶Li/⁷Li from the profile of the LiI line

As an example of this method we again use the spectrum of HD 76932. Synthetic spectra have been computed by the aid of a programme BSYN kindly made available by the stellar atmosphere group in Uppsala. The model atmosphere used has parameters, $T_{\text{eff}} = 5970$ K, $\log g = 4.4$ and $[\text{Fe}/\text{H}] = -0.8$. Details about the construction of the model and the determination of the model parameters of HD 76932 are given by Edvardsson et al. (1993). The model atmosphere computation in-

cludes thermal and microturbulent broadening with $\xi_{\text{turb}} = 1.4$ km s⁻¹ as determined by Edvardsson et al. In addition, the profiles of the lines are broadened by macroturbulent motions, rotation of the star and the instrumental profile. The synthetic spectrum was therefore folded by various broadening functions in order to reproduce the observed profiles of the FeI and CaI lines. It turns out that neither an isotropic Gaussian function nor a pure rotation profile lead to a satisfactory agreement between the observed and the synthetic profile. The best fit is obtained with a so-called radial-tangential profile (Gray 1976), which corresponds to radial and tangential motions in the atmosphere each with a Gaussian distribution of the velocities. The radial-tangential profile is more V-shaped than the U-shaped profiles corresponding to pure rotation or isotropic Gaussian broadening.

Figure 4 shows the resulting fit for the CaI line at 6717.7 Å. The equivalent width is the same for the observed and the synthetic line. A FWHM = 4.7 km s⁻¹ of the radial-tangential convolution profile is required to get the best overall fit. As seen, the fit is, however, not perfect. A slight asymmetry is apparent in the right wing of the Ca line. The observed points in the lower part of the line fall to the left of the synthetic line, whereas the points in the upper part fall to the right. Similar deviations are seen for the FeI lines in the spectrum of HD 76932. The asymmetry corresponds to a C-shaped line bisector, defined as the loci of points midway between equal-intensity points on either side of a line. C-shaped bisectors are well known for solar lines (Dravins et al. 1981) and have also been measured for a few of the brightest solar-type stars (Dravins 1987). Again, they

can be explained by convective motions. The brighter rising granules form a blueshifted component of the line, whereas the darker sinking regions form a weaker redshifted component. Although the effect on the line profile is small it has to be taken into account when one wants to determine very accurate values of the ⁶Li/⁷Li ratio.

Figure 5 shows the observed profile of the LiI line of HD 76932 compared to three synthetic profiles corresponding to ⁶Li/Li = 0.0, 0.1 and 0.2. The radial-tangential broadening function determined from the analysis of the CaI line has been applied. As seen, the profile corresponding to ⁶Li/⁷Li = 0.0 gives a nearly perfect fit to the data, especially when one takes into account the small asymmetry inherent in the observed CaI profile. Hence, like in the case of the cog-wavelength method there is no evidence of the presence of ⁶Li. From Figure 5 an upper limit ⁶Li/⁷Li < 0.03 can be set.

5. Results and the Need for VLT Observations

The spectrum of HD 76932 has been discussed in some detail above to illustrate the methods and accuracies by which the ⁶Li abundance in metal-poor stars can be determined. Results for other stars observed at ESO will be published in another paper. Here it should just be mentioned that for most of the stars studied ⁶Li seems not to be present in the atmosphere. This may well be due to the fact that these stars are too cool ($T_{\text{eff}} < 6000$ K) for ⁶Li to survive depletion at the bottom of the convection zone. Somewhat hotter stars at the very bluest point of the Pop. II turnoff sequence, like HD 84937 ($T_{\text{eff}} \approx 6200$ K) are more interesting candidates for ⁶Li determinations. But these stars are rare. One such star (CD -30°18140, $[\text{Fe}/\text{H}] = -2.1$) was observed with the fibre link to the 3.6-m. However, due to its faintness ($V = 10.0$), the S/N obtained is not quite sufficient for an accurate determination of the ⁶Li/⁷Li ratio despite the fact that a total of 10 hours of observing time was spent on the star.

There is a clear need for the light collecting power of the ESO VLT to reach a statistically significant sample of metal-poor stars at the turnoff point. With the planned UVES instrument it will be possible to reach $R = 120,000$ in the red, which is sufficient for determinations of the ⁶Li/⁷Li ratio. However, because of the use of an R4 echelle grating in UVES, the tilt of spectral lines along one order will change quite significantly ($\pm 1.4^\circ$), and the dispersion will change by about 30%. This puts high demands on the reduction software if high S/N

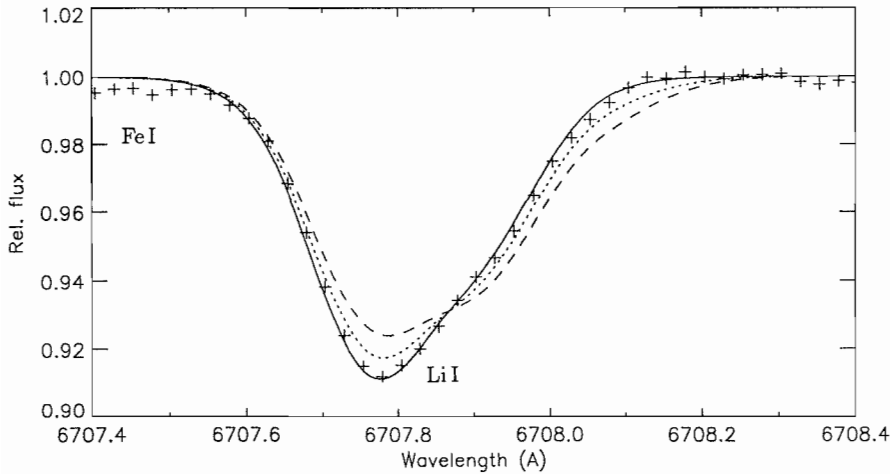


Figure 5: The observed profile of the Li I line of HD 76932 (+) compared with synthetic model atmosphere profiles convolved with a radial-tangential broadening function with the FWHM = 4.7 km s^{-1} and corresponding to ${}^6\text{Li}/\text{Li} = 0.0, 0.1$ and 0.2 , respectively. The position of a weak Fe I line at 6707.4 \AA is marked.

(> 400) and accurate wavelength calibration are to be obtained. A dedicated spectrometer with a well-defined profile similar to the CES but allowing resolutions up to $R = 300,000$ for a limited spectral region, say $\Delta\lambda = 100 \text{ \AA}$, would be a better instrument for a ${}^6\text{Li}$ programme. In addition, such an instrument

would be needed for many other programmes like studies of the hydrodynamics of stellar atmospheres and the composition of interstellar gas.

References

Andersen, J., Gustafsson, B., Lambert, D.L. 1984, *A&A* **136**, 65.

Dravins, D. 1987, *A&A* **172**, 211.
 Dravins, D., Lindegren, L., Nordlund, Å. 1981, *A&A* **96**, 345.
 Edvardsson, B., Andersen, J., Gustafsson, B., Lambert, D.L., Nissen, P.E., Tomkin, J. 1993, *A&A* **275**, 101.
 Edvardsson, B., Gustafsson, B., Johansson, S.G., Kiselman, D., Lambert, D.L., Nissen, P.E., Gilmore, G. 1994, *A&A* (in press).
 Gilmore, G., Gustafsson, B., Edvardsson, B., Nissen, P.E. 1992, *Nature* **357**, 379.
 Gray, D.F. 1976, "The Observation and Analysis of Stellar Photospheres", John Wiley and Sons, p. 426.
 Kurucz, R.L. Peytremann, E. 1975, *Smithsonian Astrophys. Obs. Spec. Rep.* 362.
 Lemoine, M., Ferlet, R., Vidal-Madjar, A., Emerich, C., Bertin, P. 1993, *A&A* **269**, 469.
 Maurice, E., Spite, F., Spite, M. 1984, *A&A* **132**, 278.
 Meissner, K.W., Mundie, L.G., Stelson, P.H. 1948, *Phys. Rev.* **74**, 932.
 Meyer, D.M., Hawkins, I., Wright, E.L. 1993, *ApJ* **409**, L61.
 Nave, G., Johansson, S., Learner, R.C.M., Thorne, A.P., Brault, J.W. 1994, *ApJS* (in press).
 Pilachowski, C.A., Hobbs, L.M., De Young, D.S. 1989, *ApJ* **345**, L39.
 Smith, V.V., Lambert, D.L., Nissen, P.E. 1993, *ApJ* **408**, 262.
 Spite, F., Spite, M. 1982, *A&A* **115**, 357.

The Kinematics of the Planetary Nebulae in the Outer Regions of NGC 1399

M. ARNABOLDI¹, K.C. FREEMAN¹, X. HUI², M. CAPACCIOLI^{3,4} and H. FORD⁵

¹Mt. Stromlo Observatory, Canberra ACT, Australia

²Astronomy Department, California Institute of Technology, Pasadena, U.S.A.

³Dipartimento di Astronomia, Università di Padova, Padova, Italy

⁴Osservatorio Astronomico di Capodimonte, Napoli, Italy

⁵Physics and Astronomy Department, The Johns Hopkins University, Baltimore, U.S.A.

1. Introduction

Integrated light observations of the inner regions of giant elliptical galaxies indicate that most of them are slow rotators (e.g. Capaccioli & Longo 1994), with specific angular momentum J/M that is 5 to 10 times less than for the disks of giant spirals (e.g. Fall 1983). Cosmological simulations (e.g. Zurek et al. 1988) show that J/M should be similar in a cluster environment (where spheroidal systems are preferentially found) and in the field (where the disk galaxies predominate). As a way around this problem, Hui et al. (1993) suggested that much of the angular momentum of these elliptical galaxies may reside in their outermost parts (beyond 20 kpc), which cannot be studied by integrated

light techniques. This suggestion was made following the recent radial velocity measurements of 500 planetary nebulae (PN) in the giant elliptical Centaurus A, extending out to about 20 kpc from the nucleus (for comparison, kinematical observations from integrated light reach out only about 5 kpc from the nucleus). The velocities of the PNe in Cen A showed a surprising result: its outer halo is rapidly rotating. The mean rotational velocity rises slowly from the centre of the galaxy and flattens to a value of about 100 km/s between 10 and 20 kpc from the centre. This property was not at all apparent from the integrated light observations of the inner regions. Another very interesting dynamical feature of Cen A is that its metal-weak

globular cluster system, which also extends out to about 20 kpc, does not appear to be rotating at all (Harris et al. 1988).

Cen A is an unusual and disturbed elliptical system. One would like to investigate the outer halo of undisturbed ellipticals to see (i) if their old stellar populations are also rapidly rotating and (ii) if their globular cluster systems are non-rotating, as in Cen A. It would be interesting to make such a study for normal giant ellipticals and also for the dominant giant ellipticals in clusters. Many of these cD galaxies have huge globular cluster populations and extended halos, and may well have different formation histories. The nearest of these giant galaxies, at distances of

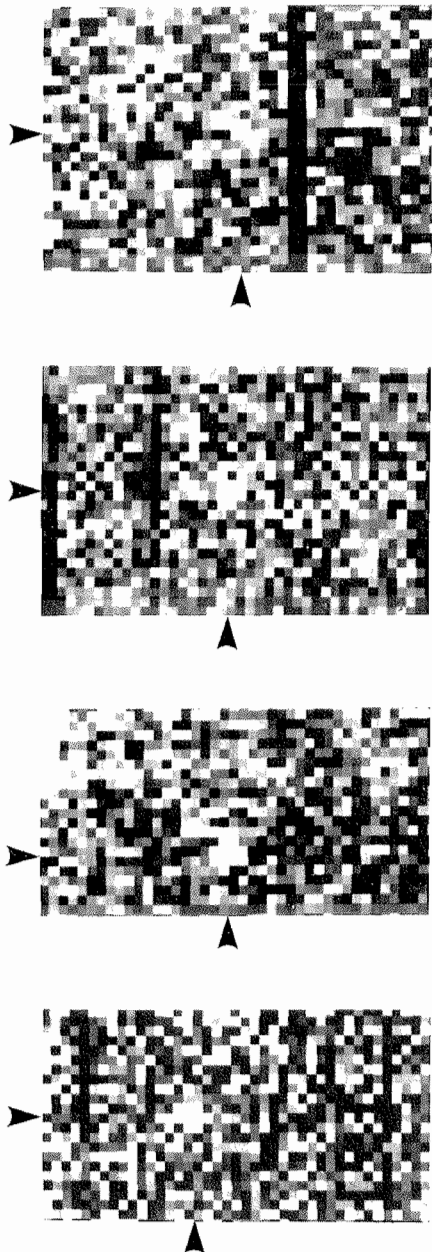


Figure 1: Images of the 2D spectra of some individual PNe in NGC 1399. In each image, the wavelength direction lies along the long axis, and the spatial direction (i.e. the direction along the slitlet) lies along the short axis. Each image shows about 40 \AA in wavelength. The spatial extent of the images varies but can be estimated from the pixel scale of 0.35 arcsec per pixel. The $\lambda 5007 \text{ \AA}$ emission is indicated by the arrows.

about 15 Mpc, have until now been out of reach for studies of PN kinematics. In this paper we present our new data, from the NTT and EMMI, on the dynamics of the PNe in the outer regions of the cD galaxy NGC 1399 in the Fornax Cluster (adopted distance $\Delta = 16.9 \text{ Mpc}$). We chose this galaxy as our first candidate, because Grillmair et al. (1994) have already studied the kinematics of its globular cluster system, showing that it has negligible rotation. Our

measurements of the PNe kinematics in NGC 1399 extend out to a radius of 4.5 arcmin or 24 kpc, where the blue surface brightness of the integrated light is about $25 \text{ mag arcsec}^{-2}$.

Under subheading 2 we describe the observations and instrumental set-up for these observations. We discuss the data reductions and the errors in our velocity measurements under 3, the results under 4, and the conclusions are drawn under subheading 5.

2. Observations

We acquired spectra for 57 planetary nebulae in NGC 1399 with the ESO NTT at La Silla on November 14–16, 1993. We used the EMMI spectrograph in the red imaging and low dispersion mode (RILD) with multi-object spectra (MOS) plates, the FA 2048 Loral CCD ($15 \mu\text{m} \equiv 0.35 \text{ arcsec}$ pixels), and the #5 grism: this gives a wavelength range of 4120 to 6330 \AA and a dispersion of 1.7 \AA per pixel. The only emission line visible in the spectra of these faint PNe is [O III] $\lambda 5007 \text{ \AA}$, so a filter with $\lambda_c = 5050 \text{ \AA}$ and $\text{FWHM} = 500 \text{ \AA}$ was used in front of the grism to reduce the wavelength range of each spectrum. This allowed us to in-

crease the number of slitlets in each MOS mask and also to get enough emission lines from the calibration exposures for an accurate wavelength calibration. The size of the slitlets punched in the MOS plates is $1.2'' \times 8.6''$. Because the intrinsic width of the [O III] $\lambda 5007 \text{ \AA}$ line in PNe is only about 0.5 \AA , the detection of faint extragalactic PNe against the sky and galaxy background will be more effective with the higher resolution of the EMMI f/5.3 camera when it becomes available.

Production of the MOS plates – Astrometry and [O III] photometry for 60 PNe in NGC 1399 came from McMillan et al. (1993). We could not use their precise (α, δ) positions directly to produce the MOS plates, since an accurate map of the distortion in the NTT focal plane (NTT-fp) was not available. McMillan et al. kindly provided us with their deep (4-hour exposure) narrow-band [O III] image of NGC 1399, acquired at the prime focus imager of the CTIO 4-m telescope with a Tektronix 1024 CCD ($8' \times 8'$ field and $0.47''$ per pixel), from which the PNe were originally discovered. We were able to map the focal plane of the CTIO telescope on to the NTT-fp in a rather lengthy procedure

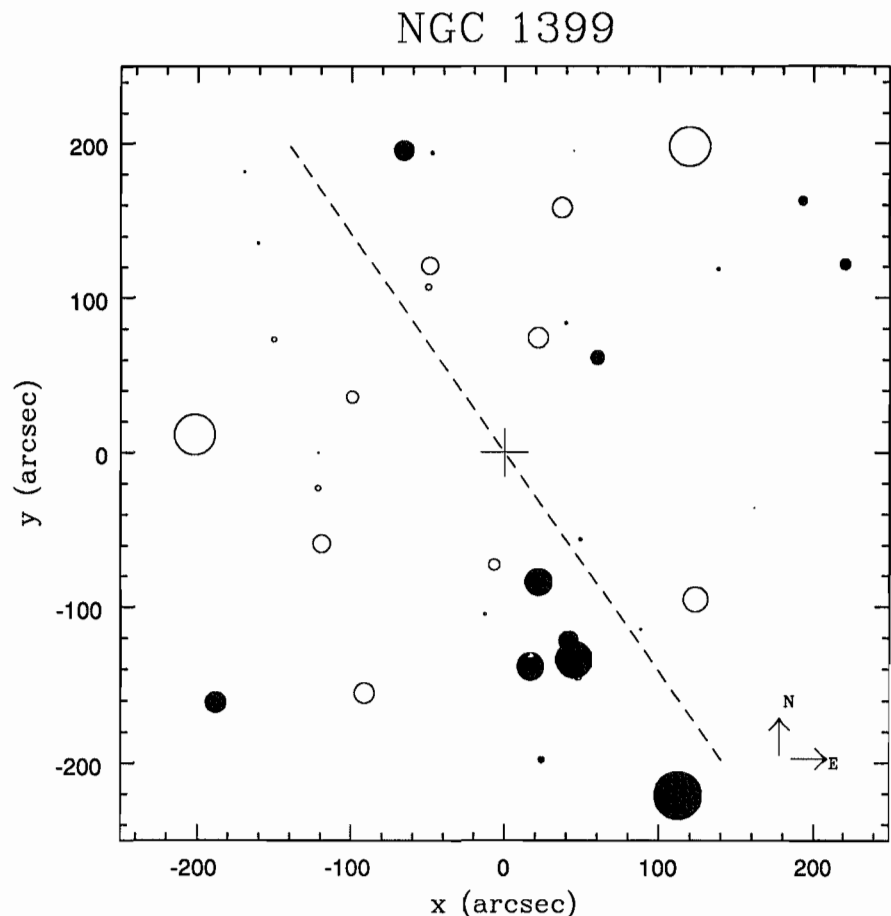


Figure 2: Positions of the PNe in the NGC 1399 field. The cross corresponds to the galaxy centre, North is up, East on the right. Full dots indicate velocities above the mean value $\bar{v} = 1503 \text{ km/s}$, open dots indicate velocities below \bar{v} . The size of the circle is proportional to the ratio $|v_{\text{obs}}/\bar{v} - 1|$. The dashed line shows the direction of maximum velocity gradient.

that was essential to the success of the observations.

To make this mapping, we requested a 5-min V-band exposure of the NGC 1399 field with the NTT, which Gauthier Mathys kindly obtained for us. We used about 40 stars in the field to derive the coordinate transformation between the CTIO and NTT images, using the IRAF processing software. (First it was necessary to filter out the effects of the steep luminosity gradient of the underlying elliptical galaxy.) The coordinate transformation over this small field turned out to be highly nonlinear: for adequate accuracy, a 3rd degree chebyshev function with cross terms was needed.

Our next problem was that the software allowed us to apply the coordinate transformation only to images: we were unable to find a way (short of writing our own programme) to obtain the NTT (x,y) coordinates directly from our CTIO (x,y) coordinate table. One quick and accurate way around this problem was to generate an artificial CTIO image with fake stars at the PNe (x,y) pixel positions. We applied the CTIO \rightarrow NTT coordinate transformation to this artificial image and then derived the PNe (x,y) positions in the NTT-fp using a centring algorithm. Finally we used the ascii file with these (x,y) positions to produce the MOS masks.

The CTIO image of NGC 1399 covered an $8' \times 8'$ field with PNe present over this entire area. The punch area for the MOS masks is $5' \times 8'$, so two MOS

masks were needed to include all the known PNe of NGC 1399. One mask was offset $75''$ East of the nucleus of NGC 1399, and the other $75''$ West, with an overlap of $2.4' \times 8'$. Our ascii file with the PN coordinates was adjusted accordingly: we decided which PNe went to which plate, and an offset to their x-coordinates was applied depending on whether they would appear on the East or West plate. The updated MIDAS tables corresponding to the East and West masks were copied to *.msk files, from which the MOS plates were punched. In addition to the slitlets punched at the PNe positions, two slitlets were punched in each MOS mask at positions correspondent to reference stars in the NGC 1399 field which we used to monitor the telescope pointing. The East mask contained 40 slitlets corresponding to 38 PNe plus the two stars, and the West mask has 42 slitlets (40 PNe and the two stars). In the overlapping region between the two masks there are 21 PNe and the two reference stars.

Before each exposure, we took an image at the mask position and then used the MIDAS task "pointing" to evaluate the x,y shifts needed to put the reference stars back at the centres of their punched slits. PNe spectra were taken only after our pointing had been checked: we noticed that the process of making calibration lamp exposures caused a significant shift of the telescope position, so a check for pointing was essential after each calibration.

The Observations. – Spectra were taken for the East field on November 14, with an average seeing FWHM = $0.9''$ and a total integration time of 3.8 hrs. The spectra for the West field were acquired on November 16, with an average seeing of FWHM = $1.0''$ and a total integration time of 4.7 hrs. One night was lost due to bad weather. The success of the observations depended very much on having the best possible image quality, so we performed imaging analysis twice a night and regularly checked the focus.

3. Data Reduction

Flat field exposures for the two MOS plates were taken with the internal lamp, the grism and the interference filter. The bias frames were flat and constant throughout each night, and so were the dark frames. Unfortunately, the performance of the Loral CCD was compromised by charge trapping problems which could not be corrected: some PNe were lost in the dark columns which extended for some tens of pixels.

Before combining all the frames obtained during one night, we carefully checked for any shifts in x and y which could possibly effect our velocity measurements. The stability of EMMI is exceptional. The average shift in the x (wavelength) direction was $\Delta x = 0.08$ pixels, which corresponds to a negligible velocity error of $\Delta v \cong 8$ km/s. The shifts in the y-direction were also very

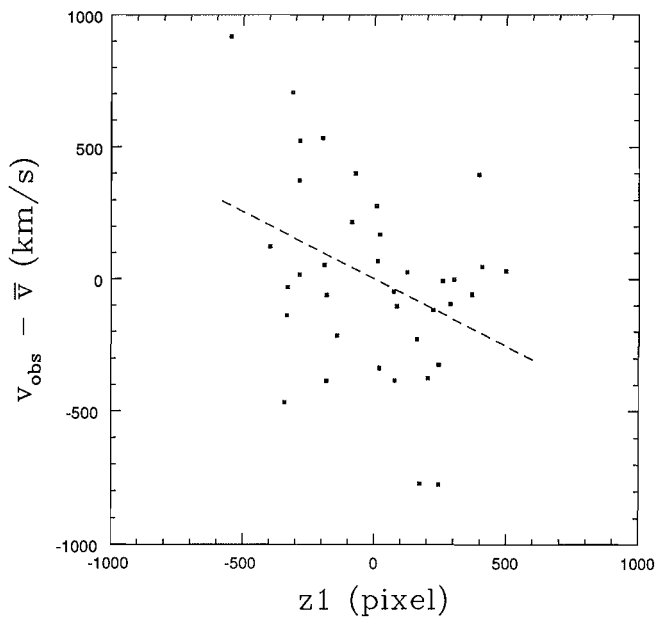


Figure 3: $v_{obs} - \bar{v}$ vs. $z1$, where $z1$ is the linear coordinate along the direction $z1$ of strongest velocity gradient. One pixel is 0.47 arcsec. The rotation is evident. The dashed line indicates the linear fit to the data.

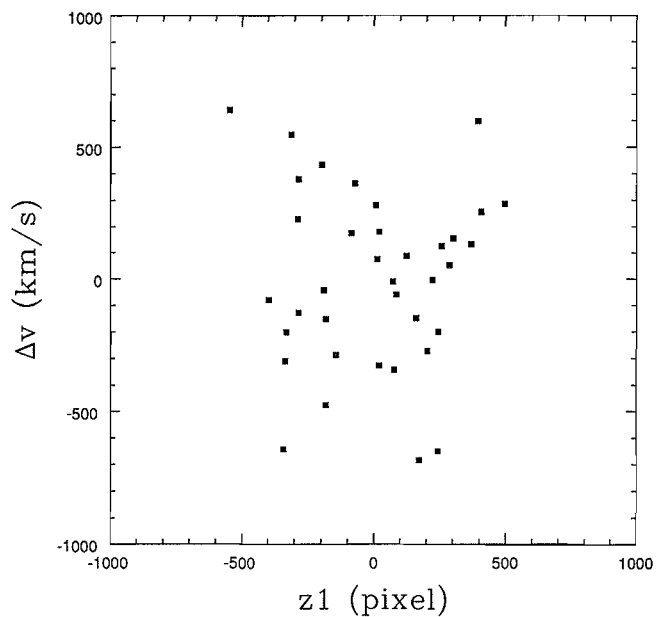


Figure 4: The velocity residual about the linear rotation fit Δv vs. $z1$, where $\Delta v = v_{obs} - v_{rot}$ and $z1$ is the linear coordinate along the direction of strongest velocity gradient. One pixel is 0.47 arcsec. The velocity residuals obtained after the subtraction of the rotation component are scattered around (0,0), and their distribution appears symmetric.

small, less than $\Delta y = 0.19$ pixels on both nights.

Therefore, we could directly combine the MOS frames and the calibration exposures obtained during a single night; after combining, the two resulting MOS frames appeared free of cosmic rays. Then the 2D spectra of each PN were extracted and wavelength calibrated using the corresponding He-Ar spectrum in the combined arc calibration frames. Figure 1 shows examples of these 2D spectra.

At this point we looked for the [O III] emission from the PN in the expected wavelength range¹ and at the expected PN y -position along the slitlet. We then subtracted the sky background, using the average of the sky rows for each individual spectrum. The rows where the [O III] emission appears were averaged and the redshifted $\lambda 5007 \text{ \AA}$ measured using a Gaussian fit.

Spectra were extracted for 54 PNe, and we were able to measure velocities for 37 PNe. Of the 21 PNe which appeared on both the East and the West MOS frames, 14 have velocity measurements, and they give us a direct estimate of the velocity errors. The distribution of their $\delta v = v_{\text{East}} - v_{\text{West}}$ gives $v_{\text{mean}} \equiv -15 \text{ km/s}$, indicating that there is no systematic velocity shift between the two nights, and a $\sigma(\delta v) = 103 \text{ km/s}$ which gives an error of $\pm 72 \text{ km/s}$ for a single velocity measurement.

4. Results

With the NTT and the EMMI/MOS facility, we have been able to measure velocities for PNe in the outer parts of the cD galaxy NGC 1399, between 5 and 24 kpc from the centre. This interesting region lies outside the limits of the integrated light observations, but overlaps the region covered by the globular cluster observations of Grillmair et al. (1994).

The PN velocities show that the outer parts of NGC 1399 are rotating. A 2D linear fit to the data gives a mean velocity $\bar{v} = 1503 \text{ km/s}$ and a maximum velocity gradient of $(1.09 \pm 0.46) \text{ km/s per arcsec}$ along P.A. = $-35^\circ \pm 26^\circ$. This maximum velocity gradient corresponds to $\pm 290 \text{ km/s}$ over $\pm 24 \text{ kpc}$. The rotation can be seen in Figure 2, which shows the PN positions in the NGC 1399 field indicated with open circles if their velocities are below \bar{v} , and with full circles if their velocities are above \bar{v} ; the size is proportional to the ratio $|v_{\text{obs}}/\bar{v} - 1|$. Figure 3 shows the observed velocity against the linear coordinate $z1$

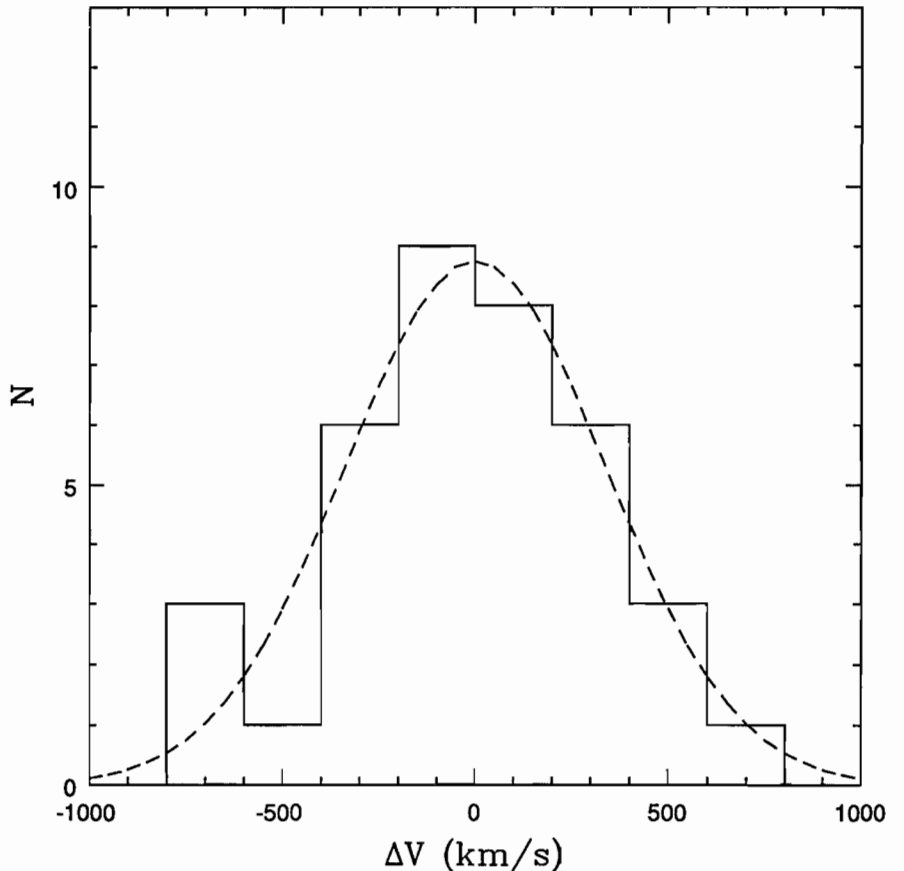


Figure 5: Histogram of Δv in bins of 200 km/s. The distribution is well approximated by a Gaussian (dashed line) with $\Delta v_{\text{mean}} = 0 \text{ km/s}$ and $\sigma = 342 \text{ km/s}$. No systematic residuals are left after the subtraction of the rotation velocity component.

along the direction of maximum gradient; again, the rotation is evident. The detailed pattern of rotation (now shown here) is more nearly cylindrical than spheroidal.

Figure 4 shows the distribution of residual velocities $\Delta v = v_{\text{obs}} - v_{\text{rot}}$ against $z1$. There is no residual velocity gradient, and the σ of the residual velocities is $\sigma_{\Delta v} = 342 \text{ km/s}$. The histogram of Δv values shown in Figure 5 is well represented by a Gaussian distribution with $\Delta v_{\text{mean}} = 0$ and $\sigma_{\Delta v} = 342 \text{ km/s}$. (The velocity dispersion of the raw observed velocities is $\sigma(v) = 364 \text{ km/s}$.)

Figure 6 shows the radial distribution of Δv . It appears that the velocity distribution of the PNe is not isothermal: the scatter of Δv increases with radius. If we divide our data into two subsamples with $r < \bar{r}$ and $r > \bar{r}$, where $\bar{r} = 2.6'$ is the average radius of the PN sample, we obtain $\bar{r}_1 = 1.9'$ and $\sigma_1 = 269 \text{ km/s}$ for the inner subset, and $\bar{r}_2 = 3.4'$ and $\sigma_2 = 405 \text{ km/s}$ for the outer subset, indicating that the velocity dispersion of the stellar component in NGC 1399 increases with radius. In Figure 7 we put together the measurements of velocity dispersion from integrated light and globular clusters (from Grillmair et al. 1994) and our

two PN points (r_1, σ_1) , (r_2, σ_2) in the $\sigma - \log r$ diagram for NGC 1399. The error bars show the measuring errors of the velocity dispersions for the integrated light data and the statistical errors for the velocity dispersion of the PNe and globular clusters. The PN velocity dispersion points fall nicely in the region between the globular clusters and the integrated light. They confirm previous indications (Grillmair et al. 1994) that the velocity dispersion increases in the outer parts of NGC 1399, giving a value for $M/L_B(4')$ greater than 80. For comparison, the dotted line in Figure 7 shows our linear (i.e. solid body) fit to the rotation of the PN system. We note that, as in Cen A, the outer stellar halo of NGC 1399 shows significant rotation, while its globular cluster system is apparently not rotating.

5. Conclusions

At present the NTT with EMMI is the only system in the world with which we can acquire spectra of distant extragalactic PNe with [O III] $\lambda 5007 \text{ \AA}$ fluxes below about $3 \cdot 10^{-17} \text{ ergs cm}^{-2} \text{ s}^{-1}$. We have used this system in multislit mode

¹ The expected wavelength range is $5031 \pm 17 \text{ \AA}$, corresponding to the galaxy redshift of 1440 km/s (RC3) $\pm 1000 \text{ km/s}$.

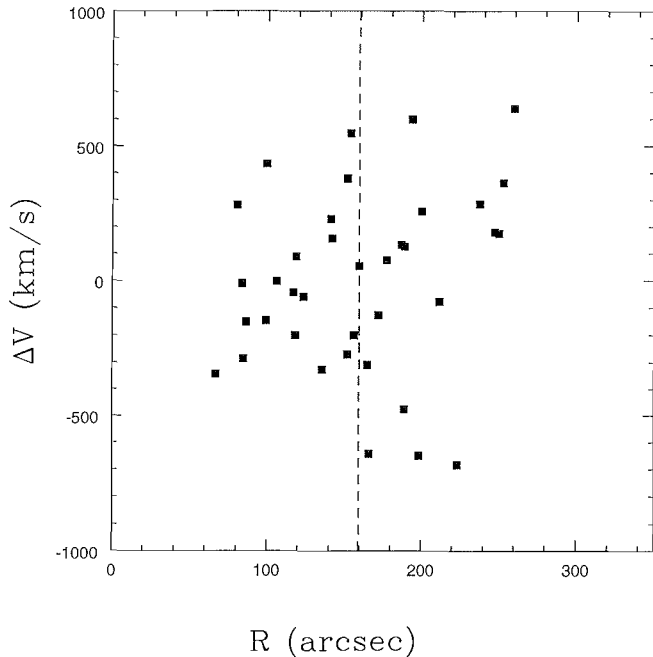


Figure 6: Δv vs. radius r : the residual velocity data appear to be more scattered at larger radii. The dashed line indicates the average radius of the distribution, at $\bar{r} = 2.65$ arcmin.

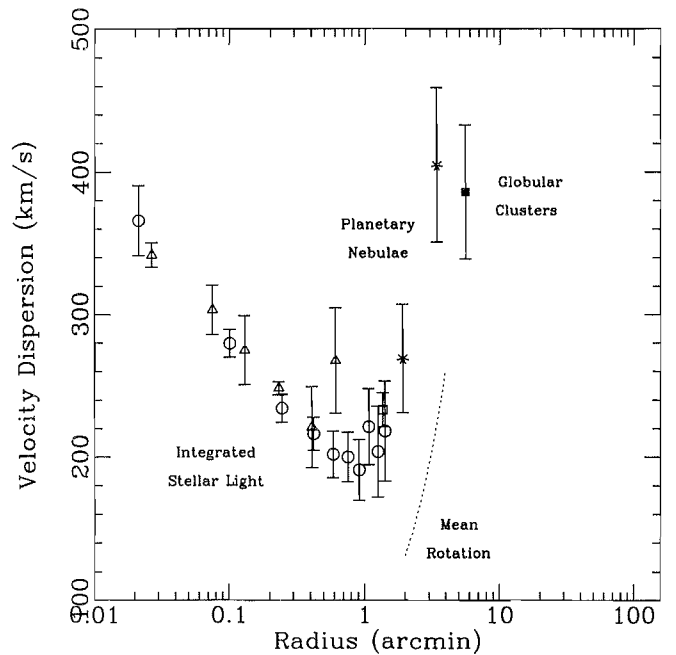


Figure 7: Velocity dispersion σ vs log r for (i) integrated light of NGC 1399 (open circles and triangles), (ii) the globular clusters in NGC 1399 (filled square) and (iii) our PNe velocity measurements (stars). The dotted curve shows the rotational velocity for our solid body rotation fit to the velocities of the PNe. For comparison, the surface brightness of NGC 1399 at a radius of 3 arcmin is $\mu_B = 24.5$ mag arcsec $^{-2}$.

to measure radial velocities of a sample of PNe in the outer regions of NGC 1399. From the PNe, the outer parts of this giant elliptical show substantial rotation. However, the velocity distribution of the globular clusters around NGC 1399 from Grillmair et al. (1994) shows no significant evidence of rotation. So it seems that the stellar halo of NGC 1399 rotates rapidly and its globular cluster system is not rotating at all (cf. Centaurus A).

The direction of maximum velocity gradient among the PNe in NGC 1399 lies in P.A. = -35° , which is close to the direction of the nearby giant elliptical NGC 1404. It is possible that the rotation of the old stars (PNe) in the outer parts of NGC 1399 could be induced by tidal interaction between the two giant ellipticals. The absence of rotation in the globular cluster system might then suggest that the very extended old stellar population in this cD galaxy, including the PNe, is part of the tidal debris, while the globular clusters belong to the original NGC 1399.

More generally, if the rapid rotation of the PN system of NGC 1399 reflects the mean motion of the bulk of the luminous component in the outer regions of this galaxy, then the outer regions contain a large amount of angular momentum. We can show that the total specific angular momentum J/M of this giant elliptical is in fact comparable with that of giant spirals. However, we know that for the inner parts of giant ellipticals (including

NGC 1399) the J/M is typically an order of magnitude lower than for spirals of comparable mass (Fall 1983). What is predicted by theoretical studies of galaxy formation? Zurek et al. (1988) and Quinn & Zurek (1988) have studied the J/M distribution for dark halos as the halos are built up by secondary infall in their cosmological simulations. Redistribution of energy and angular momentum occurs through the interaction of the clumps in the aggregating system. Clumps with lower J/M become more bound and lose J/M as they settle to the centre of the system, while the less bound objects with higher J/M gain angular momentum and form the outer parts of the resulting system. This secondary infall picture produces a system with low J/M in the inner regions and higher J/M in the outer regions. Although these models represent aggregating dark halos, the gross dynamical properties (the λ -parameter, shape distribution, mean motion v/σ) of these theoretical dark halos and the luminous components of real elliptical galaxies are very similar, and we can regard our observations of the outer parts of NGC 1399 as consistent with these secondary infall models.

Our velocity dispersion measurements for the PN confirm the previous evidence from the globular cluster kinematics for a high dark matter content in NGC 1399, and are consistent with a M/L_B ratio at least 80 within 4 arcmin.

Acknowledgements

We are grateful to S. D'Odorico, J. Melnick, G. Mathys, and the NTT night staff for much assistance before and during our run at the NTT, to P. Quinn for advice on galaxy formation, and to M. Bessell and G. Bloxham for their help with acquisition of the filter. The assistance of P. Le Saux, in modifying the EMMI punch programme and preparing the MOS masks by the non-standard process described above, was essential to the success of this observing run and is gratefully acknowledged.

References

- Capaccioli, M., & Longo, G. 1994. Preprint.
- Fall, S.M.F. 1983. In *IAU Symposium 100, Internal Kinematics and Dynamics of Galaxies*, ed. E. Athanassoula (Dordrecht: Reidel), p. 391.
- Grillmair, C.J. et al. 1994. *ApJ* **422**, L9.
- Harris, H.C., Harris G.L.H., Hesser, J.H. 1988. In *IAU Symposium 126, The Harlow-Shapley Symposium on Globular Cluster Systems in Galaxies*, eds. J.E. Grindlay and A.G. Davis Philip (Dordrecht: Reidel), p. 205.
- Hui, X., Ford, H.C., Freeman, K.C., Dopita, M.A. 1993. Preprint.
- McMillan, R., Ciardullo, R., Jacoby, G.H. 1993. *ApJ* **416**, 62.
- Quinn, P.J. & Zurek, W.H. 1988. *ApJ* **331**, 1.
- Zurek, W.H., Quinn, P.J., Salmon, J.K. 1988. *ApJ*, **330**, 519.

Milky Way Rotation from Cepheids

F. PONT, D. QUELOZ, M. MAYOR and G. BURKI

Geneva Observatory, Sauverny, Switzerland

More than one thousand radial velocity measurements of Milky Way classical Cepheids have been gathered since 1983 with the spectrometer CORAVEL¹ installed at the Danish 1.5-m telescope at La Silla. As they are bright, young disk population stars, with accurately known distances (via period-luminosity or period-luminosity-colour relations), and as their late spectral type facilitates radial velocity determinations, cepheids can be used as powerful indicators of the motion of the disk of our Galaxy. Indeed, 450 radial velocity measurements of faint cepheids were realized at La Silla specifically with the aim of studying the rotation of the Galaxy, in particular of obtaining accurate values for the Oort constant A , the curvature of the rotation curve and the distance to the galactic centre R_{\odot} . Recent developments in galactic dynamics, and N-body simulation techniques, may now permit some other finer characteristics of the local velocity field to be examined (Pont et al., 1994a, b).

As a follow-up of this programme, we began last winter measuring radial velocities of very faint galactic cepheids towards the outer parts of the Galaxy. These objects, inaccessible to CORAVEL, were observed with ELODIE², a fibre-fed echelle spectrograph installed at the 1.93-m telescope of the Haute-Provence Observatory, France. The radial velocities were computed from low signal-to-noise spectra using a cross-correlation technique, increasing the magnitude limit up to the 15th.

1. Centre-of-Mass Velocities

The measured radial velocity of a cepheid does not only reflect its movement in the Galaxy, but is a combination of this and the motion of its pulsating photosphere. Thus, a good phase coverage of the pulsation cycle is needed before the centre-of-mass velocity (or “ \dot{O} ”) can be evaluated.

Our strategy has been – in order to minimize the observation time – to get five measurements for each target cepheid evenly spread at 0.2 phase intervals. Five measurements proved sufficient to determine a cepheid \dot{O} with an

uncertainty of 2–3 km s⁻¹, small enough to be unimportant compared to the 9–11 km s⁻¹, intrinsic velocity dispersion of young stars such as the cepheids. The \dot{O} was evaluated by fitting either the light curve of the cepheid itself or the velocity curve of another cepheid of similar period to the five data points. The fitted curve can be written:

$$C(t) = v_o + A \times (\text{light or typical velocity curve } (t-t_o))$$

where the three free parameters v_o , A and t_o are the \dot{O} , the amplitude ratio and a zero-point phase shift (see Fig. 1).

The first method is justified by the fact that for extensively measured cepheids the light curve is observationally found to resemble the radial velocity curve. The second, from the fact that cepheids of similar periods tend to have similar

velocity curves (the curve shape follows the “Hertzsprung sequence”).

Only 450 measurements were sufficient to obtain a good estimate of the \dot{O} for 87 cepheids.

2. Galactic Rotation

The 87 new \dot{O} determinations were added to the existing sample of cepheids with known radial velocities, forming an extended sample of 278 galactic classical cepheids with reliable radial velocity and photometry. We then calculated distances for these objects through a Period-Luminosity-Colour relation due to Feast & Walker (1987). The position of the cepheids in the galactic disk as given by this relation is displayed in Figure 2, the cepheids measured with CORAVEL are drawn as black squares.

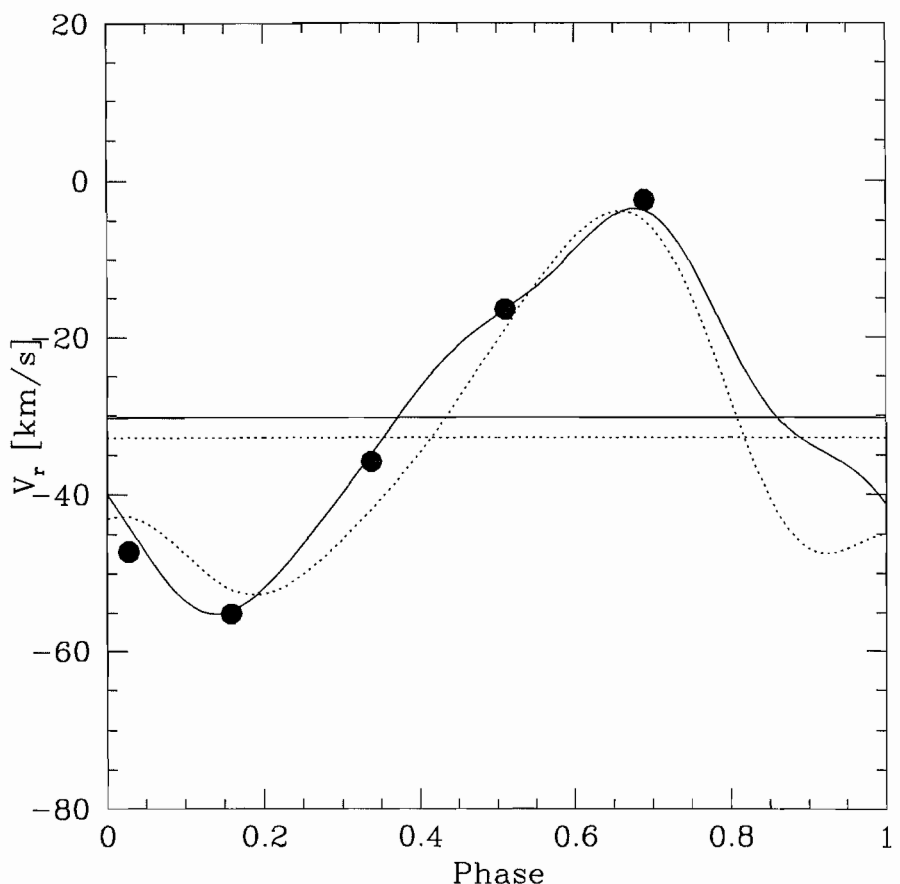


Figure 1: An example of our method of calculating the centre-of-mass velocity of a cepheid from 5 measurements with a good phase coverage. The five points are the measured radial velocities, subject to a 1–3 km s⁻¹ error, the continuous lines show the actual velocity curve and mean velocity, and the dashed lines show the fitted curve – the radial velocity curve of another cepheid with a similar period – and the recovered mean velocity. Even in this rather unfavourable case of an 11-day-period star (a period for which velocity curves are markedly heterogeneous) and with a slightly uneven phase coverage, the mean velocity is recovered within 3 km s⁻¹.

¹ For a description of CORAVEL, Baranne et al. (1979).

² A short presentation of ELODIE is given in “La lettre de l’OHP”, 1993, No. 11.

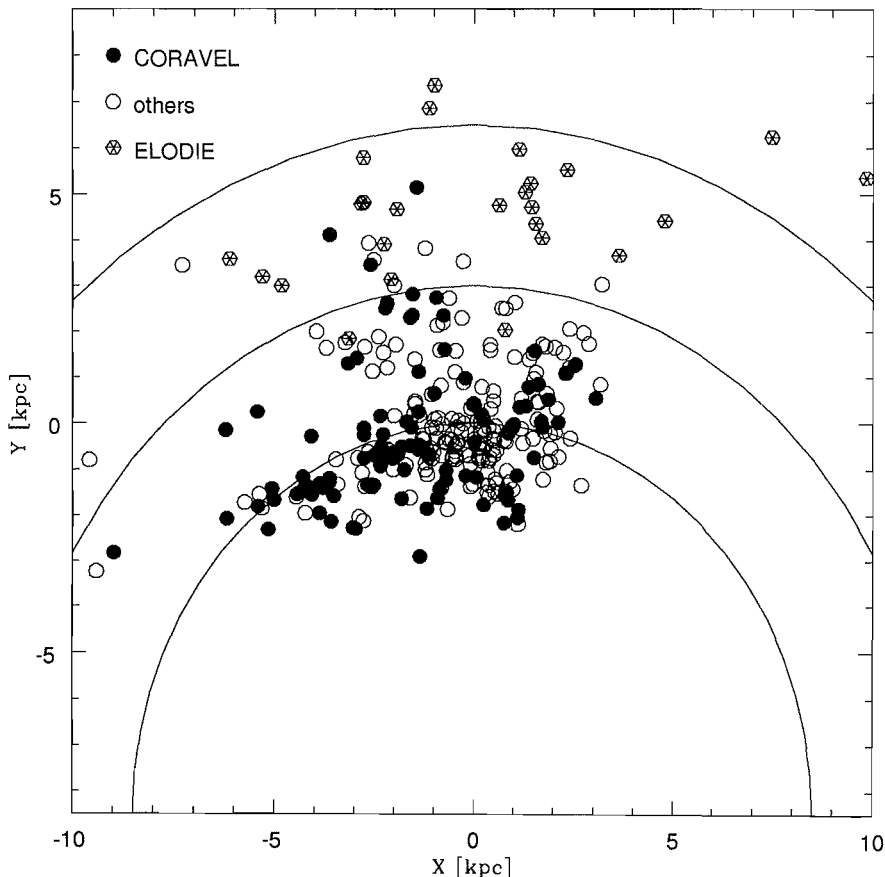


Figure 2: Position of the classical cepheids projected on the galactic plane. Coordinates are in kpc from the Sun. The galactic centre is at $(0, -8.5)$. Circles at $R=R_{\odot}$, $R=11.5$ kpc and $R=15$ kpc are shown. Black symbols indicate cepheids measured with CORAVEL, white symbols other cepheids with known radial velocity. Hexagons indicate the approximate position of the faint cepheid measured with ELODIE, if they are classical cepheids. Some of them, especially in the northern part (right), may be type II cepheids, and in that case their distance is overestimated.

The sample covers an extension of about 70° as seen from the galactic centre, and a range of galactocentric distances from 6.5 kpc to 11.5 kpc (with $R_{\odot} = 8.5$ kpc). The large size of this domain permits a firm determination of R_{\odot} and A , and a consideration of higher-order terms expressing the shape of the rotation curve near $R=R_{\odot}$.

An axisymmetric rotation model applied to these data yields the following:
 $R_{\odot} = 8.09 \pm 0.30$ kpc

distance to the galactic centre

$A = 15.92 \pm 0.34$ km s $^{-1}$ kpc $^{-1}$

Oort constant A

$u_0 = 9.32 \pm 0.80$ km s $^{-1}$

velocity of the sun relative to the LSR

$v_0 = 11.18 \pm 0.65$ km s $^{-1}$

along the U and V axes

Two additional parameters, A_2 and A_3 , the second and third derivative of the rotation curve at R_{\odot} , were also included in the fit. The corresponding rotation curve is shown in Figure 3 as a dashed line, along with rotation velocity determinations from CO measurements and H II regions (Clemens 1985, Blitz et

al. 1982). The R_{\odot} given by this analysis is slightly lower than the value currently recommended by the IAU, 8.5 kpc. The value of A is, whether or not A_2 and A_3 are used in the fits, higher than that of previous cepheid studies, indicating a steeper decrease of the rotation curve near $R=R_{\odot}$. We considered the effect of a modification in the cepheid distance scale (it is now considered unlikely that the cepheid scale zero-point is in error of more than 0.1–0.15 magnitudes). A zero-point change of plus or minus 0.15 mag brings the (A, R_{\odot}) pair to (7.6, 17.1) and (8.7, 14.8) respectively. The value $2A R_{\odot}$ is almost insensitive to a zero-point shift and remains near 260 km s $^{-1}$.

3. The Residual Velocity Field

The velocity residual of a star is defined as the difference between its observed radial velocity and the radial velocity expected from the axisymmetric rotation model.

The k-term problem

An immediate problem arises with these residuals, already recognized by Stibbs in 1956: their mean should be zero, but is observationally nearer to -3 km s $^{-1}$. We get $\langle V_{\text{obs}} - V_{\text{mod}} \rangle = -2.33$ km s $^{-1}$. This residual velocity shift has been dubbed “k-term”.

Explanations for this k-term have proceeded along two main lines: it could either be an artifact of the way the γ -velocities were calculated caused by the fact that the layers responsible for a cepheid’s spectral lines changed during the pulsation – and therefore that the zero-point of the velocity curve was shifted relative to the true centre-of-mass velocity – or be a real dynamical effect reflecting a deviation from the axisymmetric rotation model.

Both explanations run into difficulties: a 3 km s $^{-1}$ intrinsic k-term is difficult to explain with the current pulsation models for cepheids and the residuals do not correlate with period, colour or light curve amplitude, as may be expected in such a case, whereas a dynamical k-term seems suspect, since the residuals do not correlate with distance, as expected in a uniform contraction or expansion. That last fact seems to imply that the sun is in a somewhat special position relative to the residual velocity field, a rather unfashionable assumption.

The first explanation is usually favoured, and a constant shift added to the velocities in the galactic rotation analysis for cepheids.

But CORAVEL measurements for cepheids belonging to five open clusters, compared with CORAVEL radial velocities for other members of these clusters (Mermilliod et al. 1987), allowed us to reconsider the problem. The cepheids in these clusters are seen to match very closely the velocity of the other member stars. This is a strong argument against an intrinsic k-term, and makes the explanation by non-axisymmetric motions all the more plausible.

A comparison with selected fields of an N-body simulation for the galaxy, realized by R. Fux (1994), shows that k-terms of a magnitude up to 5 km s $^{-1}$ are typical when an axisymmetric rotation model is applied to a galaxy left to evolve for a few billion years and to form a bar from an initially axisymmetrical state.

Thus, we feel confident in saying that the k-term can be attributed to real dynamical effects – non axisymmetrical motions – and that the \dot{O} recovered from cepheid spectra does represent the centre-of-mass radial velocity.

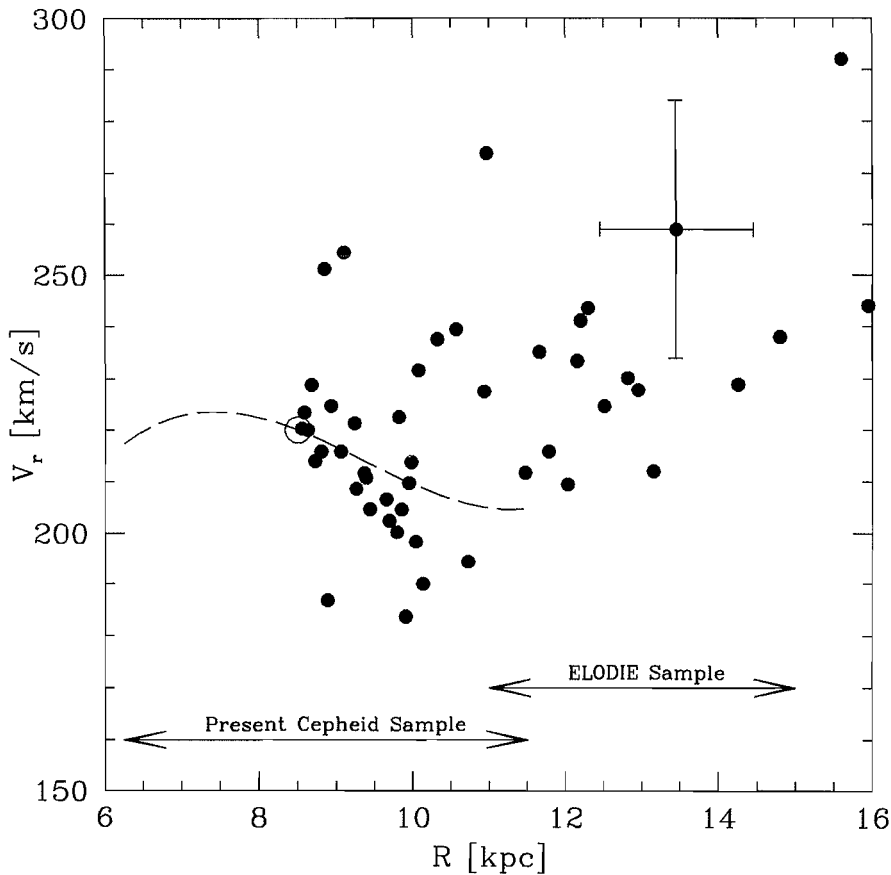


Figure 3: The circular rotation velocity as a function of the galactocentric radius R for $R=6-16$ kpc.

The dashed line shows the rotation curve obtained from the cepheid sample measured with CORAVEL, if we adopt $\theta_0 = 220 \text{ km s}^{-1}$. The white circle marks the pair (R_\odot, θ_\odot) . The black points are rotation velocity determinations from CO and H II regions data, in Clemens 1985. Typical error bars are shown for one point in the upper right.

Note that the uncertainties of the gas distances are not uncorrelated, and that a distance error moves a point diagonally from the upper right to the lower left (since the distance enters the calculation of both R and v_{rot}). Thus a systematic error in the distance scale would appear as a global increase or decrease of v_{rot} .

The range in R covered by the former cepheid sample and by the new ELODIE sample are shown at the bottom. Hopefully, this new sample could allow us to determine whether the rotation velocity decrease for $8 < R < 10$ kpc in the cepheids reflects a local motion of some type, or if it really shows a falling rotation curve for $R > R_\odot$.

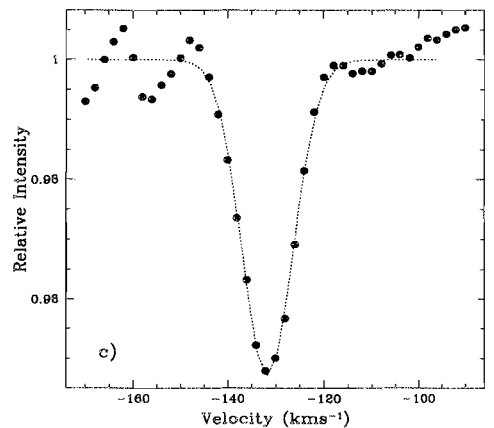
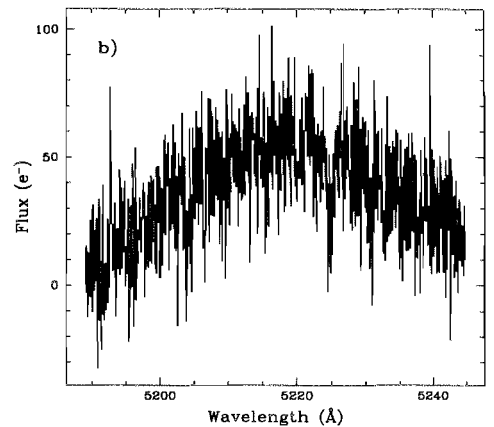
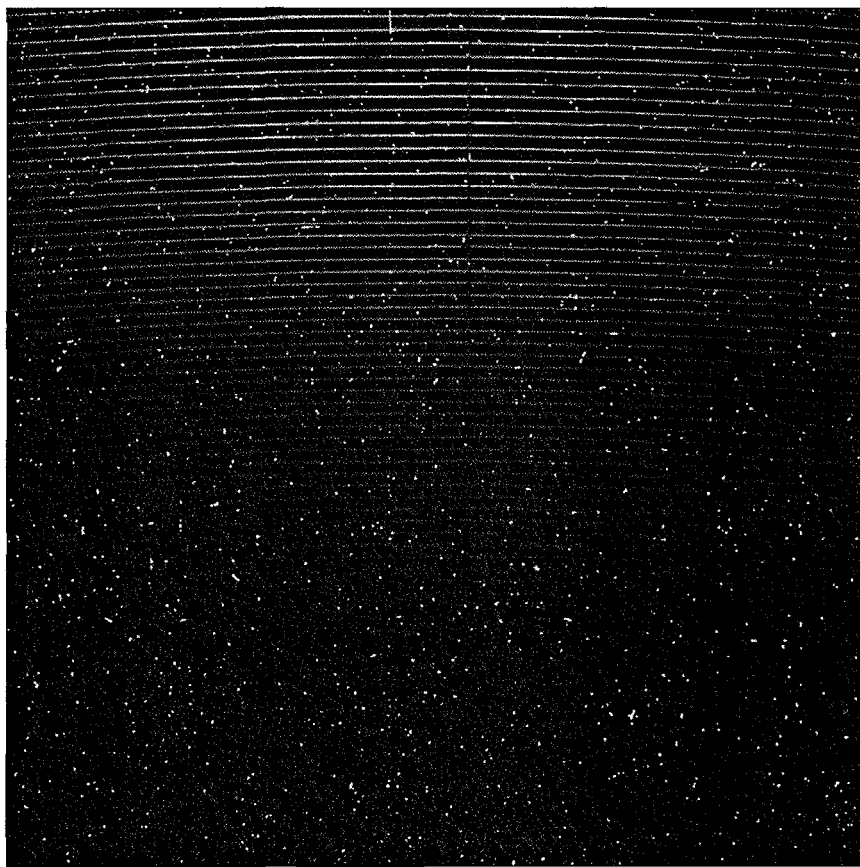


Figure 4: Typical ELODIE CCD image of a low signal-to-noise echelle spectrum ($[S/N] \approx 1$, on average) and its cross-correlation function (Fig. 4c). On the image, only half of the 67 orders are visible, the others are indistinguishable from the noise. Figure 4b displays an order located on the image at 2/3 from the bottom. The dotted line on Figure 4c is the gaussian fit used to compute the radial velocity.

4. Towards the Galactic Rotation Curve Beyond 12 kpc with ELODIE

A good knowledge of the outer rotation curve is interesting since it reflects the mass distribution of the Galaxy, and since it permits the kinematic distance determination of young disk objects. The rotation curve between 12 and 16 kpc is not clearly defined by the observations as can be seen on Figure 3. Both the gas data and the cepheid data clearly indicate a rotation velocity decrease from R_{\odot} to $R=12$ kpc, but then the gas data outline a flat or rising curve at $v_{\text{rot}} \approx 230 \text{ km s}^{-1}$ for $R > 12$ kpc. The present cepheid sample suffers an effective cutoff in radial velocity measurements around $V=12.5$ mag, so that the range in galactocentric distances that it covers is limited to the one indicated in the figure.

ELODIE is a high-resolution (45,000) fibre-fed spectrograph with a fixed wavelength range from 3900 to 6800 Å. It was built by collaboration between the Haute-Provence Observatory, the Marseilles Observatory and the Geneva

Observatory and is now permanently installed at the 1.93-m telescope of the Haute-Provence Observatory. This instrument possesses an automatic reduction programme called INTER-TACOS running on a SUN SPARC station to achieve on-line data reductions and cross-correlations in order to get the radial velocity of the target stars minutes after the observation. The cross-correlation algorithm used to find the radial velocity of stars mimics the CORAVEL process, using a numerical mask instead of a physical one (for any details, see Dubath et al. 1992). This technique allows us to extract easily the radial velocity of cool stars (later than F0) from spectra having a signal-to-noise ratio of about one and thus to get the velocity of Cepheids of 15th magnitude with an exposure time of about one hour or so (see Fig. 4).

We initiated last winter a programme of about 25 cepheids to cover the 11–15 kpc range of galactocentric distances. The approximate positions of the target cepheids are indicated as crossed hexagons on Figure 2. The analysis of this sample should constrain

the rotation curve from 12 kpc to 15 kpc and answer the question:

“Does the dip of the rotation curve at 11 kpc exist and does the rotation curve determined from cepheids follow the gas rotation curve?”

The answer will give an important clue about the reality of a local non-axisymmetric motions and will permit to investigate a possible systematic error in the gas or cepheids distance scale (due for instance to metal deficiency).

References

- Baranne A., Mayor M., Poncet J.L., 1979, *Vistas in Astronomy* **23**, 279.
Blitz, L., Fich, M., Stark, A.A., 1982, *ApJS* **49**, 183.
Clemens, D.P., 1985, *ApJ* **295**, 422.
Dubath, P., Meylan, G., Mayor, M., 1992, *ApJ* **400**, 510.
Feast M.W. & Walker A.R. 1987, *ARAA* **25**, 345.
Fux, R., 1994, in preparation.
Mermilliod J.-C., Mayor M., Burki G., 1987, *A&AS* **70**, 389.
Pont F., Mayor M., Burki G., 1994a, *A&A* in press.
Pont F., Mayor M., Burki G., 1994b, *A&AS* in press.

Interstellar Na I Absorption Towards Stars in the Region of the IRAS Vela Shell

M. SRINIVASAN SAHU^{1,2} and A. BLAAUW³

¹Nordic Optical Telescope Group, La Palma, Spain; ²Instituto de Astrofísica de Canarias, Tenerife, Spain;

³Kapteyn Laboratorium, Groningen, The Netherlands

Introduction

The H α emission associated with the Gum Nebula is confined to a circular region which has a diameter of approximately 36° (Chanot and Sivan, 1983). In the southern brighter part of the nebula, near γ^2 Velorum, the emission measure is higher by a factor of ~ 3 as compared to the fainter, outer regions. We examined the IRAS SuperSky Flux maps in the entire Gum Nebula region and discovered a ring-like structure (Fig. 1) coincident with the bright southern part, which we have termed the IRAS Vela Shell (Srinivasan Sahu, 1992; Srinivasan Sahu and Blaauw, 1994). This structure, centred around the Vela OB2 group of stars (the B-association of which γ^2 Velorum is a member, which we will refer to as Vela OB2, according to the nomenclature of Ruprecht et al., 1981), has an average radius of $\sim 8^\circ$. The section of the IRAS Vela Shell at

positive galactic latitudes is not clearly seen due to confusion with the background galactic emission. The half circle of dark clouds at negative latitudes coincident with the IRAS Vela Shell is apparent in the maps by Feitzinger and Stüwe (1986), in their study of the projected dark cloud distribution of the Milky Way. The IRAS maps clearly show that the cometary globules and dark clouds in the Puppis-Vela region, catalogued from the ESO-SERC IIIaJ plates (for example, Hawarden and Brand, 1976), are part of this ring-like structure.

The members (known and probable) of Vela OB2 lie within the IRAS Vela Shell which in fact just envelops the stars in this association. The Vela OB2 stars are therefore physically associated with the IRAS Vela Shell. Based on distance estimates to γ^2 Velorum and Vela OB2, the distance to the centre of this

ring-like structure is ~ 450 pc and its estimated mass is $\sim 10^6 M_{\odot}$. Both from the morphology on IRAS maps as well as from a study of the kinematics of the ionized gas in Puppis-Vela (Srinivasan Sahu and Sahu, 1993) the IRAS Vela Shell and the Gum Nebula appear to be two separate structures which just happen to overlap in projection.

We have analysed proper motions of the early-type stars in the region and there is strong evidence that the Vela OB2 stars are indeed part of a B-association. The association nature is further confirmed by the fact that both from position in the galactic (l, b) diagrams and its distance, Vela OB2 appears to form an extension of the string of association subgroups known as the Sco-Cen association and thereby a part of the Gould belt. Strömberg photometry by Eggen (1982) and an analysis by us using data from the homogeneous

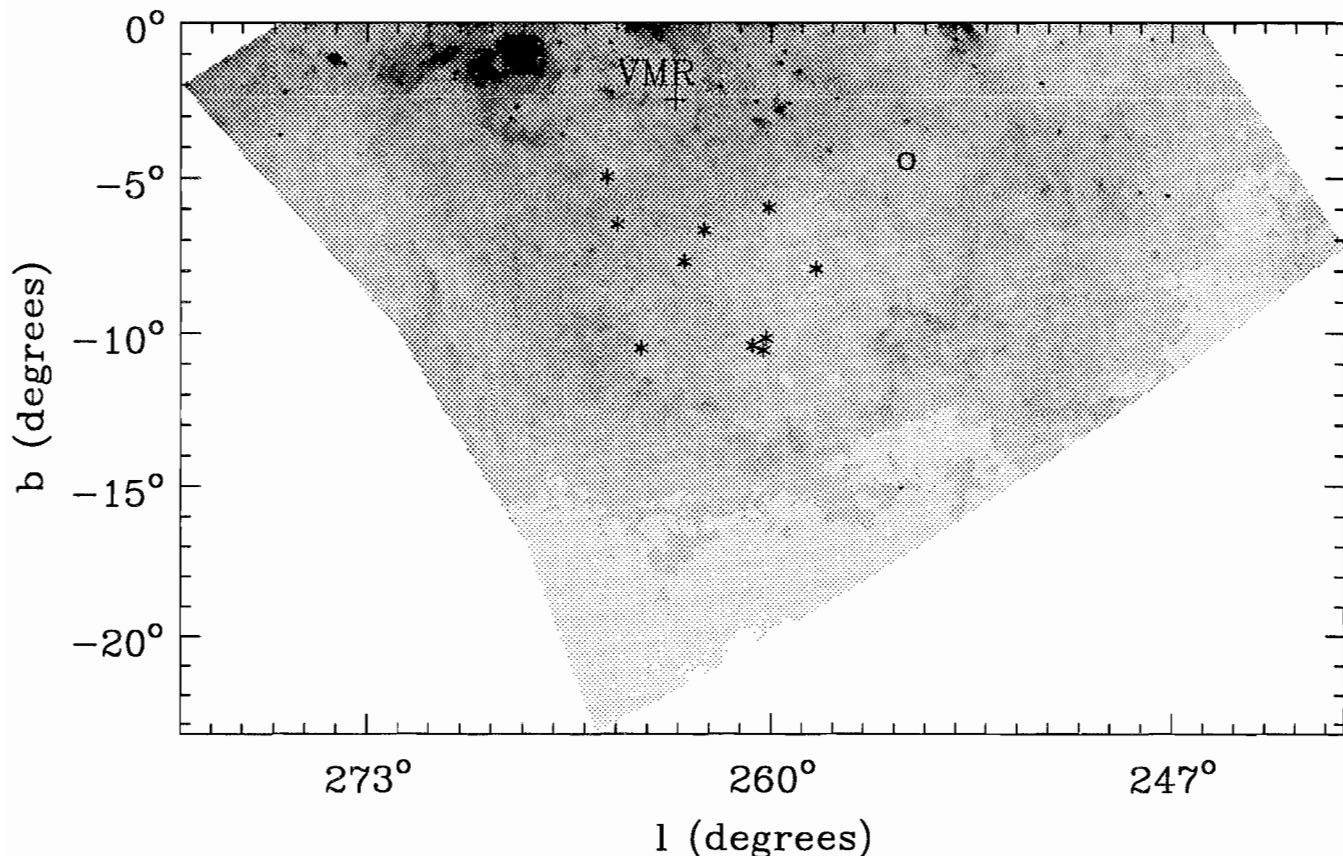


Figure 1: The IRAS Vela Shell at $60 \mu\text{m}$, obtained from the IRAS SuperSky Flux maps. The positions of the Vela OB2 stars are shown by "star" symbols, ζ Puppis by an open square and the Vela pulsar by a plus sign. ζ Puppis and the Vela pulsar are located near the edges of this shell, while the IRAS Vela Shell is clearly seen to envelop the Vela OB2 stars. This suggests that the Vela OB2 stars are physically associated with the shell and are the source of energy. The optically catalogued cometary globules and dark clouds in the Puppis-Vela region are part of the IRAS Vela Shell. The general location of the Vela Molecular Ridge (VMR) is also indicated in the plot.

ubvy-H β catalogue of Hauck and Mermilliod (1991), indicates that this association is aged (~ 2 to 3×10^7 years old) and on the verge of disintegration.

Aim of the Study

The distribution and the kinematics of the NaI absorbing gas can help to understand this component of the interstellar medium in the IRAS Vela Shell. The Goddard High-Resolution Spectrograph (GHRS) on the Hubble Space Telescope with a resolving power of $R \sim 80,000$ and wavelength range from 1150 \AA to 3200 \AA , has been used to study the properties of the highly ionized absorbing gas in each individual component for the case of γ^2 Velorum (Fitzpatrick and Spitzer, 1993). However, there are no good-quality optical data with comparable resolution which can be combined with the GHRS data to study the weakly ionized and neutral components in the IRAS Vela Shell. For these reasons, in January 1993, we initi-

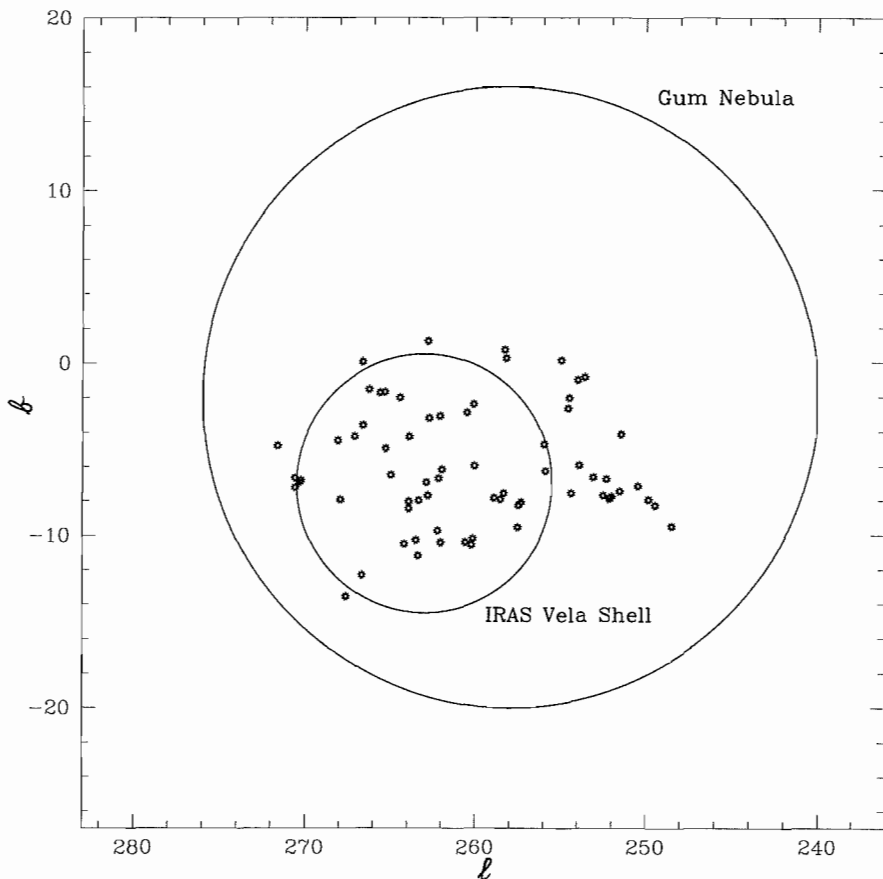


Figure 2: Schematic figure showing the locations of the IRAS Vela Shell, the Gum Nebula and the stars that we have observed.

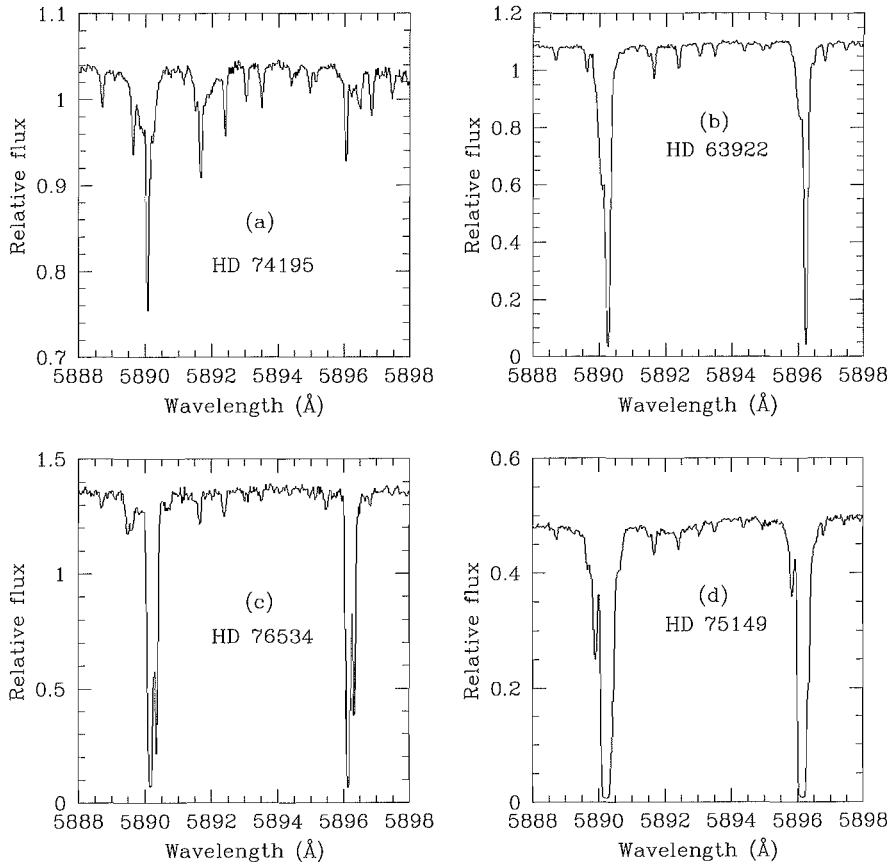


Figure 3 (a–d): The Na I D_1 and D_2 region in the spectra of four stars in our sample: (a) HD 74195, a member of the cluster IC 2391 which is at a distance of ~ 170 pc (b) HD 63922, a member of Vela OB2, located at ~ 450 pc (c) HD 76534, a member of Vela R2, located at ~ 700 pc and (d) HD 75149, a member of Vela OB1 (Humphreys, 1978) located at ~ 1500 pc. Note that the spectra have not been corrected for the influence of telluric lines.

ated a high-resolution ($R \sim 80,000$) study of the Na I D_1 and D_2 absorption lines in the line of sight to stars in the region of the IRAS Vela Shell.

Our sample consists of ~ 75 early-type stars (spectral types O9 to B7) whose locations with respect to the IRAS Vela Shell and the Gum Nebula are shown in Figure 2. The distances to these stars were determined using published spectroscopic/photometric data as well as proper motion data obtained from the Hipparcos Input Catalogue. There is fairly good agreement between the values of the distances obtained by these two methods for the case of relatively nearby stars. The distances for the stars in our sample range from ~ 150 to 2000 pc and galactic altitudes ($|z|$) range up to ~ 160 pc.

Observations and Future Prospects

We have obtained fairly high S/N (~ 60 to 500) Na D_1 and D_2 spectra for all the stars in our sample. The 1.4-m Coudé Auxiliary Telescope (CAT) and the Coudé Echelle Spectrograph (CES) in combination with the Long Camera

and the UV-coated Ford Aerospace/Loral 2048 \times 2048 CCD (#27) was used for all our observations. This CCD has a pixel size of $15 \mu\text{m} \times 15 \mu\text{m}$, a low dark current ($3 \text{ e}^-/\text{pixel}/\text{hour}$), a low readout noise ($\sim 6 \text{ e}^-$ rms) and appears to have few defects. The net efficiency of this system is: 3.8 % at 5400 \AA and 4.6 % at 6450 \AA (Pasquini et al., 1992). We have used this instrument configuration both at La Silla and by means of remote control from Garching, with satisfactory results.

We have used MIDAS for our data reduction. After the standard bias and background subtractions and flat fielding procedures, we extracted orders by using only the central 4 to 6 columns which had the highest S/N ratios, in the stellar and thorium lamp frames. This was done to avoid the contribution due to background scattered light. We opted to use a weighted average (weighted according to their S/N ratio values) of these central 4 to 6 columns rather than a simple average since the S/N ratios for the case of the weighted average method was typically higher than the simple average method by a factor ~ 1.5 to 2. Thus, normalized two-dimensional

spectra were obtained for stars and the thorium lamp. The stellar spectra were wavelength calibrated by using the thorium spectra taken either preceding or following the stellar exposure. We identified typically 30 to 35 lines in the thorium spectra with the help of the Atlas of the Thorium-Argon Spectrum (D’Odorico et al., 1987) and fitted polynomials to obtain relationships between the wavelength and pixel number. The polynomial fits had residuals with an rms scatter of $< 0.0045 \text{ \AA}$ for all the spectra. Figure 3 (a–d) shows the Na I D_1 and D_2 region in the spectra of four of the stars in our sample.

The Na I D_1 and D_2 lines fall in a spectral region which has numerous telluric lines mostly due to atmospheric water vapour. The strengths of the telluric lines caused by water vapour can vary by a factor of two or more within a matter of a few hours, even at a high altitude observatory like La Silla (A. Ardeberg, private communication). Therefore, the telluric lines contaminate the information present in the spectra and they can cause serious problems, particularly in the case of the faint components. We are now in the process of correcting the stellar spectra for the influence of the telluric lines using the synthetic telluric spectrum in the region of the D_1 and D_2 lines, constructed by Lundström et al. (1991).

We intend to pursue this observational programme and observe the Ca II absorption in the line of sight to our sample stars, to obtain Na I/Ca II ratios, whenever possible for each component. The Na I/Ca II ratio traces changes in the calcium abundance in the absorbing gas. Calcium is released in the gaseous phase when grain destruction occurs due to violent events such as, for example, supernovae. Therefore, in addition to determining the distribution and kinematics of the absorbing gas, we expect to learn more about the history of the IRAS Vela Shell through these observations.

References

- Chanot, A., Sivan, J.P.: 1983, *Astron. Astrophys.* **121**, 19.
- D’Odorico, S., Ghigo, M., Ponz, D.: 1987, ESO Scientific Report No. 6.
- Eggen, O.J.: 1982, *Astrophys. J. Suppl. Ser.* **50**, 199.
- Feitzinger, J.V., Stüwe, J.A.: 1984, *Astron. Astrophys. Suppl. Ser.* **58**, 365.
- Fitzpatrick, E.L., Spitzer, L.: 1993, Princeton Observatory Preprint No. 541.
- Hauck, B., Mermilliod, M.: 1991, obtained through the SIMBAD data retrieval facility.
- Hawarden, T.G. and Brand, P.W.J.L.: 1976, *Monthly Notices Roy. Astron. Soc.* **175**, 19P.

Humphreys, R.M.: 1978, *Astrophys. J. Suppl.* **38**, 309.
 Lundström, I., Ardeberg, A., Maurice, E., Lindgren, H.: 1991, *Astron. Astrophys. Suppl. Ser.* **91**, 199.

Ruprecht, J., Balazs, B., White, R.E.: 1981, *Catalogue of Star Clusters and Associations*, Supplement I, Part B2, ed. B. Balazs (Akademiai Kiado, Budapest), p. 471.
 Srinivasan Sahu, M.: 1992, Ph. D. thesis,

University of Groningen.
 Srinivasan Sahu, M. and Blaauw, A.: 1994, *Astron. Astrophys. Main Journal* (subm.).
 Srinivasan Sahu, M. and Sahu, K.C.: 1993, *Astron. Astrophys.* **280**, 231.

A Radial Velocity Search for Extra-Solar Planets Using an Iodine Gas Absorption Cell at the CAT + CES

M. KÜRSTER¹, A.P. HATZES², W.D. COCHRAN², C.E. PULLIAM², K. DENNERL¹
 and S. DÖBEREINER¹

¹Max-Planck-Institut für Extraterrestrische Physik, Garching, Germany

²McDonald Observatory, The University of Texas at Austin, Austin, U.S.A.

Introduction

The origin of the solar system is a fundamental problem in astrophysics for which many basic questions remain to be answered. Is planet formation a common or rare phenomenon? Is it a natural extension of the star formation process or is a different mechanism involved? Unlike most stars, the Sun is not found in a binary system. Is its single status related to the fact that it has a planetary system? Unfortunately, the answers to these and other important questions are hampered by the fact that the only known example of a planetary system (around a non-degenerate star) is the one around the Sun. Clearly, before one can develop general theories of planet formation, one must collect a large body of astronomical data that includes the frequency of planetary systems, the planetary mass function, and the correlation of such systems with mass, age, stellar composition, etc. of the primary star.

Although a number of direct and indirect techniques have been proposed for extra-solar planet detections, radial velocity measurements are proving to be a cost effective means of using ground-based facilities to search for planets. What radial velocity precision is needed to detect Jovian-sized planets? Naturally, one uses the Jupiter-Sun system as a guide where the Sun orbits around the barycentre with an average velocity of 12 m s^{-1} and a period of 12 years. Thus, an instrument capable of measuring relative stellar radial velocities to a precision better than 10 m s^{-1} and with a decade-long stability should be able to detect the presence of a Jovian-massed planet orbiting 5 AU from a solar-type star. Lower mass objects can be detected in orbits with smaller semi-major axes.

Radial Velocity Technique

Traditional radial velocity measurement techniques rarely exceed a precision of $200\text{--}500 \text{ m s}^{-1}$. The reason for this is that the wavelength reference is taken at a different time and often traverses a different light path than that of the stellar spectrum. Use of radial velocity standard stars circumvents the problem of different light paths for the reference and stellar spectra, but the standard observation is still made at a different time and there is always the danger that the standard star is a low-amplitude variable.

The instrumental errors can be

minimized by superimposing the wavelength reference on top of the stellar observation. One means of accomplishing this is to pass the starlight through an absorbing gas prior to its entrance into the spectrograph. The gas produces its own set of absorption lines against which velocity shifts of the stellar spectrum are measured. Since instrumental shifts now affect both the wavelength reference and stellar spectrum equally, a high degree of precision is achieved.

Griffin and Griffin (1973) first proposed using telluric O_2 lines at 6300 \AA as a radial velocity reference. In this

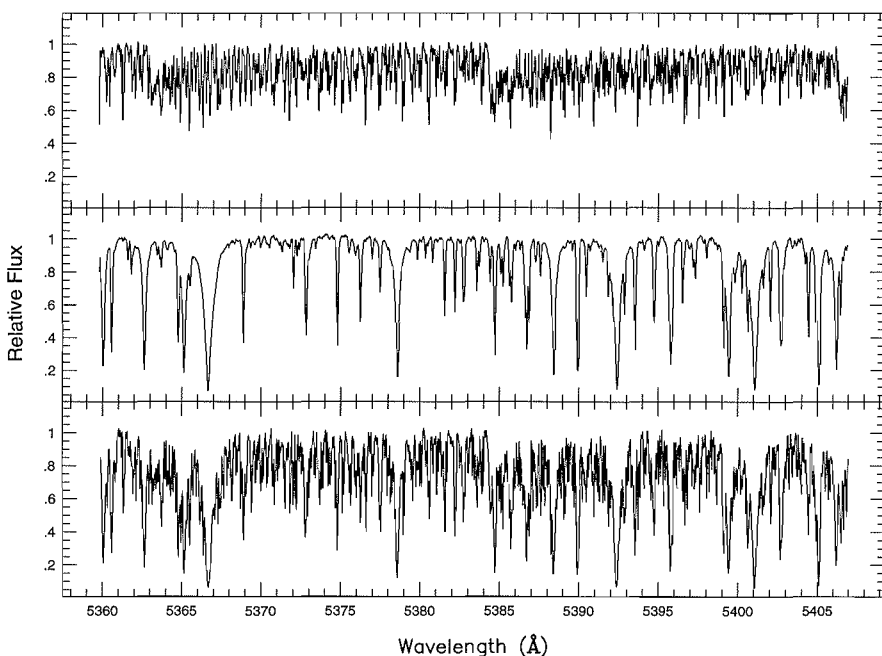


Figure 1: (Top) Absorption spectrum of the I_2 cell obtained by taking a dome flatfield through the cell. (Middle) Spectrum of $\alpha \text{ Cen B}$ without the I_2 cell from 5360 \AA to 5407 \AA . (Bottom) Spectrum of $\alpha \text{ Cen B}$ taken with the I_2 cell in front of the entrance slit of the ESO CES. All spectra have been normalized to the continuum.

case the absorbing medium is naturally provided by the earth's atmosphere. This technique was extensively used at McDonald Observatory as part of a planet search programme and a long-term precision of about $15\text{--}20\text{ m s}^{-1}$ was demonstrated (Cochran and Hatzes 1990). The ultimate precision of this method is determined by pressure and temperature changes of the earth's atmosphere as well as by Doppler shifts of the O_2 lines due to winds. These errors can be eliminated if the observer has some control over the absorbing gas.

Modern improvements to the simple telluric technique enclose a gas in a cell that can be temperature and pressure regulated. Use of such a gaseous absorption cell was pioneered for stellar applications by Campbell and Walker (1979) who chose hydrogen fluoride (HF) as the absorbing gas. They have demonstrated in more than a decade of use that the HF cell can measure relative radial velocities with a long-term precision of about 13 m s^{-1} (Campbell et al. 1988). Although the HF cell has proved capable of achieving the desired precision needed for detecting Jovian-sized planets around solar-type stars, there are a number of disadvantages to using such a device. The path length of the cell that is required to produce reasonably deep HF absorption lines is about 1 m and this could pose a problem if space in front of the spectrograph slit were limited. HF also has significant pressure shifts and must be regulated to a rather high temperature of 100°C . This is a highly reactive chemical, and prolonged exposure of the cell to HF will destroy the container walls. Consequently, the absorption cell must be made of inert material and has to be refilled for each observing run. The greatest disadvantage, however, is the hazardous nature of HF, and human exposure to this gas is fatal.

Gaseous molecular iodine (I_2) is a benign alternative to HF and the advantages of using this substance in an absorption cell are numerous. I_2 has a strong electronic band ($\text{B}^3\Pi_{\text{ou}}^+ - \text{X}^1\Sigma_{\text{g}}^+$) in the $5000\text{--}6000\text{ \AA}$ spectral region producing a rich spectrum of extremely narrow lines. Pressure shifts of I_2 are much smaller than for HF and this results in a very stable reference spectrum (Schweizer et al. 1973). The vapour pressure is high enough (about 0.5 torr) to produce significant absorption at room temperature in a cell $10\text{--}20\text{ cm}$ in length. Iodine gas does not react with glass so that the construction of the cell is relatively easy and can be done by any glassblower. Also, a fixed number of I_2 molecules are permanently sealed in the cell for its entire lifetime, so there is no need to refill it prior to each observ-

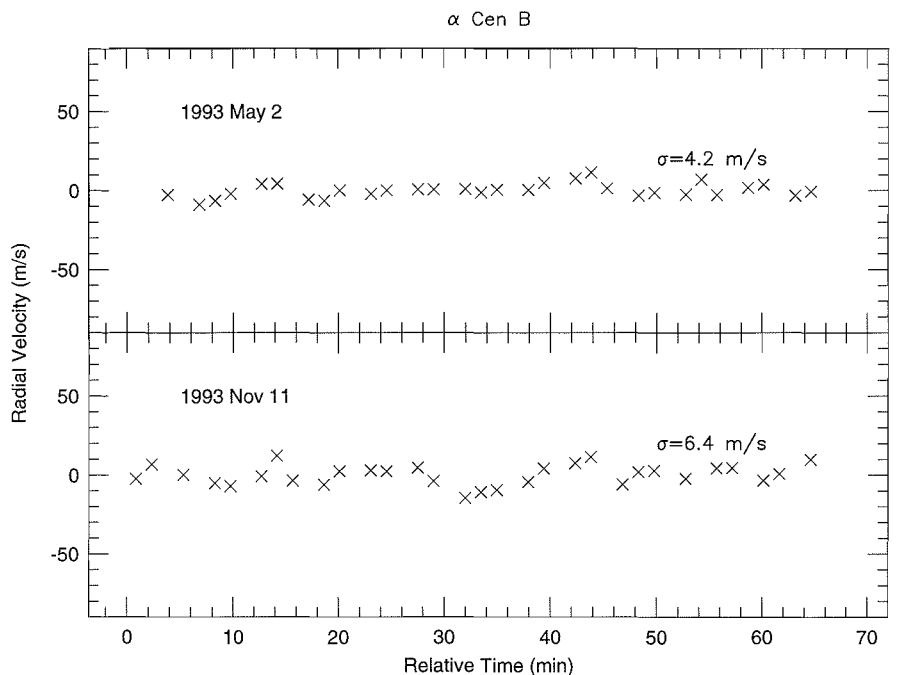


Figure 2: The short-term radial velocity variations of α Cen B on 1993 May 2 (top) and 1993 Nov. 11 (bottom). The standard deviations of the measurements are 4.2 m s^{-1} and 6.4 m s^{-1} , respectively.

ing run. This guarantees that there is no variation in the amount of absorbing iodine from run to run. The device operates at a modest temperature of 50°C and its small mass can be temperature regulated using commercially available temperature controllers. In short, iodine absorption cells require virtually no maintenance and are easy, and above all, safe to use.

Use of I_2 as a wavelength standard has been employed by numerous investigators. Beckers (1973) used an iodine absorption cell to study material motions in sunspot umbrae. More recently, Libbrecht (1988) and Marcy and Butler (1992) have pioneered using the I_2 technique to measure relative stellar radial velocities. Iodine absorption cells are routinely used at McDonald Observatory as part of a planetary search programme (Cochran and Hatzes 1994) and to study low-amplitude variability in stars (Hatzes and Cochran 1993, 1994a, b). These studies have shown that, depending on the spectral resolution of the data, a long-term radial velocity precision of $7\text{--}20\text{ m s}^{-1}$ is possible using an iodine absorption cell.

There are a number of programmes using precision radial velocity measurements to search for extra-solar planets. Campbell et al. (1988) have used their HF absorption cell at the CFHT 3.6-m telescope. Radial velocity surveys using iodine absorption cells are being conducted with the Lick 3-m telescope by Marcy and Butler (1992) and the McDonald Observatory 2.7-m telescope

by Cochran and Hatzes (1994). McMillan et al. (1993) use a Fabry-Perot in transmission along with the Steward 0.9-m telescope for their planet search programme. In spite of the variety of telescopes and radial velocity techniques employed, these programmes share the common feature that they are all conducted from the northern hemisphere. There is one radial velocity survey for low-mass companions among southern hemisphere objects carried out by Murdoch et al. (1993) on a sample of 29 solar-type stars. However, the mean accuracy of their measurements, computed using digital cross-correlation techniques, is only 55 m s^{-1} , too large for the detection of Jovian-sized planets. In November 1992 we began a higher precision radial velocity survey of southern hemisphere stars at ESO in order to increase the statistical sample of stars being surveyed for planets.

It was realized that the many advantages of the iodine gas absorption cell made it the ideal device for use at the ESO 1.4-m Coudé Auxiliary Telescope (CAT) and Coudé Echelle Spectrograph (CES). The space in front of the entrance slit to the CES allowed for a device no more than about 10 m in length (no problem for an iodine cell), otherwise it would obscure the guide camera. A hazardous gas such as HF would not have been desirable to use since we did not wish for the ESO staff to handle potentially lethal chemicals. Finally, since all the observing was to be conducted remotely from Garching it was

Table 1: Comparison of Radial Velocity Programmes

Telescope	Technique	Resolving power	$\Delta\lambda$ [Å]	σ [m s ⁻¹]	Reference
Mt. John 1.0-m	Digital CC	100,000	45	55	Murdoch et al. 1993
McDonald 2.7-m	Telluric O ₂	200,000	12	15–20	Cochran & Hatzes 1990
Steward 0.9-m	Fabry-Perot	74,000	300	8–14	McMillan et al. 1993, MS
CFHT 3.6-m	HF cell	40,000	133	13	Campbell et al. 1988
Lick 0.6-m CAT	I ₂ cell	40,000	200	20	Marcy & Butler 1993
McDonald 2.1-m	I ₂ cell	48,000	24	20–25	Hatzes & Cochran 1993
McDonald 2.7-m	I ₂ cell	200,000	9	10–15	Cochran & Hatzes 1994
ESO 1.4-m CAT	I ₂ cell	100,000	48	4–7	This work

paramount to have a device that was not only safe, but could be used with minimal training of the personnel.

Construction and Use of the Iodine Cell

The ESO iodine absorption cell was constructed at the University of Texas and shipped to La Silla in August 1992. The construction of the cell was very straightforward. A glassblower first attached two optical quartz windows, 0.63 cm thick and 5 cm in diameter, to the ends of a quartz tube 10 cm in length. A feed-through tube 1 cm in diameter was then fused through the cylindrical walls near the centre of the cell and the free end of this tube was attached to a glass manifold. At one end of the manifold was a sample tube containing solid iodine and at the other end was a valve with an exit tube that first passed through a liquid nitrogen trap on its way to a vacuum pump. The cold trap prevented iodine from entering and damaging the pump. After air was evacuated from the manifold, the valve was sealed so as to allow gaseous I₂ (which had sublimated from the solid I₂) to fill the entire chamber (manifold + the cell). The glassblower then detached the cell by applying a torch to the feed-through tube. Since this tube was now under vacuum, as the glass became molten the tube collapsed on itself and permanently sealed gaseous iodine in the cell.

Surrounding the cell is heating foil and a 0.65 cm thick layer of insulation. The cell is regulated by a commercial temperature controller which measures the temperature of the cell and provides power to the heater foil as needed. The cell is regulated at a temperature of 50°C. Our experience indicates that temperatures below this may result in iodine condensing out of the gaseous phase within the cell; regulating the cell at higher temperatures may create unnecessary heat dissipation that could create air currents in the slit room that may affect the seeing conditions.

The decision whether the iodine cell

should be used with the short camera (R=50,000) or the long camera (R=100,000) of the CES depends on the desired radial velocity accuracy and the magnitudes of the objects studied. The radial velocity precision is proportional to $R^{-3/2}(S/N)^{-1}$ where R is the resolving power and S/N is the signal-to-noise ratio (Hatzes and Cochran 1992). For the planet detection programme the highest precision possible was desired and since most of the programme objects are bright, the lower photon count rate of the long camera/CCD#30 setup did not present a problem. Furthermore, higher resolution data are less sensitive to changes in the instrumental profile of the spectrograph (Hatzes and Cochran 1992). For radial velocity work on faint objects the increased speed of the short camera may outweigh its lower velocity resolution (dispersion) and a higher radial velocity precision may result.

The ESO iodine cell has been used successfully on nine observing runs with

the 1.4-m CAT and the long camera of the CES spanning November 1992 to March 1994. All observing runs, including the inaugural run, were smoothly conducted remotely from Garching. This is a testament to the ease of using such a device. At first the ESO staff installed the cell and temperature controller prior to each run; now they permanently reside in the slit room. During the course of observing the night assistant is requested to move the cell in or out of the light path as needed.

Although the iodine cell can be used anywhere in the wavelength region 5000–6000 Å, for the planetary search programme a region centred on 5385 Å was chosen. Solar-type stars (the predominant objects of our survey) have a high density of spectral lines in this wavelength region and this wavelength also corresponds to the blaze peak of the echelle grating of the CES. The detector was CCD#30 which has 2048×2048 pixels. The spectra had a wavelength range of 48 Å at a spectral resolution of 0.054 Å (dispersion = 0.024 Å pixel⁻¹).

In order to compute radial velocities with an iodine absorption cell one requires a spectrum of pure iodine, a spectrum of the programme star, and a spectrum of the star taken through the iodine cell. Figure 1 shows typical radial velocity data taken with the I₂ cell at the 1.4-m CAT/CES. The top panel shows a spectrum of molecular iodine produced by observing a continuum calibration lamp (dome flatfield) with the cell in place. The central panel shows an ob-

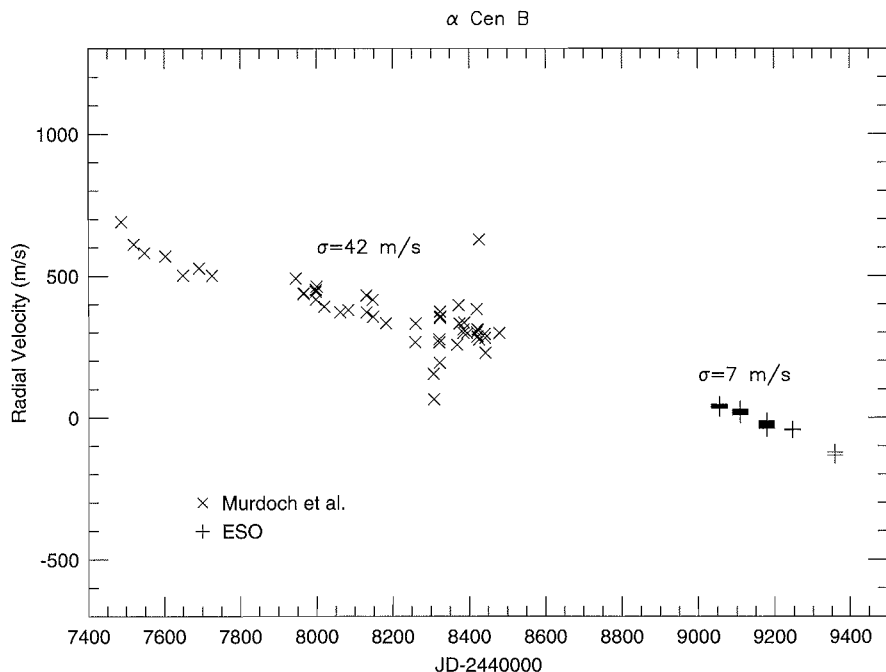


Figure 3: The radial velocity variations of α Cen B. Data from Murdoch et al. (1993) are indicated by 'x' and the ESO I₂ cell measurements are depicted by '+'. The long-term trend is due to the orbit around α Cen A.

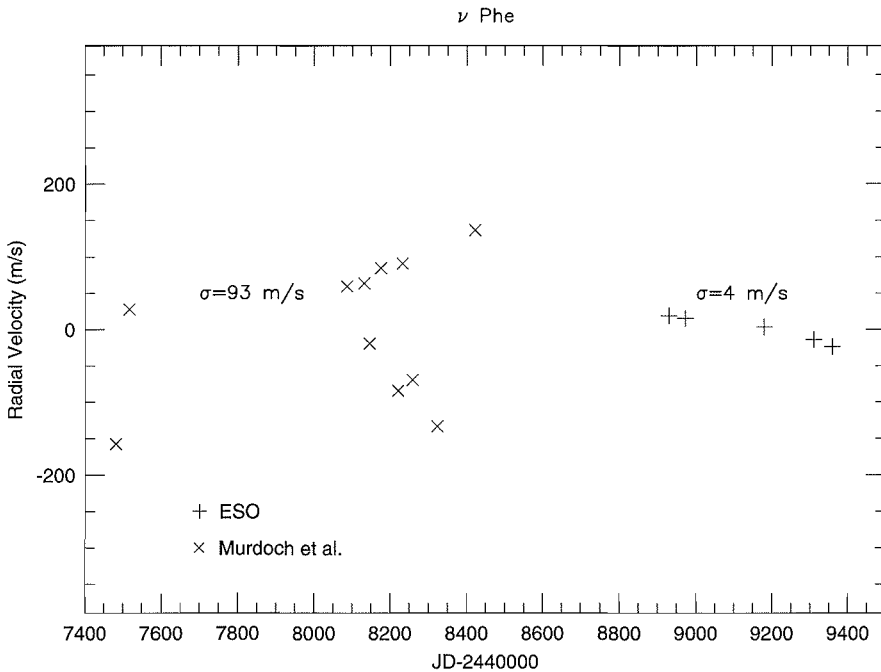


Figure 4: The relative radial velocity of ν Phe. Once again the '+'s represent data from Murdoch et al. 1993 and 'x's indicate the ESO measurements.

servation of one of the planet search programme stars, the K1V star α Cen B, taken without the iodine cell. The bottom panel shows an observation of α Cen B taken with the iodine cell in front of the entrance slit of the spectrograph.

Performance of the Iodine Cell

The ESO iodine cell has been in use long enough so that both the long- and short-term radial velocity precision can be quantified. Short-term precision is defined to be the radial velocity accuracy achievable on a given night whereas the long-term precision is determined by the month-to-month scatter of the radial velocity measurements. The short-term precision is expected to be higher than the long-term one since the instrumental profile of the spectrograph is not expected to change in the course of several hours. On the other hand, degradation of the long-term precision can result from a variety of sources. A slightly different spectrograph focus from run to run, different CCD noise, of different temperature of the spectrograph optics can all affect the instrumental response of the spectrograph and this can result in systematic radial velocity errors.

Central to quantifying the precision of any radial velocity technique is the problem of finding a radial velocity "standard", particularly when determining the long-term precision. One can always look at an object of known radial velocity such as the moon, but this is an

extended source that uniformly fills the spectrograph entrance slit thereby minimizing possible errors related to variable seeing, telescope focus, or guiding. Instead we chose to quantify the radial velocity precision by using actual observations of our programme stars. The radial velocity precision thus represents an upper limit as some scatter may be due to intrinsic stellar variability of unknown nature rather than to instrumental effects.

Radial velocities were computed using a stellar spectrum taken with and without the cell and a pure molecular I_2 spectrum. A "model" spectrum was produced by shifting and combining the stellar and iodine spectra and comparing it to the data. The relative shift between the stellar and I_2 spectra as well as all coefficients of the dispersion function were varied until the rms difference between the model and data (star+iodine as in the lower panel of Fig. 1) were minimized. A more refined calculation can take into account the instrumental response or point spread function (PSF) of the spectrograph. Changes in PSF from run to run can cause significant radial velocity errors at this level of precision. Marcy and Butler (1992) have pioneered a technique for modelling the PSF using the iodine absorption lines. The radial velocity data presented here do not include PSF modelling and thus provide a better gauge of spectrograph stability.

All radial velocities were corrected for the earth's motion using the JPL DE200 Planetary Ephemeris.

(a) Short-term precision

The short-term precision of the iodine cell + CES was determined by taking a series of observations on α Cen B covering approximately 1 hour on each of two nights. The exposure time for each observation was 45 s. Figure 2 shows the resulting radial velocities on 2 May 1993 and 11 November 1993. The rms scatter of the velocities on the first night was 4.2 m s^{-1} and 6.4 m s^{-1} on the second.

(b) Long-term precision

The '+' symbols in Figure 3 show the ESO long-term relative radial velocity measurements of α Cen B using the iodine absorption cell. Also shown (as 'x') are the radial velocity measurements of Murdoch et al. (1993). Since both data sets represent relative radial velocities, they each have their own zero-point velocity. Therefore, an offset was applied to the Murdoch et al. data so as to align the two data sets. The long-term trends evident in both data sets are due to the long-period orbit of the α Cen AB binary system. The rms scatter about a straight line fit to the ESO measurements result in a standard deviation of 7 m s^{-1} , considerably smaller than the 42 m s^{-1} (also about a straight line fit) for the Murdoch et al. measurements.

Figure 4 shows the ESO and Murdoch et al. radial velocity measurements for the F8V star ν Phe after aligning the mean values of both data sets. Again, there is a greatly improved precision in the ESO data which has a standard deviation of 4 m s^{-1} compared to the 93 m s^{-1} of the Murdoch et al. measurements. There is a slight downward trend in the ESO data, possibly indicating the presence of a low-mass companion, but more measurements are needed to confirm this.

The ESO radial velocity measurements for the G8V star τ Cet are shown as filled circles in Figure 5. The standard deviation of these measurements is 19 m s^{-1} . Also shown (as 'x') are the radial velocity measurements taken at McDonald Observatory using an iodine absorption cell and the coude spectrograph of the 2.7-m telescope. Note how well the ESO data track the McDonald data. In particular, the large decrease in the radial velocity (by about 50 m s^{-1}) between about Julian day 2449300 and 2449350 is present in both data sets. A similar amplitude in the scatter was also evident in the radial velocity measurements of this star made by Campbell et al. (1988). This strongly suggests that the rather high scatter seen in the radial velocity measurements of τ Cet (com-

pared to ν Phe and α Cen B) may actually be intrinsic to the star.

(c) Comparison to other high precision radial velocity programmes

Table 1 compares the radial velocity precision of the ESO I₂ cell + CES to other high-precision radial velocity programmes. The columns list the telescope used for the programme, the radial velocity technique, the resolving power, the approximate wavelength coverage, the long-term radial velocity precision, and the reference for the work. The radial velocity precision quoted for these techniques should not be taken as the ultimate precision that can be achieved. In particular, all radial velocity measurements made with iodine cells did not take into account modelling of the point spread function. Such PSF modelling may remove any systematic errors introduced by changes in the instrumental profile and thus improve the radial velocity precision. Clearly, the ESO 1.4-m CAT + CES + iodine cell together with a simple data reduction procedure can produce a long-term precision that is at least as good, if not better, than any other high-precision radial velocity programme. This is a testament not only to the radial velocity measurement technique, but to the overall stability of the CES.

Other Applications

Although the ESO I₂ cell was installed as part of a programme to search for extra-solar planets, it is also an excellent means of studying low-amplitude radial velocity variability in stars. Iodine cells have been used to study the variability of K giants (Hatzes & Cochran 1993, 1994a, b), to measure the radial velocity amplitude of rapidly oscillating Ap stars (Libbrecht 1988; Hatzes & Kürster 1994), and to search for variability among the non-Cepheid stars in the instability strip Butler (1992).

Summary

We have started a programme of using precise radial velocity measurements to search for extra-solar planets with the ESO 1.4-m CAT + CES. The technique uses an iodine gas absorption cell placed before the entrance slit of the

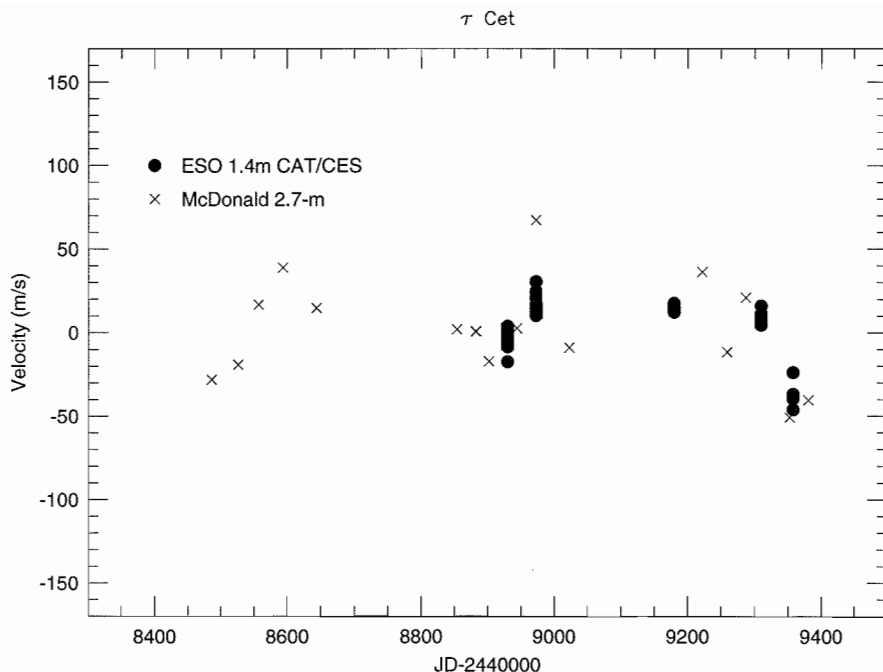


Figure 5: (Top) The relative radial velocity measurements of τ Cet. The 'x' symbols represent data taken with the McDonald Observatory 2.7-m telescope and an iodine absorption cell. The solid circles represent the ESO measurements which consist of 5–11 individual measurements per observing run.

spectrograph. The iodine absorption spectrum that is superimposed on the stellar spectrum provides a stable reference for measuring relative stellar radial velocities. Preliminary measurements indicate that the I₂ cell + CAT + CES is capable of achieving a long-term radial velocity precision of 4–7 m s⁻¹ on bright, solar-type stars. This precision is comparable, if not better, to that of other precise radial velocity surveys currently in place. Continued observations of the programme stars should be able to detect planets with Jovian masses if they are indeed present around these stars.

Acknowledgements

This project could not have been started without the assistance of the ESO staff. We especially thank Luca Pasquini and Alain Gilliotte for installing the iodine cell at the CES.

References

Beckers, J.M., 1973, *ApJ*, **213**, 900.
Butler, R.P., 1992, *ApJ*, **394**, L25.
Campbell, B., & Walker, G.A.H., 1979, *PASP*, **91**, 540.

Campbell, B., Walker, G.A.H., & Yang, S., 1988, *ApJ*, **331**, 902.
Cochran, W.D. & Hatzes, A.P., 1990, *Proc. SPIE*, **1318**, 148.
Cochran, W.D. & Hatzes, A.P., 1994, *Ap&SS*, in press.
Griffin, R. & Griffin, R., 1973, *MNRAS*, **162**, 243.
Hatzes, A.P. & Cochran, W.D., 1992, in *High Resolution Spectroscopy with the VLT*, ed. Ulrich, M.-H., European Southern Observatory, Garching, p. 275.
Hatzes, A.P. & Cochran, W.D., 1993, *ApJ*, **413**, 339.
Hatzes, A.P. & Cochran, W.D., 1994a, *ApJ*, **422**, 366.
Hatzes, A.P. & Cochran, W.D., 1994b, in press.
Hatzes, A.P. & Kürster, M., 1994, *A&A*, in press.
Libbrecht, K.G., 1988, *ApJ*, **330**, L51.
Marcy, G.W. & Butler, R.P., 1992, *PASP*, **104**, 270.
Marcy, G.W. & Butler, R.P., 1993, *BAAS*, **25**, 916.
McMillan, R.S., & Smith, P.H., 1987, *PASP*, **99**, 849 (MS).
McMillan, R.S., Moore, T.L., Perry, M.L., & Smith, P.H., 1993, *ApJ*, **403**, 901.
Murdoch, K.A., Hearnshaw, J.B., & Clark, M., 1993, *ApJ*, **413**, 349.
Schweitzer, W.G., Kessler, E.G., Deslattes, R.P., Layer, H.P., & Whetstone, J.R., 1973, *Applied Optics*, **12**, 2927.

The 94MAY Release of ESO-MIDAS

Science Data Analysis Group

Although in principle ESO-MIDAS is released only once a year, on an exceptional basis we decided to prepare a minor release in May 1994 (94MAY version). This decision was made to provide, as soon as possible, a POSIX and ANSI-C compatible version for developers of reduction packages for VLT instruments. This release will also fully support the DEC OSF/1 systems. The 94MAY minor release will only be available through networks (i.e. ftp). No special documentation will be generated except for a new version of the ESO-MIDAS Environment document applicable to this and future MIDAS releases.

Although it contains a number of new features and upgrades of the 93NOV release, it is only recommended for sites which either require full POSIX and ANSI-C compatibility or have DEC OSF/1 systems on which 93NOV cannot be installed. The 93NOV release will still be the official and fully supported release of ESO-MIDAS for all other systems, until 94NOV becomes available. Some of the new features are described in the following section, a more detailed account can be found in the March issue of the ESO-MIDAS Courier.

1. Redirection of Input/Output

For some time the MIDAS user community has expressed the wish for an easy and robust method of communication between MIDAS and the host system. Thus, one could employ host sys-

tem utilities for MIDAS reduction tasks and on the other hand, system utilities could profit from MIDAS functionality. Because we didn't want to introduce a completely new twist to the MIDAS command syntax, the input/output redirection for MIDAS commands was implemented very similar to the Unix concept using the '<' and '>' characters. Note, that this redirection is also valid for VMS/Open VMS.

2. Refurbishment of PLOT Package

The MIDAS PLOT package of the 94MAY release was rewritten in C which (hopefully) will be noticed by its improvement in performance. Also, a number of limitations are lifted. For example, the PLOT/CONTOUR command no longer has restrictions on the frame size, in particular PLOT/PERSPECTIVE is much faster, and PLOT/TABLE is now ready for 3D tables. We have given it some nice options which are also useful for 2D tables.

3. Changes in the Standard Interfaces

This 94MAY release will be the first release in which the modified type definitions of arguments in the C-routines of the Standard Interfaces are implemented. The modifications are: a change of the arguments of type 'long int' to 'int' in all SC and TC routines and

a type change of the parameter 'unit' (e.g. in SCKRDC) from type 'char **' to 'int *'. At the same time ANSI-C prototype definitions of the interfaces were provided.

These modifications were necessary in order to provide a clean port of MIDAS to a CPU with a 64-bit architecture, e.g. the Alpha chip from DEC running under the OSF/1 operating system (HP, IBM and SUN are also currently working on 64-bit chips).

A notification of these changes and a more detailed technical explanation were sent to all MIDAS sites in the summer of last year to obtain feedback from the user community and objections, if any. No negative response was received, so the modifications were implemented as proposed.

Nothing has changed with respect to the Fortran implementation of the Standard Interfaces, therefore users who wrote MIDAS applications in Fortran are not affected. Also the applications written in C will not feel the impact of these modifications as long as they are running on a 32-bit machine. However, we strongly recommend to update the relevant code as soon as possible.

New in the MIDAS Environment is a standard MIDAS Graphics library. The library is meant for those who want to incorporate graphics into their Fortran or C applications that are fully compatible with graphics created by MIDAS commands. The library becomes available in the 94MAY release.

ESO's New On-Line Information System

THE ESO WEB CONSORTIUM¹

A new information system is being set up, based on the system called the World-Wide Web. This article describes why it was set up, what is now available, and how it can be accessed.

ESO as an Information Provider

One of the specific tasks of ESO is the rationalization and distribution of information about ESO facilities. This central task of ESO relates both to external and internal users. Information may exist, but accessibility, consistency and comprehensiveness are all very important considerations which need constant attention.

ESO's information production and distribution activities include the following:

- Science Information: bibliographical – abstracts, papers, books; preprints; news; data; conferences, meetings, talks.
- Facilities: telescopes, instruments, detectors, computers, measuring machines.
- Tools: data analysis software, appli-

¹ Includes: H.-M. Adorf, M. Albrecht, P. Ballester, T. Bedding, P. Benvenuti, P. Bristow, P. Dierckx, M. Fendt, C. Madsen, J. Mendez, F. Murtagh, J. Schwarz, R. West, and W. Zeilinger. Membership open!

cations software, electronic mail, network services, word processing, desktop publishing, presentation software.

Information on such topics exists, but it is mostly spread around, not well organized, inhomogeneous, irregularly updated, and difficult to access. ESO has an obligation to provide such information to its user community. Additionally, the life of internal and external ESO users should be made as productive as possible, through the use of the best available, modern information-handling tools.

A number of people from the Space Telescope – European Coordinating Facility (ST-ECF), ESO's new Data Management Division (DMD), and from ESO's Science Division, have been putting together a scheme for collecting and presenting ESO-wide information. Earlier work was also carried out at La Silla.

The preferred technical infrastructure is the multi-platform, public toolset associated with the Internet's World-Wide Web. The information system being built up is not yet complete. However, what is currently available shows, already, what can be done.

ESO information is geographically distributed. The information system prototyped allows instrument information to be maintained at La Silla, and to be effortlessly integrated into an overall presentation structure in Garching. The coming roof-to-roof 2 Mb link between La Silla and Garching will obviate any bandwidth-related difficulties.

The Internet and the World-Wide Web

The number of Internet users has been growing ever faster, and currently stands at 20 million. A simplistic extrapolation shows an Internet connection for every human being on earth by the year 2002.

An additional trend in the past year or two has been the wide use of reliable, userfriendly, freely available tools for distributed free-text searching, and for resource finding. Examples of such tools include the World-Wide Web (WWW, or Web) browsers such as Mosaic and Lynx. The number of users of Mosaic stands now at 2 million, and (as of one or two months ago) is the fastest-growing Internet application. Web browsers are available on a range of common platforms – Unix, Macintosh, VMS, Windows, and PC. For hardware with limited graphics – e.g. VT100 terminals, or when dialing up ESO via modem from home – line mode operation can be used (e.g. Lynx).

The ESO Portal is based on the Web.

The ESO Portal homepage on a Unix workstation, mid-May 1994.

It was set up following the successful experience of Web-based information servers in the ST-ECF and the Archive Group in ESO. Internal Unix users automatically access this ESO Portal when they execute the command `xmosaic`. For external users, the URL (address) is <http://http.hq.eso.org/eso-homepage.html>.

To read further about the World-Wide Web, Adorf (1994) provides an introduction.

ESO Portal Contents

The following are a number of topics which can now be accessed in the ESO Portal:

- All press releases issued by ESO in 1994 are accessible, including the accompanying images. The images are displayed, by clicking within the article at the appropriate place.
- Up-to-the-minute information on such topics as the Shoemaker-Levy/Jupiter event is available.
- A major current drive is to have comprehensive instrument information available. This builds on the earlier work of making such information available, and prototyping a Web

server, which was carried out at La Silla.

- Meteorological satellite images of Chile are continually uploaded to the Portal.
- Seminar and Lunch-Talk information is made available as soon as it is on hand.
- Extensive practical information is available with regard to ESO computing topics.
- A link to other network-based astronomical resources is available – around 700 sites.
- A small but growing number of ESO preprints are now accessible on the ESO Web.

Work on the ESO Portal began only recently, but it has grown fast. It is not yet at the level which we would like it to be, and to achieve this goal, your help is needed.

Feedback on the contents of the ESO Portal is welcome at all times. So also are comments on presentation and layout.

Reference

H.-M. Adorf, "Electronic access to HST information. II. The World-Wide Web", *ST-ECF Newsletter*, No. 21, April 1994, pp. 31–34.

The Light Element Abundances

A LIGHT REVIEW OF THE RECENT ESO/EIPC WORKSHOP

P. CRANE, ESO, and J. FAULKNER, Lick Observatory, University of California, Santa Cruz, U.S.A.

The ESO/EIPC Workshop on *The Light Element Abundances* was held during the week of May 23 at the Elba International Physics Centre on the Island of Elba. The 78 participants, only a small number of whom even noticed their email exile, represented the major fraction of the active researchers in this field.

The main focus of the workshop, the abundances of the elements with $Z \leq 5$, encompasses a very broad range of topics in astronomical research. These stretch from the synthesis of elements in the early Universe through stellar and galactic evolution to the Intergalactic Medium. The interplay between the theorists and observers in these seemingly diverse topics generated interesting and at times lively exchanges, just as a workshop should.

New observational opportunities with the Keck Telescope, with the refurbished HST, and with observational procedures that push old telescopes to new limits provided the most exciting new results.

The recently reported Keck observations of an absorption feature in the spectrum of Q0014+813 (Songaila et al., 1994, Carswell et al., 1994) which has been interpreted as a strong deuterium feature was touched on by many speakers. Curiously the standard Big Bang Nucleosynthesis (BBN) can accommodate almost a factor of 10 more D than is seen in the local ISM. However, theories of galactic evolution and the ^3He abundance cannot easily be made to agree with such a high value for D. Several participants suggested (or hoped) the “deuterium feature” in Q0014+813 would prove to be due to a weak hydrogen cloud.

Keck observation of Be in several low metallicity stars (Boesgaard) may be showing a plateau in the Be abundance which would present difficulties for theory if true. However, more observations are needed.

HST provided two of the most beautiful new pieces of data. Linsky presented spectra of D lines in the local ISM of unprecedented quality. His results confirm and strengthen the previous values for the abundance of D in the ISM. Jakobsen presented a truly convincing spectrum of a HeII absorption feature at rest wavelength of 304 Å. This feature was seen in the spectrum of a high redshift quasar where the original HeII line was redshifted to the region acces-

sible to HST. Essentially no radiation at all was seen shortward of 304 Å suggesting that the Universe is opaque at these wavelengths. This is the first time the presumed diffuse intergalactic medium has been detected.

The $^7\text{Li}/^6\text{Li}$ isotope ratio determination is being measured in stars and in the ISM using improved data and methodology. Nissen reviewed the observational situation in old stars and showed convincing evidence that his techniques can determine this important isotope ratio. Lemoine showed new observations of exceptional quality to determine this ratio in the ISM toward Zeta Oph. The $^7\text{Li}/^6\text{Li}$ ratio in the ISM is close to solar or slightly below.

The new and old of BBN was reviewed by Audouze and elaborated on by Hoyle and Steigman. Hoyle in particular produced a characteristically bold alternative to the BBN by proposing that the light elements form in unusually hot and dense fireballs which are the end products of decay of Planck particles at 10^{-43} sec. This theory apparently can produce similar abundances for the light elements as does the BBN theory. In spite of this and over the silent protests of Burbidge, who had left early, Schramm proclaimed in his summary that the Big Bang is still healthy and basically the only game in town.

Theoretical models for galactic evolution of the light elements were the focus of many authors. Whether the observed total of $\text{D} + ^3\text{He}$ was consistent with the BBN picture and galactic evolution theory occupied the discussions by Steigman, Tosi, and Galli; new observations by Rood and his colleagues of galactic ^3He did not show a pattern consistent with an overall chemical enrichment scenario, and only added to the perceived problems if the deuterium mentioned above is taken seriously. Clearly, a further advance in understanding of this area requires less data. Reeves discussed the relations between the boron isotopic ratio and galactic cosmic rays, while Matteucci and Kunth each presented models of galactic evolution involving various stellar processes and mixing. The motto for this part of the meeting was “Those who cannot destroy an element are destined to produce it” – and so they did, in a dense and tangled thicket of parameters, although the final fits were always termed “predictions” by their perpetrators. Beckman, however, distin-

guished himself by bravely presenting a new and quite plausible model in which low energy cosmic ray $\alpha + \alpha$ reactions combined with an adequate chemical evolution model intriguingly reproduced the dependence of Li on Fe in the galactic disk, as well as fairly representing aspects of Be and the Li and B isotopic ratios. He was also able to explain the observed delay in the onset of Li production compared with that of Fe.

Lithium's study has far to go, and so, appropriately, almost all of Thursday, and more, was devoted to this particular element. Faulkner presented a self-consistent, and purely classical, parameter free explanation of the Hyades G- and K-dwarf (Li, T_{eff}) relation that appears to resolve this 30-year-old problem. Delyannis not only discussed Be- (in addition to Li-) depletion in stars, but was a persistent proponent of the view that Li depletion was dominated by age and rotational spin-down considerations. Pallavicini produced evidence from tidally locked binaries tending to support the idea that in them, at least, rotationally-induced mixing played a part in the Li depletion. However, when he remarked that the picture was greatly confused in Pop I field stars, perhaps by the influence of other parameters, Delyannis rose smoothly to interject (and to hoist himself upon) one of the best petards of the meeting: “You need to know the *complete* rotational and mass-loss history of a star before you can predict its surface lithium content.” How such post-pre-science was to be achieved remained unclear. His rotational enthusiasm remained undampened even when Soderblom revealed that new Keck HIRES observations of Li in low-mass Pleiades stars ($T_{\text{eff}} \sim 4200 \pm 300$ K) suggested that the previously seen correlation between excess Li and excess rotation is weak or absent – or, indeed on the face of the evidence presented, inverted!

Nevertheless, the Light Element Abundances is hardly a topic to be taken lightly and the proceedings should prove to be a tome of some intellectual weight.

References

- Carswell, R.F., Rauch, M., Weymann, R.J., Cooke, A.J., and Webb, J.C., *MNRAS* **268**, L1 (1994).
- Songaila, A., Cowie, L.L., Hogan, C.J., and Rugers, M., *Nature*, **368**, 599 (1994).

Shoemaker-Levy 9/Jupiter Collision to be Observed at ESO

The upcoming collision between comet Shoemaker-Levy 9 and giant planet Jupiter has led to intensive preparations by astronomers all over the world and it is obvious that this unique event has also caught the imagination of the public. According to the latest calculations the impacts will commence in the evening of July 16 and end in the morning of July 22, 1994. There will be no less than 12 different investigations at the ESO La Silla observatory during this period.

A Unique Event

This is the first time ever that it has been possible to predict such a collision. Although it is difficult to make accurate estimates, it is likely that there will be important, observable effects in the Jovian atmosphere.

High-resolution Hubble Space Telescope images have shown that the comet has broken up into 21 or more individual fragments (termed "nuclei"), whose diameters probably range between a few kilometres and a few hundred meters. There is also much cometary dust visible around the nuclei; it is probably a mixture of grains of different sizes, from sub-millimetre sand up to metre-sized boulders. No outgassing has so far been observed from Shoemaker-Levy 9, but this is not unusual for a comet at a heliocentric distance of 5 A.U.

Accurate determinations of the positions of the individual nuclei have permitted to calculate quite precise orbits and it is certain that all of them will indeed collide with Jupiter. The points of impact are in the Jovian southern hemisphere, at $\sim -45^\circ$ latitude. Unfortunately, these impacts will happen just behind Jupiter's limb, i.e., out of sight from the Earth. However, due to the rapid rotation of the planet, the impact sites will come into view only ~ 10 – 20 minutes later at the very limb, where they will be seen "from the side". It is also fortunate that the American spacecraft Galileo, now approaching Jupiter, will have a direct view of the impact sites.

On the basis of the recent astrometric observations, including some with the Danish 1.5-m telescope at La Silla, the impact times can now (June 20) be predicted to about ± 30 minutes (2σ). The first, rather small nucleus ("A") will hit the upper layers of Jupiter's atmosphere on July 16, 1994 at about 20^h (UT); the apparently biggest nucleus ("Q") on

July 20, at 20^h UT, and the last one in the train ("W"), on July 22 at about 8^h UT.

Possible Effects

The comet nuclei will hit Jupiter at a high velocity, ~ 60 km/sec. The correspondingly large motion energy (the "kinetic energy") will all be deposited in the Jovian atmosphere. For a 1 km fragment, this is about equal to 10^{28} erg ($\sim 250,000$ Megatons).

When one of the cometary nuclei enters the upper layers of the Jovian atmosphere, it will be heated by the friction, exactly as a meteoroid in the Earth's atmosphere, and its speed will decrease very rapidly. Depending on the size of the fragment, it may evaporate completely within a few seconds, while it is still above the dense cloud layer that forms the visible "surface" of Jupiter, or it may plunge right through these clouds (and therefore out of sight) into increasingly denser, lower layers, where it ultimately comes to a complete stop and disintegrates in a giant explosion.

All of the kinetic energy is released during this process. One part will heat the surrounding atmosphere to very high temperatures; this will result in a flash of light that lasts a few seconds. Within the next minutes, a plume of hot gas will begin to rise over the impact site. It may reach an altitude of several hundred kilometres above the cloud layers and will quickly spread out in all horizontal directions.

Another part of the energy will be transformed into shock waves that will propagate into the interior of Jupiter, much as seismic waves from an earthquake do inside the Earth. When these waves again reach the upper layers of the atmosphere, they may be seen as slight increases in the local temperature along expanding circles with the impact sites at their centres (like waves in a water surface). The shock waves may also start oscillations of the entire planet, like those of a ringing bell.

During the past year, atmospheric scientists have attempted to calculate the details of these impacts, but the uncertainties are still rather large. Moreover, the magnitudes of the overall effects are entirely dependent on the energies involved, i.e., on the still not well determined sizes (masses) of the cometary nuclei.

It is also expected that there will be some kind of interaction between the cometary dust and Jupiter's strong

magnetic field. The fast-moving dust grains may become electrically charged. This will possibly have a significant influence on Jupiter's radio emission and therefore be directly observable with Earth-based radio telescopes, as well as from several spacecraft, including *Ulysses*, now en route towards its first pass below the Sun. There may also be changes in the plasma torus that girdles Jupiter near the orbit of the volcanic moon Io, and some cometary dust particles may collect in Jupiter's faint ring.

All in all, this spectacular event offers a unique opportunity to study Jupiter and its atmosphere. It may also provide a first "look" into its hitherto unobservable inner regions. Nobody knows for sure, how dramatic the effects of the impacts will actually be, but unless we are prepared to observe them, we may lose a great chance that is unlikely to come back in many years, if ever.

Some Recent Developments

Both Jupiter and the cometary nuclei have been extensively observed during the past months. However, while we now possess more accurate information about the comet's motion and the times of impact, there is still great uncertainty about the effects which may actually be observed at the time of the impacts. This is first of all due to the fact that it has not been possible to measure the sizes and masses of the individual cometary nuclei and thereby to estimate the amount of energy which will be liberated at the collisions.

Despite intensive spectroscopic observations, no gas has yet been detected in any of the nuclei. We only see dust around the nuclei which are completely hidden from our view within these clouds. The amount of the dust has been steadily decreasing; this is because the dust production from the individual nuclei – which began when the parent body broke up at the time of the near-collision with Jupiter in July 1992 – is slowly diminishing with time.

Some of the smaller nuclei have recently disappeared from view, probably because they have ceased to produce dust. It is not clear, however, whether this also implies that they no longer exist at all, or whether they are just too small to be seen with available telescopes.

The Observations at ESO

In November 1993, a group of 25 cometary and planetary specialists from

Europe and the U.S.A. met at ESO to discuss possible observations from the ESO La Silla observatory in connection with the cometary impacts at Jupiter. In a resulting report, they emphasized that ESO is in a particularly advantageous situation in this respect, because the excellent site of this observatory is located in the south and Jupiter will be 12° south of the celestial equator at the time of the event and therefore well observable from here; the time available from observatories in the northern hemisphere will be much more restricted. Moreover, many different observing techniques are available at La Silla; this provides optimal conditions for effective coordination of the various programmes, in particular what concerns imaging and spectral observations in the infrared and submillimetre wavebands.

During its November 1993 meeting, the OPC granted extensive observing time for observations with the ESO telescopes of this event.

Some of the observations at ESO are aimed at the accurate determination of the positions of the individual nuclei in order to improve the determination of their orbits. By continuing this work until the very last day before the impacts, it will hopefully be possible to achieve a final timing uncertainty of a few minutes for these events. This will be of importance for all other observations, both from the ground, and especially for those carried out from the spacecraft.

A team from the Munich Observatory (Germany) under the leadership of Heinz Barwig will perform rapid brightness measurements of Jupiter's moons at the predicted times of the impacts with their special high-speed photometer attached to the ESO 1-metre telescope. The flashes from the impacts will be reflected from the surfaces of those Jupiter moons which are in view of the impact sites. If this happens when a moon is in full sunlight, the relative increase of intensity will probably only be of the order of 1%. However, if one of the moons is located in the shadow of Jupiter and is at the same time visible from the Earth, then the relative brightening may be very conspicuous. Whether this will be the case will of course depend on the exact moments of the impacts.

Also at the time of the impacts, a group of French astronomers, headed by Bruno Sicardy of the Observatoire de Paris, will mount a special CCD camera at the Danish telescope, which will be used for different types of observations. They also hope to be able to detect some of the expected light flashes from the Jupiter moons. In addition, this programme will monitor changes in the

cloud structure around the impact sites. It may also be possible to obtain low-resolution spectra which will show the temperature of the flashes, but in view of their very short duration, a few seconds at most, this will not be easy.

The same instrument will also be used by Nick Thomas of the Max-Planck-Institut für Aeronomie (Lindau, Germany) to image the Jupiter plasma torus in order to detect possible changes after the impacts.

Spectral observations of the comet have been made with the ESO 1.5-m telescope in April by Heike Rauer, also from the Max-Planck-Institut für Aeronomie. They are expected to lead to a better knowledge about the physical and chemical state of the impacting bodies. For instance, are they really so "dusty", as present observations seem to indicate, or do they contain large amounts of gas? If so, what kind of molecules are present? This will help to refine the predictions of the impact effects.

Imaging and spectral observations of the comet for the same general purposes will also be obtained in early July with the EMMI instrument at the 3.5-m New Technology Telescope by an international team headed by Rita Schulz, formerly at the University of Maryland and now at the Max-Planck-Institut für Aeronomie.

No less than 46 observing hours have been allocated at the Swedish-ESO Submillimetre Telescope (SEST) to an international group headed by Daniel Gautier, Observatoire de Paris-Meudon. During the impacts, the cometary molecules will be mixed with those in the Jovian atmosphere, some of which may come from very deep layers. Together they will be carried upwards in the plume, described above. This may provide a rare opportunity, not only to register the submillimetre emissions from those molecules which are already known to be present in the comet and on Jupiter, but also to detect new and unknown molecules otherwise not accessible for direct observations, either from the interior of the cometary nuclei or from deep down in Jupiter's enormous atmosphere.

Infrared observations will play a very important role during the ESO campaign. A new ESO-developed instrument, TIMMI (Thermal Infrared Multi-Mode Instrument) will be mounted at the ESO 3.6-m telescope and will provide detailed infrared images of the impact areas when they become visible at the limb. Two teams will be active here; one is led by Timothy A. Livengood from NASA Goddard Space Flight Center (U.S.A.) and includes several ESO staff astronomers. Thanks to the excellent

imaging capabilities of TIMMI in the far-infrared spectral region, this group will be able to look far down into the atmosphere and to measure minute temperature variations. This should make it possible to register the effects of the shockwaves that arise when the cometary energy is deposited in the atmosphere.

The second group at the 3.6-m telescope, led by Benoit Mosser from Institut d'Astrophysique, Paris, will be looking for short- and long-term oscillations of the entire planet during the days and nights following the impacts. It is agreed that such observations will not be easy, but they offer the best hope we presently have of learning about the internal structure of Jupiter. It may be deduced from the observed frequencies and modes of oscillation. A particularly interesting problem is whether Jupiter really possesses a core of metallic hydrogen, as postulated by some scientists.

Infrared images will also be made by Klaus Jockers from the Max-Planck-Institut für Aeronomie with the ESO infrared IRAC camera at the MPI/ESO 2.2-m telescope. Since they will be obtained at shorter wavelengths than those at TIMMI, they will show higher layers of the atmosphere and the possible changes (streaming motions, new whirls and eddies?) which may result from the impacts. These programmes will therefore complement each other.

A total of no less than 13 half-nights have been allocated at the 3.5-m New Technology Telescope. They will be shared between two groups which will both use the IRSPEC instrument to obtain detailed infrared spectra of the impact sites. One team is headed by Rita Schulz, the other by Thérèse Encrenaz from Observatoire de Paris. Among many others, they hope to observe some of the molecules which may be present in the deeper layers of the Jovian atmospheres, e.g., water, ammonium and phosphine (PH₃).

Altogether, there are 12 individual programmes at all of the major telescopes, including the 3.6-m, the NTT, the SEST, the 2.2-m MPI/ESO, the 1.4-m CAT and the Danish 1.54-m telescope.

The Observations Are Difficult

The observers at ESO will profit from the simultaneous observations with many different telescopes and observing techniques at one site. In particular, they will have contact with observers at the South African Astronomical Observatory (SAAO), where observations will start a few hours before each evening. They will then be able to better prepare them-

selves for unexpected developments, should such be observed at SAAO.

It is clear that these observations will be difficult, in particular because of the relatively short time that Jupiter and the comet will be well above the horizon at La Silla, at most a few hours each evening. When Jupiter is very low in the sky, the viewing conditions are less favourable, since the light must traverse a longer distance through the turbulent and absorbing terrestrial atmosphere. However, since Jupiter will be south of the celestial equator, observing conditions will be even worse from observatories located in the northern hemisphere.

To record the best possible data (images, spectra, light curves, etc.), the telescopes must follow the motion of Jupiter very accurately. Due to its orbital motion in the solar system, Jupiter moves rather rapidly in the sky, and the telescope motion must be precisely offset to continuously track the planet without "smearing" the images. This is not a simple task, also since the planet's rate of motion changes with time and new corrections must be made several times each hour.

All in all, the observers face a difficult task and must be extremely alert, especially around the predicted moments of impact. This will demand very high concentration and necessitate "training runs" before the real observations begin. Some of these have already taken place – not surprisingly, various technical problems were uncovered and are now in the process of being resolved.

ESO's Special Services to the Media

In view of the unique nature of this event and the associated astronomical observations, ESO has decided to provide special services to the media. In particular, it is the intention to ensure that the media will be able to follow the developments at La Silla closely and in near-real time, and at the same time will be kept informed about the observational results at other observatories all over the world.

This service will be available from the ESO Headquarters in Garching near Munich, Germany, and special arrangements are also being made for the media in Chile. It will have the following elements:

- Background material in the form of text and images, as well as related video clippings (broadcast quality) will be available at request from July 5.
- From July 11, ESO will issue daily bulletins with the latest predictions and other news, related to the preparations of observations at La Silla and elsewhere in the world.
- Press Conferences will be arranged at the ESO Headquarters in Garching and at the ESO Office in Santiago de Chile on Saturday, July 16, just before the first impacts. Following an in-depth briefing, some of the media representatives will pass the night at the ESO Headquarters from where they can follow the first observations at La Silla at distance.
- There will be a Press Conference at the ESO HQ each following day at 11:00 (CEST), summarizing the previous night's results. Selected images obtained at ESO the night before will be available on these occasions. Special arrangements are also being made for the Chilean media.

*Based on ESO Press Releases
02/94 and 10/94*

Adriaan Blaauw at 80

S.R. POTTASCH, Kapteyn Laboratorium, Groningen, Netherlands

On 12 April 1994, Adriaan Blaauw celebrated his 80th birthday. He neither looks nor acts this age: he still spends much of his time actively engaged in scientific work. His impact on (European) astronomy has been great and it is useful to examine it more closely.

Short Sketch of his Career

Adriaan was born in Amsterdam in 1914. In 1932 he began his studies of Astronomy at Leiden University. He became an "Assistant" at the Kapteyn Institute in Groningen in 1938, although he was officially still a student at Leiden, obtaining his "doctoraal" degree there in 1941. He spent the war years in Groningen, moving to a staff position at Leiden in October 1945. He defended his thesis "A study of the Scorpio-Centaurus Cluster" in 1946 at Groningen (advisor, P.J. van Rhijn). In 1948 Adriaan became Associate Professor of Astronomy at Leiden University. He resigned from this position in 1953 to accept a similar position at the University of Chicago (Yerkes Observatory) where he remained for four years. During the last year of his stay he was also Associate Director of Yerkes and McDonald Observatories.

At the end of 1957 Adriaan returned to the Netherlands as Professor at Groningen University and Director of the Kapteyn Institute, which he remained until 1970. His growing involvement with ESO (see below) led to his formal "half-time" appointment as Scientific Director of ESO in 1968. In 1970 he reversed these associations, becoming Director General of ESO and part-time Professor at Groningen. This situation lasted five years, after which Adriaan returned to the Netherlands, but this time as Professor at Leiden. He retired from there in 1981 to settle in his beautiful, centuries old, farmhouse in the province of Drenthe, not far from Groningen University. Here he became Advisor to the Department of Astronomy, a function which he actively fulfils at present.

Scientific Research in Astronomy

Adriaan's name is mostly associated with investigations on massive stars, the O and B-type Stars. Of these we summarize (1) the observational confir-

mation of the occurrence of stellar groups of recent formation, (2) the discovery of the process of sequential star formation, and (3) his work on the class of early-type stars with anomalously high velocities, the "runaway" stars. These investigations would bear fruit also in studies of the star formation process.

1. In the late 1940's, there was accumulating evidence that besides the majority of stars with ages of the order of that of the solar system, to be counted in billions of years, the ages of the most massive stars in the Galaxy would have to be counted in millions of years only. The evidence was based, on the one hand, on the new understanding of stellar nuclear energy sources (closely related to work on nucleosynthesis in the years during and immediately after the Second World War) and, on the other hand, on the study of the structures and equilibrium conditions of loose stellar groups, the Stellar Associations. Adriaan studied known OB-Associations and identified new ones (the Sco-Cen, the Per OBII, the Lac OBI Associations), and provided direct confirmation of these very young ages by means of investigations of their internal motions. These revealed a general expansion, confirming that they are unbound systems that must have been born only millions of years ago. An important implementation of these various lines of evidence was that star formation in the Galaxy must still be going on today.

2. His study of the structures and stellar content of the OB Associations revealed that these consist of spatially separated subgroups, separated in age by intervals of several millions of years, and this led him to the conclusion that star formation occurs stepwise. The process has since become known as "sequential star formation", and is now recognized as a general characteristic of the formation of massive stars. In many cases there is close association of the youngest of these subgroups with the interstellar molecular cloud medium from which the association has emerged. Examples are the Sco-Cen Association with at least four subgroups formed over the last 15 million years, and the

Orion OBI Association with four subgroups formed over the past 12 million years.

3. Regarding the runaway stars, it was already known in the early 1930's that early-type stars have small random velocities. However, about 10 % of the O stars have high radial velocities which did not fit into the universal property of slow moving luminous stars. The possibility that these motions were due to undiscovered spectroscopic binaries was ruled out, as was the possibility that they were due to systematic atmospheric motions. A study of the proper motions indicated that at least some of these stars had transverse motions which were equally large. Adriaan concluded that these high velocities were real motions in space.

How had these motions originated and why was there a clear-cut dichotomy between fast and slow moving stars? An important clue was that these runaway stars were mostly single stars. Adriaan suggested that these stars had originally been part of a massive binary system which had suddenly been disrupted because the primary of the system became a supernova, so that the component was released at a velocity of the order of the orbital velocity. This relatively simple solution was first published in 1961. An interesting aspect of these studies is that for nearby runaway stars with accurate proper motions it is possible to identify the OB Association from which the star originated. In such cases the epoch of the supernova explosion can be fixed with high accuracy (of the order of several tenths of a million years) and it is also possible to determine the distance, and hence the absolute magnitude of the star with high accuracy. These studies therefore also bear fruit in other ways, for instance for stellar astrophysicists working on models of atmospheres of early-type stars. A recent example is his study of the bright runaway star Zeta Puppis.

Some Details on the Association with ESO

Discussion about the need for a joint European observatory in the southern

hemisphere first began to take form after the last war. In 1953 at a conference on galactic structure in Groningen (IAU Symposium 1), informal talks were held the day before the conference began among various European astronomers about the possibilities. Adriaan took part in these discussions but just after this conference he accepted the position at Yerkes Observatory. Because he expected to remain there he took no further part in the ESO planning until the end of 1957, at which time he returned to Europe as Professor of Astronomy (and Director of the Kapteyn Institute) at Groningen. Although a "statement of intent" had been signed in 1954, only limited progress was made in the early years. Positive was the beginning of site testing in South Africa. The financial basis remained weak and dependent on voluntary contributions of the future member states. In October 1957 the committee of astronomers which was meeting periodically (about once a year) to discuss the project assumed a more formal form with the appointment of a Chairman (Oort) and a Secretary (Banner). In May 1959 Adriaan succeeded Banner as Secretary of this "provisional council" until succeeded by Heckmann in 1963. During this period substantial progress had been made in the organization of ESO, leading to the signing of the Convention in October 1962.

Adriaan continued to be involved in the development of ESO. At the beginning of 1968 this was formalized by his appointment as Scientific Director of ESO. This was a "half-time" function and he combined it with his work in Groningen by driving to and from Hamburg (where ESO had its headquarters at the time). In January 1970 he succeeded Heckmann as Director General. His position at Groningen became "part-time" and he remained Director General of ESO until the beginning of 1975 and continued as advisor for some time after that. He is the author of "ESO's Early History" which was published in 1991.

Astronomy and Astrophysics: a European Journal

The founding of *Astronomy and Astrophysics* took place in 1968 for essentially the same reasons ESO was formed: the individual European countries could not compete in this case with the large American journals. Europeans

began to feel that their work was not widely read and some were considering publishing their best work in the *Astrophysical Journal*. The initiative to merge the national journals came, as might be expected, from their editors, especially J.-L. Steinberg and myself. A meeting took place in April 1968 of astronomers from Belgium, Denmark, France, Germany and the Netherlands to prepare a possible merger. It was immediately clear that scientifically the difficulties of such a merger were relatively minor (but not non-existent). A much greater problem were the financial and administrative aspects. If the same procedure had been followed as by the creation of ESO, a journal might have been formed many years before.

Adriaan, as ESO representative at the meeting, suggested circumventing the difficult procedure. He offered the services of ESO as "legal person" responsible for the financial and administrative state of the journal. This would make it easy for national governments to make financial contributions to an international organization, since an official treaty already existed. A Board of Directors with representatives of the sponsoring countries was set up, which took over the financial and administrative dealings of the journal. The editors were then only responsible for the scientific dealings of the journal. The Board fixed general policy (e.g. which languages were acceptable, who were to be the editors) but was not involved in the processing of articles. Adriaan was elected the first Chairman of the Board of Directors in October 1968 and held the position until March 1979. When he resigned, the journal was well established and both financially and scientifically "healthy".

Other European and International Activities

Since 1981 Adriaan has been associated with the Hipparcos satellite project, as Chairman of the Scientific Evaluation Committee. In this position he has worked closely with the scientists who have designed and built the instrument. In particular he has advised on many aspects of the scientific programme. This association was "natural" since Adriaan's scientific research is closely related to the Hipparcos goal. The fruits of this association will only be known in detail in the coming years as the Hipparcos data are released for publication.

Mention must also be made of Adriaan's work for the International Astronomical Union, of which he was President from September 1976 to August 1979. He is especially remembered for his efforts to include China and the vast majority of Chinese astronomers as members of the IAU. These efforts bore fruit as Chinese membership was confirmed at the Patras meeting in 1982. A discussion of the details of these negotiations as well as a general history of the IAU has just been completed by Adriaan and should be available before the General Assembly of this year.

Non-Astronomical Scientific Activity

Adriaan has also been scientifically active in a field quite different from astronomy: the early history of farmers-settlements. It started with research on the history of the structure and inhabitants of the 17th-century farmhouse he acquired and restored in the 1960's. This gradually developed into his systematically investigating aspects of the history of a nearby village, typical for the settlements in the north-east of the Netherlands. These studies were based on archival data in Dutch State Archives. After having published several articles in professional History Journals, he published a book on the village Westervelde in 1987, in which he covered cultural, agricultural and social aspects in the 17th, 18th and 19th century. This study has turned out to be useful in courses on legal anthropology at Groningen University.

Concluding Remarks

The picture describes an international, and especially European-oriented astronomer. The European orientation has partly to do with the fact that astronomy has turned rapidly to large projects which can no longer be supported by individual institutes or even small countries. It has partly to do with larger historical (and political) changes.

Finally, I personally would like to thank Adriaan for one of his minor decisions: his invitation in 1962 to me to come to Groningen, without which I would not have become a "European" astronomer.

ESO Studentship Programme

The European Southern Observatory has positions available for 12 research students. Six of these positions are at the ESO HQ in Garching, the other six at the Observatory, La Silla, Chile. Since students normally stay approximately 2 years, this means that each year a total of 6 students (3 at each location) may be accepted. These are available to students enrolled in a Ph.D. (or equivalent) programme in the member states and exceptionally at a university in other countries.

Potential candidates or their supervisors may obtain detailed information about the programme by requesting the updated brochure and application forms from the Personnel Administration and General Services at ESO HQ, Karl-Schwarzschild-Str. 2, D-85748 Garching bei München, Germany.

The closing date for applications is October 15.

ESO Fellowships

The European Southern Observatory (ESO) will award up to six post-doctoral fellowships tenable at the ESO Headquarters in Garching near Munich. The tenure of the Fellowships can begin between January and October 1995. Fellows have the opportunity to participate in the ongoing activities at ESO Headquarters.

Inquiries, application forms and other information may be requested from:

European Southern Observatory
Fellowship Programme
Karl-Schwarzschild-Str. 2
D-85748 Garching bei München
Germany

The deadline for applications is October 15, 1994.

Studentships at La Silla

Two studentships are offered at La Silla, one starting in January 1995, the other in April 1995.

Students in the ESO Research Student Programme work on an advanced research degree under the formal tutelage of their home university, but come to La Silla and work under the daily guidance of an ESO staff member. In addition to the opportunities offered by the infrastructure and guidance, ESO may also provide logistical and financial support if necessary.

Students are appointed initially for one year, and, if appropriate, reappointed for an extension of up to one year. The home institute of the student must guarantee that a position is available upon returning which enables the student to complete his/her degree.

Students at La Silla will normally be part of the team of astronomers in the Astronomy Support Department that provides introductions and observational support to Visiting Astronomers. Typically, one third of their official working time will be occupied by these duties.

The research interests of the members of the staff in the Astronomy Support Department at La Silla include low-mass star formation, protoplanetary nebulae, chemistry of molecular clouds, high-resolution spectroscopy of cool stars, supernovae and their remnants, the distance scale, compact groups of galaxies, and observational cosmology. Staff members and senior fellows act as co-supervisors for students of European universities who spend up to 2 years on La Silla working towards a doctoral dissertation. The staff of the Astronomy Support Department consists of about 20 astronomers including staff, post-doctoral fellows, and students. Most of the ESO scientists are from the member states of ESO (Belgium, Denmark, Germany, France, Italy, the Netherlands, Sweden and Switzerland), but several are from other countries.

The research facilities at La Silla consist of 12 telescopes, including the SEST 15-m submillimetre antenna, and the 3.5-m New Technology Telescope. There are ample computing facilities including a number of networked SUN workstations.

Applications for both studentships should be submitted to ESO **not later than October 15, 1994**. Applicants will be notified before December 1, 1994. The ESO Studentship Application Form must be used, and two letters of recommendation should be sent directly to ESO before the same deadline.

Potential candidates or their supervisors may obtain detailed information about the programme by requesting the ESO Student Brochure. Requests for the brochure and application forms and applications should be addressed to:

European Southern Observatory, Studentship Programme, Karl-Schwarzschild-Strasse 2, D-85748 Garching bei München, Germany

Fellowships at La Silla

A post-doctoral fellowship is offered on La Silla starting at the beginning of 1995. The position is open to young astronomers with an interest in observational astronomy. The ESO fellowships are granted for a period of one year, normally renewed for a second and exceptionally for a third year.

For the present fellowship, applicants with experience in infrared imaging are particularly encouraged to apply. However, all qualified applicants will be considered irrespective of their field of observational experience.

The successful applicant will be required to spend 50 % of his/her time doing support activities and 50 % of the time on research.

Applicants normally should have a doctorate awarded in recent years. Applications should be submitted to ESO **not later than September 15, 1994**. Applicants will be notified by November 1, 1994. The ESO Fellowship Application Form should be used and be accompanied by a list of publications. In addition, three letters of recommendation from persons familiar with the scientific work of the applicant should be sent directly to ESO. These letters should reach ESO **not later than September 15, 1994**.

The research interests of the members of the staff in the Astronomy Support Department at La Silla include low-mass star formation, protoplanetary nebulae, chemistry of molecular clouds, high resolution spectroscopy of cool stars, supernovae and their remnants, the distance scale, compact groups of galaxies, and observational cosmology. Staff members and senior fellows act as co-supervisors for students of European universities who spend up to 2 years on La Silla working towards a doctoral dissertation. The staff of the Astronomy Support Department consists of about 20 astronomers including staff, post-doctoral fellows, and students. Most of the ESO scientists are from the member states of ESO (Belgium, Denmark, Germany, France, Italy, the Netherlands, Sweden and Switzerland), but several are from other countries.

The research facilities at La Silla consist of 12 telescopes, including the SEST 15-m submillimetre antenna, and the 3.5-m New Technology Telescope. There are ample computing facilities including a number of networked SUN workstations.

Enquiries, requests for application forms and applications should be addressed to:

European Southern Observatory, Fellowship Programme, Karl-Schwarzschild-Strasse 2, D-85748 Garching bei München, Germany

Senior Visitor Programme at La Silla

The European Southern Observatory (ESO) invites experienced astronomers to spend periods ranging from a few months to one year at La Silla in Chile within the framework of the ESO Senior Visitor Programme. The research facilities at La Silla consist of 12 telescopes, including the SEST 15-m submillimetre antenna, and the 3.5-m New Technology Telescope. There are ample computing facilities with a number of networked SUN workstations which run, among other things, the MIDAS image-processing system.

The astronomy group at La Silla has 18 members divided into 6 staff astronomers, 6 post-doctoral fellows and 6 students. The research projects currently pursued by the astronomical staff include low-mass star formation (Herbig-Haro flows, young binaries, disk accretion), protoplanetary nebulae, supernovae and their remnants, chemistry of molecular clouds, high-resolution spectroscopy of cool stars, the distance scale, compact groups of galaxies, and observational cosmology.

The purpose of the Senior Visitor Programme is to provide stimulus to the ESO Astronomy Group in Chile. Thus, applicants are expected to have or to begin collaborations with one or more ESO astronomers during their visit. A series of lectures on the research field of the Senior Visitor is welcomed, although not mandatory. Except for the requirement to participate in the scientific life of the observatory staff, there are no constraints on the research activities of the Senior Visitor.

Most of the scientists in ESO come from the member states of ESO, but several are from other countries. The member states of ESO are: Belgium, Denmark, Germany, France, Italy, the Netherlands, Sweden and Switzerland. Applicants of all nationalities can apply. Senior Visiting Scientists will be paid an appropriate stipend. Applications may be submitted to ESO at any time. Applicants will be notified within two months. The ESO Senior Visitor Application Form should be used and be accompanied by a list of publications. Enquiries, requests for application forms, and applications should be addressed to:

European Southern Observatory
Senior Visitor Programme
Karl-Schwarzschild-Strasse 2
D-85748 Garching bei München
Germany

New ESO Preprints

March–June 1994

Scientific Preprints

986. P. Ballester: Hough Transform for Robust Regression and Automated Detection. *Astronomy and Astrophysics*.
987. M. Einasto et al.: The Structure of the Universe Traced by Rich Clusters of Galaxies. *M.N.R.A.S.*
988. L. Pasquini, Q. Liu and R. Pallavicini: Lithium Abundances of Nearby Solar-like Stars. *Astronomy and Astrophysics*.
989. Th. Müller, M.R. Rosa and S. Röser: Astrometry in the Galactic Center Region. *Astronomy and Astrophysics*.
990. J.J. Clariá et al.: An Abundance Calibration for DDO Photometry of Populations II G and K Giants. *M.N.R.A.S.*
991. N.N. Chugai: The Oxygen Mass in SN 1987A: Making Use of Fluctuations in (OI) 6300, 6364 Å Profile. *Astrophysical Journal (Letters)*.
N.N. Chugai: Supernovae with Dense Circumstellar Winds *Astrophysical Journal (Letters)*.
992. H. Kjeldsen and T.R. Bedding: Amplitudes of Stellar Oscillations: the Implications for Asteroseismology. *Astronomy and Astrophysics*.
993. A. Franceschini et al.: X-Ray versus Optically Selected Active Galactic Nuclei: A Comparative Study of the Luminosity Functions and Evolution Rates. *M.N.R.A.S.*
994. P. Petitjean, M. Rauch and R.F. Carswell: The $Z_{\text{abs}} \sim Z_{\text{em}} \sim 2$ QSO Absorption Line Systems: Evidence for Abundances in Excess of Solar. *Astronomy and Astrophysics*.
995. A.A. Zijlstra et al.: Radio and Infrared Emission from a (WC)-Type Planetary Nebula in the LMC. *Astronomy and Astrophysics*.
996. S.R. Pottasch and A.A. Zijlstra: VLA Measurements of a Sample of Planetary Nebulae. *Astronomy and Astrophysics*.
997. E. Giallongo and P. Petitjean: The Temperature of the Lyman Alpha Clouds and the UV Ionizing Background at High Redshifts. *The Astrophysical Journal (Letters)*.
998. T.R. Bedding, J.G. Robertson and R.G. Marson: An Optical Interferometer with Wavelength Dispersion. *Astronomy and Astrophysics*.
999. G. Marconi, F. Matteucci and M. Tosi: Element Abundances in Blue Compact Galaxies. *M.N.R.A.S.*
1000. C.M. Carollo and I.J. Danziger: Colours, Line-Strengths and Stellar Kinematics of NGC 2663 and NGC 5018. *M.N.R.A.S.*

ANNOUNCEMENT ESO Workshop on QSO Absorption Lines

ESO, Garching
21 – 24 November 1994

An ESO workshop on QSO absorption lines will be held from 21 to 24 November 1994, at the Headquarters of the European Southern Observatory, Garching bei München, Germany.

The workshop is intended to discuss the theory and observations of QSO absorption lines in relation to the following topics:

- Galactic halo and interstellar medium
- Low-redshift systems
- Intrinsic absorption lines and BAL systems
- Ly-alpha clouds
- Damped systems
- Metal systems
- Probing the large scale structure
- Probing the Universe at high redshifts

Organizing Committee:

J. Bergeron, G. Meylan, P. Petitjean, P. Shaver, J. Wampler, ESO

Contact Address:

Georges Meylan, European Southern Observatory
Karl-Schwarzschild-Str. 2, D-85748 Garching bei München,
Germany
e-mail: gmeylan@eso.org fax: + 49 89 320-06-480/320-23-62

1001. O. Hainaut et al.: Imaging of Very Distant Comets – Current and Future Limits. *Astronomy and Astrophysics*.
1002. L. Jorda, O. Hainaut and A. Smette: Photometric Study of Comets P/Faye 1991 XXI and Zanotta-Brewington 1992 III. *Planetary and Space Science*.
1003. C.M. Carollo and I.J. Danziger: Dynamics and Stellar Populations in Early-Type Galaxies. *M.N.R.A.S.*
1004. M. Della Valle: Spectroscopic Observations of the Mt. Stromlo MACHO Candidate. *Astronomy and Astrophysics (Letters)*.

1005. P. Dubath and G. Meylan: High-Resolution Kinematical Mapping of the Core of the Globular Clusters M15 = NGC 7078. *Astronomy and Astrophysics*.
1006. M. Della Valle, I.F. Mirabel and L.F. Rodríguez: The Optical and Radio Counterpart of the X-Ray Nova Oph 1993. *Astronomy and Astrophysics*.
1007. J. Storm, B.W. Carney and D.W. Latham: Distances and Luminosities for RR Lyrae Stars in M5 and M92 from a Baade-Wesselink Analysis. *Astronomy and Astrophysics*.
1008. G.C. Van de Steene and A.A. Zijlstra: On an Alternative Statistical Distance Scale for Planetary Nebulae. *Astronomy and Astrophysics*.
1009. F. La Franca et al.: Deep VLA Observations of an Optically Selected Sample of Intermediate Redshift QSOs and the Optical Luminosity Function of the Radio Loud QSOs. *The Astronomical Journal*.
1010. G. Bertin et al.: A Search for Dark Matter in Elliptical Galaxies: Radially Extended Spectroscopic Observations for Six Objects. *Astronomy and Astrophysics*.
1011. S. Pellegrini: ROSAT PSPC Observation of the X-Ray Faint Early-Type Galaxy NGC 5866. *Astronomy and Astrophysics*.

Technical Preprints

63. VERY LARGE TELESCOPE (Instrumentation in Astronomy VIII). Papers submitted to S.P.I.E.'s 1994 Symposium on Astronomical Telescopes and Instrumentation for the 21st Century. 13–18 March 1994, Kona, Hawaii, U.S.A.
64. VERY LARGE TELESCOPE (Advanced Technology Optical Telescopes V). Papers submitted to S.P.I.E.'s 1994 Symposium on Astronomical Telescopes and Instrumentation for the 21st Century. 13–18 March 1994, Kona, Hawaii, U.S.A.
65. VERY LARGE TELESCOPE (Amplitude and Intensity Spatial Interferometry; Adaptive Optics in Astronomy). Papers submitted to S.P.I.E.'s 1994 Symposium on Astronomical Telescopes and Instrumentation for the 21st Century. 13–18 March 1994, Kona, Hawaii, U.S.A.

STAFF MOVEMENTS

Arrivals

Europe

AHRA, Margarete (AUS), Administrative employee (Pers.)
 BIANCAT MARCHET, Fabio (I), Electronics Engineer
 CHIESA, Marco (I), Software Engineer
 CHIOZZI, Gianluca (I), Software Engineer
 CROCKER, James (USA), Head of Programme Office
 CUBY, Jean-Gabriel (F), Paid Associate
 DUHOUEY, Philippe (F), Software Engineer
 FORSTMANN, Pierre (F), Software Engineer
 HERLIN, Thomas (DK), Software Engineer
 KAPER, Lex (NL), Fellow
 KNUDSTRUP, Jens (DK), Software Support Engineer
 KRETSCHMER, Gerhard (D), Mechanical Engineer
 NASTVOGEL-WÖRZ, Michael (D), Software Engineer
 MANIL, Emmanuel (F), System Engineer
 PHAN, Duc Thanh (B), Software Engineer

RÖNNBACK, Jari (S), Fellow
 SANDROCK, Stefan (D), Software Support Engineer
 SPYROMILIO, Jason (GB), Infrared Astronomer
 THIMM, Guido (D), Fellow

Chile

BENETTI, Stefano (I), Fellow
 CHATZICHRISTOU, Eleni (GR), Student
 KOWASCH, Wolfgang (D), Civil Engineer (Cerro Paranal)
 LEMKE, Roland (D), Paid Associate (SEST)
 LUNDQVIST, Göran (S), Paid Associate (System Analyst)

Departures

Europe

MARCONI, Gianni (I), Fellow
 MATTEUCCI, Francesca (I), Paid Associate
 VAN DER WERF, Paul (NL), Fellow

Chile

GREBEL, Eva (D), Student

ESO Publications Still Available

A number of books published by ESO are still available. To permit you to complete the series or simply to inform you about any volume that you may have missed, we reproduce here a list of some of the more recent ESO publications.

Proceedings

No.	Title and year of publication	Price
41	Fourth ESO/ST-ECF Data Analysis Workshop, 1992	DM 25.—
42	Progress in Telescope and Instrumentation Technologies, 1993	DM 90.—
43	Astronomy from Large Data Bases II, 1993	DM 70.—
44	Science with the Hubble Space Telescope, 1993	DM 80.—
45	Structure, Dynamics and Chemical Evolution of Elliptical Galaxies, 1993	DM 90.—
46	Mass Loss on the AGB and Beyond, 1993	DM 70.—
47	Fifth ESO/ST-ECF Data Analysis Workshop, 1993	DM 30.—
48	ICO-16 Satellite Conference on Active and Adaptive Optics, 1994	DM 90.—

Other Publications

ESO's Early History: The European Southern Observatory from Concept to Reality (A. Blaauw), 1991	DM 25.—
The Strasbourg-ESO Catalogue of Planetary Nebulae, Part I and II (eds. A. Acker, F. Ochsenbein, B. Stenholm, R. Tylenda, J. Marcout, C. Schohn), 1992	DM 135.—

Written-Off Items Available at ESO Headquarters

The following electronic parts, in good condition for further use, have recently been written off at ESO, Garching bei München, and are immediately available for the scientific institutes at a small nominal fee or even free of charge, provided that:

– a request is presented to ESO, Contracts & Procurement (Mr. F. Palma, Tel. 0049-89-32006-205; Fax: 0049-89-3207327) until August 31, 1994;

– agreements are taken on the terms and conditions of delivery.

Assignment will be made mainly by taking into account the order of presentation of the formal request and by giving priority to astronomical institutes in the ESO Member States.

F. PALMA, ESO

ESO Reference	Manufacturer	Description	Model	S/N	Year of manufacture
C30	Digital Equipment	Micro Vax	MVAX II	870342446	1987
MT26	Digital Equipment	Tape Unit TU 81	TU81E-CB	KB01212	1986
D46	Digital Equipment	Disk Drive RA 81	RA81-HD	KB22207	1987
D52	Digital Equipment	Disk Drive RA 81	RA81-AD	KB09171	1987
D53	System Industries	Disk Drive 906 MByte	SI93	4947	1988
D67	System Industries	Disk Drive 906 MByte	SI93	20532	1989
D71	System Industries	Disk Drive 906 MByte	SI93	500834	1990
D72	System Industries	Disk Drive 906 MByte	SI93	508839	1990
V1	Versatek	Printer Plotter	V80-711	B521198	1981
V4	Versatek	Printer Plotter	V80-711	B541162	1981
V5	Versatek	Printer Plotter	V80-211	C531680	1982
V6	Versatek	Printer Plotter	V80-211	B621095	1986
LA15	Agfa	Laser Printer	P3400PS	9P00315	1989
LA18	Agfa	Laser Printer	P3400PS	85220	1989
LA19	Agfa	Laser Printer	P3400PS	9P00190	1989
LA20	Agfa	Laser Printer	P3400PS	85498	1989
LA5	Agfa	Laser Printer P400PS	9350/190	73247	1988
NB13	NBI-BTO	Laser Printer	4045	3203002636	1988
W2	Wang	Phoenix Disk	2266V2	PB6208	1984
W3	Wang	Phoenix Disk	2266V2	ZV1917	1986
W4	Wang	Storage Cabinet	2295V-CO	UO2930	1988
TK1	Tektronix	Colour Terminal	4111	B021151	1986
TK4	Tektronix	Colour H/Copy	4692	B013226	1986
HC3	Seiko	Hardcopy device A3	CH-5312S	73B414A	1987
CC2	Seiko	Hardcopy controller A3 cont	CH-501F	60A393C	1987
	Hewlett Packard	Disk Drive 614120	HP7920	2126A03547	
LP3	Hewlett Packard	Printer	2631A	1841A04BO	1981
T35	Hewlett Packard	Graphics Terminal	2648A	2016F01302	1981
HC1	Honeywell	Printer	4VIEODTO	130006JAJ84	1983
LP6	Centronics	Printer	6600	D8K0096	1978
LP7	Centronics	Printer	6600	043003	1980
LP11	Centronics	Printer	6080	241006	1981
XT1	NCD	x Terminal	16P1E	936SF004TL1	1989
XT0	NCD	x Terminal	192P2E	313125	1989
	Phillips	Black/white Monitor			1988
DG1	Hewlett Packard	Digitizer	9874A	1811A01607	1982
LP17	TAB	Matrix Printer	GE8232A	13009651	1983
PC107	Olivetti	PC286	M290	7134112	1988
PC104	Olivetti	PC286	M280	2143496	1987
C14	Hewlett Packard	21MX Computer	2112A	1621F00321	1979
C10	Hewlett Packard	21MX Computer	2112A	1706F00401	1979
WS101	Texas Inst.	Explorer Workstation	2,249E+10	2342370002	1987
M18	Philips	B/W Monitor	LDH2122	14505	1982
M9	Philips	B/W Monitor	LDH2123	11714	1982
M5	Cotron	B/W Monitor	PM50B	111813	1978
M6	Cotron	B/W Monitor	IM50b	111812	1978
T56	Hewlett Packard	Terminal	2645A	2203F13490	1982
T50	Hewlett Packard	Terminal	2645a	2121F12222	1982
T51	Hewlett Packard	Terminal	2645a	2121F12223	1982
	Hewlett Packard	Desk Jet	2225BB	2737S02317	1987
	Hewlett Packard	Desk Jet	2225BB	2610S00031	1986
	Hewlett Packard	Desk Jet	2225BB	2442S00389	1984
PC12	IBM	PC	8350021	552100853	1987
M38	Philips	B/W Monitor	LDH2154	502850	1988
C45	DEC	VAX Station	3100	VL95002616	1989
	DEC	VAX Station	3100	AY92200713	
T8	Hewlett Packard	Terminal	2645A	1649A00823	1976

ESO, the European Southern Observatory, was created in 1962 to . . . establish and operate an astronomical observatory in the southern hemisphere, equipped with powerful instruments, with the aim of furthering and organizing collaboration in astronomy . . . It is supported by eight countries: Belgium, Denmark, France, Germany, Italy, the Netherlands, Sweden and Switzerland. It operates the La Silla observatory in the Atacama desert, 600 km north of Santiago de Chile, at 2,400 m altitude, where fourteen optical telescopes with diameters up to 3.6 m and a 15-m sub-millimetre radio telescope (SEST) are now in operation. The 3.5-m New Technology Telescope (NTT) became operational in 1990, and a giant telescope (VLT=Very Large Telescope), consisting of four 8-m telescopes (equivalent aperture = 16 m) is under construction. It will be erected on Paranal, a 2,600 m high mountain in northern Chile, approximately 130 km south of the city of Antofagasta. Eight hundred scientists make proposals each year for the use of the telescopes at La Silla. The ESO Headquarters are located in Garching, near Munich, Germany. It is the scientific-technical and administrative centre of ESO where technical development programmes are carried out to provide the La Silla observatory with the most advanced instruments. There are also extensive facilities which enable the scientists to analyze their data. In Europe ESO employs about 200 international Staff members, Fellows and Associates; at La Silla about 50 and, in addition, 150 local Staff members.

The ESO MESSENGER is published four times a year: normally in March, June, September and December. ESO also publishes Conference Proceedings, Preprints, Technical Notes and other material connected to its activities. Press Releases inform the media about particular events. For further information, contact the ESO Information Service at the following address:

EUROPEAN
SOUTHERN OBSERVATORY
Karl-Schwarzschild-Str. 2
D-85748 Garching bei München
Germany
Tel. (089) 32006-0
Telex 5-28282-0 eo d
Telefax: (089) 3202362
ips@eso.org (internet)
ESO::IPS (decnet)

The ESO Messenger:
Editor: Marie-Hélène Ulrich
Technical editor: Kurt Kjär

Printed by Universitäts-Druckerei
Dr. C. Wolf & Sohn
Heidemannstraße 166
80939 München 45
Germany

ISSN 0722-6691

Contents

R. Giacconi: Message from the Director General – Summary of a Report to the ESO Staff	1
-------------------------------------------------------------------------------------------------	---

TELESCOPES AND INSTRUMENTATION

D. Enard: Work Starts on the VLT M2 Unit	2
B. Koehler: Hunting the Bad Vibes at Paranal	4
Recent Photographs of Paranal	11
M. Sarazin: Site Surveys, from Pioneering Times to the VLT Era	12
M. Sarazin: Seeing Update: La Silla Back on the Track	13
S. D'Odorico: A F/5.2 Camera with a Thinned 2048 ² CCD at the EMMI Red Arm	15
H. Dekker, S. D'Odorico and A. Fontana: Test of an R4 Echelle Mosaic	16
J. Melnick: News from La Silla	20
NTT BITS & PIXELS	21

SCIENCE WITH THE VLT

A.-M. Lagrange: Studies of Disks Around Main-Sequence Stars with the VLT . . .	23
--------------------------------------------------------------------------------	----

REPORTS FROM OBSERVERS

A. Vallenari, G. Bertelli, C. Chiosi and S. Ortolani: The History of Star Formation in the Large Magellanic Cloud	30
R. Mignani, P.A. Caraveo and G.F. Bignami: Geminga, 10 Years of Optical Observations	32
M. Shaw, C. Tadhunter, N. Clark, R. Dickson, R. Morganti, R. Fosbury and R. Hook: Jet/Cloud Interactions in Southern Radio Galaxies?	34
P.E. Nissen, D.L. Lambert and V.V. Smith: The Lithium Isotope Ratio in Metal-Poor Stars	36
M. Arnaboldi, K.C. Freeman, X. Hul, M. Capaccioli and H. Ford: The Kinematics of the Planetary Nebulae in the Outer Regions of NGC 1399	40
F. Pont, D. Queloz, M. Mayor and G. Burki: Milky Way Rotation from Cepheids . .	45
M. Srinivasan Sahu and A. Blaauw: Interstellar Na I Absorption Towards Stars in the Region of the IRAS Vela Shell	48
M. Kürster, A.P. Hatzes, W.D. Cochran, C.E. Pulliam, K. Dennerl and S. Döbereiner: A Radial Velocity Search for Extra-Solar Planets Using an Iodine Gas Absorption Cell at the CAT + CES	51

OTHER ASTRONOMICAL NEWS

Science Data Analysis Group: The 94MAY Release of ESO-MIDAS	56
The ESO Web Consortium: ESO's New On-Line Information System	56
P. Crane and J. Faulkner: The Light Element Abundances – a Light Review of the Recent ESO/EIPC Workshop	58
Shoemaker-Levy 9/Jupiter Collision to be Observed at ESO	59

ANNOUNCEMENTS

S.R. Pottasch: Adriaan Blaauw at 80	62
ESO Studentship Programme	64
ESO Fellowships	64
Studentships at La Silla	64
Fellowships at La Silla	64
Senior Visitor Programme at La Silla	65
New ESO Preprints (March-June 1994)	65
Announcement of an ESO Workshop on QSO Absorption Lines	65
Staff Movements	66
ESO Publications Still Available	66
F. Palma: Written-Off Items Available at ESO Headquarters	66